(19) Europäisches Patentamt
European Patent Office
Office européen des brevets

(11) **EP 3 396 729 A1**

(12) EUROPEAN PATENT APPLICATION

(43) Date of publication:
31.10.2018 Bulletin 2018/44

(51) Int Cl.:
H01L 51/42 *(2006.01)* ***H01L 21/20*** *(2006.01)*

(21) Application number: **18168162.8**

(22) Date of filing: **28.05.2015**

(84) Designated Contracting States:
AL AT BE BG CH CY CZ DE DK EE ES FI FR GB GR HR HU IE IS IT LI LT LU LV MC MK MT NL NO PL PT RO RS SE SI SK SM TR

(30) Priority: **28.05.2014 US 201462004020 P**
08.10.2014 US 201462061475 P
14.01.2015 US 201562103277 P

(62) Document number(s) of the earlier application(s) in accordance with Art. 76 EPC:
15800233.7 / 3 149 765

(71) Applicant: **Alliance for Sustainable Energy, LLC**
Golden, CO 80401 (US)

(72) Inventors:
- **ZHU, Kai**
  GOLDEN, CO 80401 (US)
- **LUTHER, Joseph**
  GOLDEN, CO 80401 (US)
- **ZHAO, Yixin**
  SHANGHAI, GUANGDONG 200240 (CN)

(74) Representative: **Studio Torta S.p.A.**
Via Viotti, 9
10121 Torino (IT)

Remarks:
This application was filed on 19-04-2018 as a divisional application to the application mentioned under INID code 62.

(54) METHODS FOR PRODUCING AND USING PEROVSKITE MATERIALS AND DEVICES THEREFROM

(57) The present disclosure describes solution methods for manufacturing perovskite halide films for use in solar cells. The methods include the use of additives that facilitate the formation of transitory, intermediate films that are later transformed into the final target perovskite halide films, such that the final films provide improved physical characteristics and operational performance.

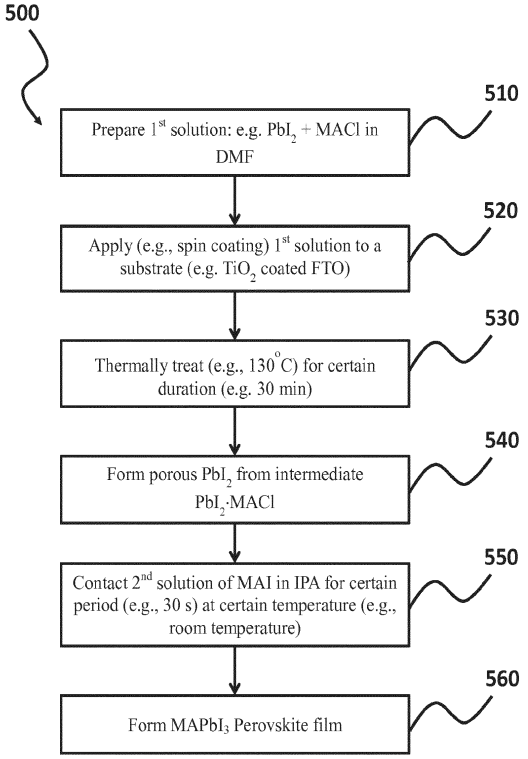

Fig. 5

EP 3 396 729 A1

Printed by Jouve, 75001 PARIS (FR)

Description

Background

[0001] Perovskite halides (e.g., $CH_3NH_3PbI_3$) represent a new class of light absorbers that have demonstrated tremendous progress in solar cell performance from 3.8% in 2009 to 20.1% in 2015. One attraction for perovskite halides is their bandgap tuning capability. For example, perovskite halide $CH_3NH_3PbI_2Br$ has a bandgap of about 1.8 eV, which makes it suitable for developing tandem or multijunction perovskite-based solar cells. However, perovskite halides have the capability of bandgap tuning by modifying their components building blocks. Moreover, high-efficiency perovskite solar cells can be made by low-cost processing methods. In addition, perovskite halides are not only direct-bandgap absorbers with strong absorption coefficients, but they also demonstrate long electron and hole diffusion lengths. For these and other reasons, perovskite halide solar cell technology is expected to attract strong interest from solar manufacturers and start-ups looking for their next-generation solar cell products.

[0002] However, current manufacturing methods typically produce unsatisfactory perovskite halide films. For example, many of the films produced are not full coverage, continuous films, free from pin-holes. In addition, it is very difficult to produce perovskite halide films that are highly crystalline and phase-pure; e.g. films that do not possess residual impurities such as lead iodide. Thus, there remains a need for both better performing perovskite halide films, and solar cells made therefrom, but also improved manufacturing methods for making high performance perovskite halide films.

Summary

[0003] An aspect of the present invention is a "two-step" method of forming a perovskite film, where the method includes applying a solution onto a substrate, the solution containing at least two alkyl ammonium halides and a metal halide in a solvent. The method then includes thermally treating the solution, such that the treating removes substantially all of the solvent and at least a portion of at least one of the alkyl ammonium halides from the solution, and the remaining alkyl ammonium halides and the metal halide crystallize to form a final alkyl ammonium metal halide perovskite film on the substrate.

[0004] In some embodiments of the present invention, the solution may include two alkyl ammonium halides. The first alkyl ammonium halide may be an alkyl ammonium chloride and the second alkyl ammonium halide may be an alkyl ammonium iodide.

[0005] In some embodiments of the present invention, during the treating, an intermediate alkyl ammonium metal halide perovskite film may forms where the intermediate film may include at least two halogen elements, which then transform to the final perovskite film that includes at least one halogen element. In other embodiments, the intermediate perovskite film may include two halogen elements and the final perovskite film comprises one halogen element. In still further embodiments, the two halogen elements may be chlorine and iodine and the one halogen element may be iodine.

[0006] In some embodiments of the present invention, the intermediate perovskite film may incude at least one of a methyl ammonium metal iodide and a methyl ammonium metal chloride, or a methyl ammonium metal dihalide comprising iodide and chloride. In some embodiments of the present invention, the final perovskite film may be a methyl ammonium metal iodide.

[0007] In some embodiments of the present invention, the alkyl group for the at least two alkyl ammonium halides may be at least one of a methyl group, an ethyl group, a propyl group, or a butyl group. In some embodiments of the present invention, each of the at least two alkyl ammonium halides may have a halogen from at least one of fluorine, chlorine, bromine, iodine, or astatine, such that the halogen for each alkyl ammonium halide is different from the halogen of each of the remaining alkyl ammonium halides. In some embodiments, a first alkyl ammonium halide may be alkyl ammonium chloride with a second alkyl ammonium halide with a halogen selected from bromine, iodine, or astatine.

[0008] In some embodiments of the present invention, a metal of the metal halide may be at least one of lead, tin, germanium, or any other metal in the 2+ valence state. In some embodiments of the present invention, the solvent may be at least one polar solvent. In still further embodiments of the present invention, the solvent may be at least one of dimethysulfoxide, dimethylformamide, γ-butyrolactone, or N-methyl-2-pyrrolidone.

[0009] In some embodiments of the present invention, the metal halide and the alkyl ammonium iodide may be present in the solution at a molar ratio of about one to one (1:1). In still further embodiments, the alkyl ammonium iodide and the alkyl ammonium chloride may be present in the solution at a molar ratio ranging from about 1:0.1 to about 1:4. In still further embodiments, at least one of the alkyl ammonium halides, or the metal halide may be present in the solution at a concentration ranging from about 0.1 M to about 3.0 M.

[0010] In some embodiments of the present invention, the thermally treating may include heating the solution at a temperature ranging from about 20°C to about 250°C. In some further embodiments of the present invention, the thermally treating comprises heating the solution for a period of time ranging from about 30 seconds to about 6 hours.

[0011] A further aspect of the present invention is a "three-step" method of forming a perovskite film, where the method includes applying a first solution onto a substrate, the first solution containing in a first solvent, a first alkyl ammonium halide with a first halogen, and a metal halide with a second halogen different from the first halogen. The method then includes completing a first thermal treatment of the first solution to form a first film of the metal halide on the substrate, followed by contacting a second solution with the first film, the second solution containing in a second solvent, a second alkyl ammonium halide with the second halogen, such that the second alkyl ammonium halide reacts with the first film to form a final crystalline alkyl ammonium metal halide perovskite film that is substantially free of the first film and the first halogen.

[0012] In some embodiments of the present invention, the "three-step" method may further include, during at least a portion of the contacting, completing a second thermal treatment of the second solution and the first film. In some embodiments of the present invention, the first thermal treatment may form an unstable intermediate film that may include the metal halide and an alkyl ammonium metal halide with the first halogen, such that the intermediate film subsequently changes to form the first metal halide film.

[0013] In some embodiments of the present invention, the first halogen and the second halogen may include fluorine, chlorine, bromine, iodine, or astatine. In other embodiments, the first halogen may have a lower molecular weight than the second halogen. In still further embodiments, the first halogen is chlorine and the second halogen is iodine.

[0014] In some embodiments of the present invention, an alkyl group for at least one of the first alkyl ammonium halide or the second alkyl ammonium halide may include at least one of a methyl group, an ethyl group, a propyl group, or a butyl group. In some embodiments of the present invention, a metal of the metal halide may include at least one of lead, tin, germanium, or any other metal in the 2+ valence state.

[0015] In some embodiments of the present invention, the first solvent may include at least one polar solvent. In some further embodiments, the second solvent comprises isopropyl alcohol.

[0016] In some embodiments of the present invention, the metal halide and the first alkyl ammonium halide may be present in the first solution at a molar ratio ranging from about 1:0.1 to about 1:3. In some further embodiments, at least one of the metal halide and the first alkyl ammonium halide may be present in the first solution at a concentration ranging from about 0.1 M to about 3.0 M. In still further embodiments, the second alkyl ammonium halide may be present in the second solution at a concentration ranging from 0.1 mg/ml solvent to about 100 mg/ml solvent.

[0017] In some embodiments of the present invention, at least one of the thermal treatments may include heating at least one of the solutions at a temperature ranging from about 40°C to about 250°C. In further embodiments, at least one of the thermal treatments may include heating at least one of the solutions for a period of time ranging from about 30 seconds to about 6 hours.

[0018] A further aspect of the present invention is a method for manufacturing a solar cell, the method including in order, forming a perovskite film on a substrate by any one of the methods described herein, depositing a hole-transport layer on the perovskite film, depositing a molybdenum oxide layer on the hole-transport layer, and depositing an aluminum layer on the molybdenum oxide layer.

[0019] A further aspect of the present invention is a solar cell include in order, transparent conducting oxide substrate, an electron-transport layer on the transparent conducting oxide substrate, a perovskite halide film on the electron-collecting layer, a hole-transport layer on the perovskite halide film, a molybdenum oxide layer on the hole-transport layer, and an aluminum layer on the molybdenum oxide layer.

[0020] In some embodiments of the present invention, the electron-transport layer may be titanium oxide. In further embodiments of the present invention, the hole-transport layer may be spiro-OMeTAD.

Brief Description of the Drawings

[0021]

Figure 1 illustrates alkyl ammonium metal halide perovskite crystal structure, according to exemplary embodiments of the present invention.

Figure 2 illustrates a solar cell constructed with a perovskite halide film and molybdenum oxide/aluminum top contact, according to exemplary embodiments of the present invention.

Figure 3 illustrates a schematic of a "one-step" method for making a methyl ammonium lead iodide perovskite, according to exemplary embodiments of the present invention.

Figure 4 illustrates a schematic of a "one-step" method for making a methyl ammonium lead iodide bromide perovskite, according to exemplary embodiments of the present invention.

Figure 5 illustrates a schematic of a "three-step" method for making an alkyl ammonium metal halide perovskite, according to exemplary embodiments of the present invention.

Figure 6 provides images of the perovskite films prepared from $CH_3NH_3PbI_3$ precursors with different amounts of CH_3NH_3Cl and annealed at 100°C with varying duration.

Figures 7a-d are UV-vis absorption spectra of perovskite $CH_3NH_3PbI_3$ on mesoporous TiO_2 films as a function of annealing time at 100°C using precursors containing (a) 0 methyl ammonium chloride ("MACl"), (b) 0.5 MACl, (c) 1 MACl, and (d) 2 MACl.

Figures 8a-c depict (a) XRD patterns of $CH_3NH_3PbI_3$ on mesoporous TiO_2 film as a function of the MAC1 amount in the precursors for different annealing times at 100°C; magnified views of the XRD patterns (b) near 14 degrees for perovskite films using 0-2 MACl with their respective optimum annealing time; and magnified views of the XRD patterns (c) for the 2-MACl sample with different annealing time (1-45 min).

Figures 9a-h are typical SEM images of perovskite $CH_3NH_3PbI_3$ grown on (a-d) mesoporous TiO_2 film and (e-h) planar TiO_2 compact layer with different MAC1 amount (a, e: 0; b, f: 0.5; c, g: 1; d, h: 2).

Figures 10a-b are graphs showing the effect of MACl on the *J-V* curves of (a) mesostructured and (b) planar perovskite $CH_3NH_3PbI_3$ solar cells.

Figures 11a-b are graphs showing the effect of MACl on the recombination resistance (R_{rec}) as a function of voltage for (a) mesostructured and (b) planar perovskite $CH_3NH_3PbI_3$ solar cells.

Figures 12a-b are dark *J-V* curves of (a) mesostructured and (b) planar perovskite solar cells as a function of added amount of MACl in the precursor solution for growing $CH_3NH_3PbI_3$.

Figure 13 is a graph showing the effect of annealing time (at 100°C) on the XRD patterns of perovskite films prepared from precursor containing equimolar PbI_2 and MACl. In addition to the main perovskite (110) peak near 14 degrees, two new peaks appear at about 12.6 (denoted by pound) and 15.5 degrees (denoted by asterisk).

Figures 14a-b are graphs displaying the effect of MACl on (a) electron diffusion coefficient as a function of photoelectron density and (b) recombination lifetime as function of voltage in mesostructured perovskite $CH_3NH_3PbI_3$ solar cells.

Figure 15 is a graph displaying UV-vis absorption spectra of perovskite film as a function of annealing time at 100°C using a precursor containing equimolar mixture of MACl and PbI_2.

Figures 16a-c are (a) SEM image, (b) XRD patterns, and (c) EDX analysis of the mixed halide $CH_3NH_3PbI_{3-x}Cl_x$ prepared from the precursor containing MAI and $PbCl_2$ (3:1 molar ratio).

Figure 17 is a graph showing recombination resistance R_{rec} as a function of voltage for a planar perovskite solar cell based on the mixed halide $CH_3NH_3PbI_{3-x}Cl_x$ prepared from the precursor containing MAI and $PbCl_2$ (3:1 molar ratio).

Figure 18 is a *J-V* curve of a planar perovskite solar cell based on the mixed halide $CH_3NH_3PbI_{3-x}Cl_x$ prepared from the precursor containing MAI and $PbCl_2$ (3:1 molar ratio). The cell efficiency is 11.86% with a J_{sc} of 20.57 mA/cm^2, V_{oc} of 0.995 V, and FF of 0.579.

Figures 19a-c are Typical SEM images of $MAPbI_2Br$ films deposited on c-TiO_2/FTO substrates from various precursor solutions; (a) PbI_2+MABr; (b) PbI_2+MABr+MACl; and (c) PbI_2+MABr+2MACl.

Figures 20a-c are graphs showing the effect of annealing time (as indicated) at 125°C on the XRD patterns of $MAPbI_2Br$ films deposited on c-TiO_2/FTO substrate from various precursor solutions: (a) PbI_2+MABr; (b) PbI_2+MABr+MACl; and (c) PbI_2+MABr+2MACl.

Figure 21 is a graph showing the photocurrent density-photovoltage (J-V) curves of perovskite solar cells prepared from different precursor compositions (i.e., PbI_2+MABr or 0 MACl; PbI_2+MABr+MACl or 1 MACl; and PbI_2+MABr+2MACl or 2MAC1).

Figures 22a-b are graphs showing the effect of the dipping time in the 10 mg MAI/mL IPA solution on the evolution of (a) XRD patterns and (b) UV-vis absorption spectra for the perovskite films deposited from 1.0 M PbI2 precursor on mesoporous TiO_2 film.

Figures 23a-b are graphs showing the effect of PbI_2 concentration (0.4-1.0 M) on the (a) XRD patterns and (b) UV-vis absorption spectra of the perovskite films deposited on mesoporous TiO_2 film after dipping in 10 mg MAI/mL IPA solution for 10 min.

Figures 24a-b are graphs showing (a) UV-vis absorption spectra and (b) XRD patterns of the films in each of the three production steps: (1) initial film formation from precursor of mixed PbI_2 and MACl; (2) thermally decomposed PbI_2 film from the second step; (3) final $CH_3NH_3PbI_3$ formed after dipping in MAI solution after the third step.

Figure 25 is a curve showing the *J-V* characteristic of a perovskite solar cell based on the CH3NH3Pbb film prepared from the three-step approach.

Figures 26a-d are (a) UV-vis absorption spectra and (b) XRD patterns of $CH_3NH_3PbI_3$ films grown via the standard two-step sequential solution deposition using pure PbI_2 precursor film with different MAI solution dipping times. SEM images of (c) the typical spin-coated PbI_2 film and (d) the converted $CH_3NH_3PbI_3$ film with 20-min dipping (reaction) time in MAI solution are also depicted.

Figure 27 depicts typical *J-V* curves of planar $CH_3NH_3PbI_3$ solar cells prepared from PbI_2 precursor films with different MAI solution dipping time from 0.5 to 20 min.

Figures 28a-d are (a) UV-vis absorption spectra and (b) XRD patterns of PbI_2·xMAI films (with varying x values as indicted) before the second conversion step; (c) UV-vis absorption spectra of CH3NH3PbI3 films prepared from PbI_2·xMAI films after the second conversion step; (d) evolution of UV-vis absorption spectra using the PbI_2·0.15MAI precursor film with different dipping times in the MAI solution.

Figure 29 is a graph showing XRD patterns of $PbI_2 \cdot xMAI$ (x: 0.1-0.3) films after dipping in MAI solution for 1-3 min.

Figures 30a-h are typical SEM images of $PbI_2 \cdot xMAI$ (x = 0.1, 0.15, 0.2, and 0.3) precursor films (a-d) and $CH_3NH_3PbI_3$ films prepared from their respective precursor films as indicated (e-h).

Figures 31a-b are (a) a schematic illustration of the crystal phase transformation from PbI_2 to $CH_3NH_3PbI_3$ in the standard two-step sequential deposition process and (b) a plot of the film thickness (or volume) expansion ratios of converting $PbI_2 \cdot xMAI$ to $CH_3NH_3PbI_3$ films as a function of the relative amount *x* MAI used. The solid line is the best fit as discussed in the Detailed Description.

Figure 32 is a graph showing the typical *J-V* curves of planar $CH_3NH_3PbI_3$ solar cells prepared from $PbI_2 \cdot xMAI$ precursor films.

Figure 33 shows plots of recombination resistance R_{rec} as a function of voltage for solar cells prepared with different $PbI_2 \cdot xMAI$ precursor compositions (*x*: 0-0.3).

Figures 34a-b are (a) the *J-V* curve of a planar $CH_3NH_3PbI_3$ solar cell prepared from $PbI_2 \cdot 0.15MAI$ precursor with the highest efficiency of 16.76% (J_{sc}=20.86 mA/cm^2, V_{oc}=1.09 V, FF=0.737) under simulated one-sun illumination; and (b) the stability of power conversion efficiency as a function of time for the same cell in (a) under simulated one-sun illumination.

Figures 35a-c are the sequence (a) to (c) of the color change of a $(CH_3NH_3)PbI_3$ film (deposited on a mesoporous TiO_2 film on FTO) passing through the top opening of a 3% NH_3 solution bottle.

Figure 36a-b are (a) UV-vis absorption spectra of a $(CH_3NH_3)PbI_3$ film in the absence and in the presence of NH_3 gas; and (b) the photoresponse (transmitted light intensity) of a $(CH_3NH_3)PbI_3$ film at 660 nm as measured by a silicon detector in response to the introduction (on) and removal (off) of NH_3 gas.

Figure 37 depicts XRD patterns of the TiO_2/FTO substrate (black line), a PbI_2 film on TiO_2/FTO, a $(CH_3NH_3)PbI_3$ film on TiO_2/FTO, and the NH_3-treated $(CH_3NH_3)PbI_3$ film on TiO_2/FTO. The asterisks denote the characteristic XRD peaks for $(CH_3NH_3)PbI_3$.

Figure 38 depicts XRD patterns and UV-vis absorption spectra of perovskite $CH_3NH_3PbI_3$ deposited on a compact TiO_2 layer on the FTO substrate.

Figures 39a-b illustrate (a) typical cross-sectional SEM image of a planar FTO/TiO_2/$CH_3NH_3PbI_3$/spiro-MeOTAD/MoO_x/Metal (Ag or Al) solar cell; and (b) the effect of MoO_x interlayer thickness on the *J-V* characteristics of perovskite $CH_3NH_3PbI_3$ solar cells using Ag top contact.

Figures 40a-b are a comparison of (a) *J-V* characteristics and (b) IPCE of perovskite $CH_3NH_3PbI_3$ solar cells using different top-contact structures as indicated.

Figures 41a-b are (a) typical Nyquist plots of the impedance responses (Z) for a planar perovskite cell (using HTM/10-nm MoO_x/Ag) with three different bias voltages; and (b) a comparison of recombination resistance (R_{rec}) as a function of voltage for planar perovskite solar cells using different top-contact structures.

Figure 42 shows the pictures of the perovskite solar cells after 15 hour continuous light soaking under simulated one sun illumination.

Figure 43 shows the dependence of solar cell efficiencies as a function of continuous light soaking under simulated one sun illumination for 15 hours.

Detailed Description

[0022] Figure 1 illustrates that perovskites halides may organize into cubic crystalline structures and may be described by the general formula ABX_3, where X (130) is an anion and A (110) and B (120) are cations, typically of different sizes (A typically larger than B). In a cubic unit cell, the B-cation 120 resides at the eight corners of a cube, while the A-cation 110 is located at the center of the cube and is surrounded by 6 X-anions 130 (located at the face centers) in an octahedral $[MX_6]^{4-}$ cluster (unit structure). Typical inorganic perovskites include calcium titanium oxide (calcium titanate) minerals such as, for example, $CaTiO_3$ and $SrTiO_3$. In some embodiments of the present invention, the cation A(110) may include a nitrogen-containing organic compound such as an alkyl ammonium compound. Cation (120) may include a metal and anion B (120) may include a halogen.

[0023] Additional examples for cation A (110) include organic cations and/or inorganic cations. Organic cations of A (110) may be an alkyl ammonium cation, for example a C_{1-20} alkyl ammonium cation, a C_{1-6} alkyl ammonium cation, a C_{2-6} alkyl ammonium cation, a C_{1-5} alkyl ammonium cation, a C_{1-4} alkyl ammonium cation, a C_{1-3} alkyl ammonium cation, a C_{1-2} alkyl ammonium cation, and/or a C_1 alkyl ammonium cation. Further examples of organic cations of A (110) include methylammonium (CH_3NH^{3+}), ethylammonium ($CH_3CH_2NH^{3+}$), propylammonium (CH_3CH_2 CH_2NH^{3+}), butylammonium (CH_3CH_2 CH_2 CH_2NH^{3+}), formamidinium ($NH_2CH{=}NH^{2+}$), and/or any other suitable nitrogen-containing organic compound. In other examples, a cation A (110) may include an alkylamine. Thus, a cation A (110) may include an organic component with one or more amine groups. For example, cation A (110) may be an alkyl diamine halide such as formamidinium ($CH(NH_2)_2$).

[0024] Examples of metal cations 120 include, for example, lead, tin, germanium, and or any other 2+ valence state metal that can charge-balance the perovskite halide 100. Examples for the anion X (130) include halogens: e.g fluorine, chlorine, bromine, iodine and/or astatine. In some cases, the perovskite halide may include more than one anion X (130), for example pairs of halogens; chlorine and iodine, bromine and iodine, and/or any other suitable pairing of halogens. In other cases, the perovskite halide 100 may include two or more halogens of fluorine, chlorine, bromine, iodine, and/or astatine.

[0025] Thus, cation A (110), cation B (120), and anion X (130) may be selected within the general formula of ABX_3 to produce a wide variety of perovskite halides 100, including, for example, methylammonium lead triiodide ($CH_3NH_3PbI_3$), and mixed halide perovskites such as $CH_3NH_3PbI_{3-x}Cl_x$ and $CH_3NH_3PbI_{3-x}Br_x$. Thus, a perovskite halide 100 may have more than one halogen element, where the various halogen elements are present in none integer quantities; e.g. x is not equal to 1, 2, or 3. In addition, perovskite halides, like other organic-inorganic perovskites, can form three-dimensional (3-D), two-dimensional (2-D), one-dimensional (1-D) or zero-dimensional (0-D) networks, possessing the same unit structure.

[0026] As stated above, the anion A (110) may include an organic constituent in combination with a nitrogen constituent. In some cases, the organic constituent may be an alkyl group such as straight-chain or branched saturated hydrocarbon group having from 1 to 20 carbon atoms. In some embodiments, an alkyl group may have from 1 to 6 carbon atoms. Examples of alkyl groups include methyl (C_1), ethyl (C_2), n-propyl (C_3), isopropyl (C_3), n-butyl (C_4), tert-butyl (C_4), sec-butyl (C_4), iso-butyl (C_4), n-pentyl (C_5), 3-pentanyl (C_5), amyl (C_5), neopentyl (C_5), 3-methyl-2-butanyl (C_5), tertiary amyl (C_5), and n-hexyl (C_6). Additional examples of alkyl groups include n-heptyl (C_7), n-octyl (Cs) and the like.

[0027] Figure 2 illustrates a solar cell 200 constructed with a perovskite halide absorbing layer 240. In this example, the perovskite halide absorbing layer 240 is positioned between an electron-transport layer 250 and a hole-transport layer 230. In some cases, the electron-transport layer 250 may be constructed from titanium dioxide and the hole-transport layer 230 may be constructed from Spiro-OMeTAD (2,2',7,7'-tetrakis-(*N,N*-di-*p*-methoxyphenyl-amine)-9,9'-spirobifluorene). In addition, Figure 2 illustrates that the solar cell 200 has a bottom contact layer 260 positioned on a transparent substrate 270. The bottom contact layer 260 may be any suitable transparent conducting oxide layer, for example fluorine-doped tin oxide. The transparent substrate 270 may be glass or any other suitable material. Figure 2 also illustrates that the solar cell 200 may include a top contact constructed from a layer of molybdenum oxide 220 and aluminum 210. Embodiments of the present invention similar to that shown in Figure 2 have demonstrated superior results, especially regarding performance stability over time.

[0028] In some embodiments of the device summarized in Figure 2, a solar cell utilizing a molybdenum oxide/aluminum (i.e., MoO_x/Al) top contact with a CH3NH3PbI3 absorber layer demonstrated an efficiency of about 11.4%. The molybdenum oxide/aluminum may replace noble/precious metals (e.g., Au or Ag) as a top contact for extracting photogenerated holes. As described in detail herein, the device performance of perovskite solar cells using a MoO_x/Al top contact may be comparable to that of cells using the silver as the standard top contact. In addition, analysis of impedance spectroscopy measurements suggests that using a thin (e.g., 10-nm thick) MoO_x/Al top contact does not appear to affect charge-recombination properties of perovskite solar cells.

[0029] Figure 3 illustrates a method 300 of making perovskite halide films. The method may begin at 310 with preparing a solution that may include a solvent, a metal halide, and at least two alkyl ammonium halides. For example, the solvent may be dimethylformamide (DMF), the metal halide may be lead iodide (PbI_2) and the two alkyl ammonium halides may be methyl ammonium iodide (MAI - CH_3NH_3I) and methyl ammonium chloride (MACl - CH_3NH_3Cl).

[0030] Once the solution is prepared, it may be deposited or applied 320 to a suitable substrate; e.g. a titanium oxide surface on a transparent conducting oxide layer. The depositing 320 may be accomplished by any suitable means, for example, spin coating, dip coating, curtain coating, etc. In the process of depositing 320, at least a portion of the solvent may be removed from the solution. The depositing 320 may be followed by thermal treatment 330. Thermal treatment 330 may include heating the solution to at least one specified target temperature, resulting in the removal of any remaining solvent and at least one of the alkyl ammonium halides. In some cases the thermal treatment 330 may include a temperature ramp, such that the solution is heated over a specified range of temperature over a specified period of time. Alternatively, the solution may be allowed "dry" in ambient conditions, for example, at room temperature. For example, referring again to Figure 3, a solution of DMF, lead iodide, MAI, and MACl may be heated to about 100°C where the solution is maintained at that temperature for about 30 minutes, resulting in the removal of substantially all of the DMF and substantially all of the MAC1, resulting in the formation 340 of the target perovskite halide film on the substrate; methyl ammonium lead halide perovskite ($CH_3NH_3PbI_3$).

[0031] In some cases the thermal treatment step 330 may remove substantially all of the solvent. However, in other cases small amounts of solvent may remain in the final target perovskite film. In addition,

[0032] However, the methods described herein need not be limited to producing halide perovskites containing only one halogen element. Figure 4 illustrates another example of the present invention, a method 400 that may produce a perovskite dihalide (e.g. containing two halogen elements). In this example, the method may begin with preparing 410 a solution containing a metal halide and two alkyl ammonium halides in a solvent (e.g. DMF), where each of these three compounds contain a different halogen. For example, the metal halide may be lead iodide, the first alkyl ammonium halide may be methyl ammonium bromide (MABr), and the second alkyl ammonium halide may be MACl. Once the solution preparation 410 is completed, it may be applied 420 to a suitable substrate (e.g. spin coating). After applying 420, the solution may then be thermally treated 430 to form 440 the final perovskite halide film on the substrate. Referring again to Figure 4, the final perovskite halide film may be methyl ammonium lead di-iodide bromide ($CH_3NH_3PbI_2Br$).

[0033] As will be demonstrated later in this disclosure, the methods summarized in Figures 3 and 4 may provide significantly improved final perovskite halide films, and better performing solar cells that incorporate these films. Referring again to the example illustrated in Figure 3, referred to herein as a "one-step" method, the solution may begin with an equimolar mixture of MAI and PbI_2 in the solvent. The use of the second alkyl ammonium halide, the MAC1, strongly affects the crystallization process during the thermal treatment step 330 leading to the formation 340 of the final $CH_3NH_3PbI_3$ film. The final $CH_3NH_3PbI_3$ film made by this method demonstrates enhanced absorption of light and significantly improved coverage of the $CH_3NH_3PbI_3$ film on its substrate. This method has been shown to provide measurable improvement relative to some of the standard one-step solution methods used to manufacture $CH_3NH_3PbI_3$ films. For example, usage of MACl as the second alkyl ammonium halide has shown solar cells performance improvement from about 2% to 12% for a planar cell structure and from about 8% to 10% for a mesostructured device architecture, relative to one-step methods utilizing only one alkyl ammonium halide (MAI).

[0034] Figure 5 illustrates another exemplary method 500 for forming final perovskite halide films, according to some embodiments of the present invention. This method 500 may begin with preparing 510 a first solution containing a metal halide and an alkyl ammonium halide in a first solvent, where the metal halide and the alkyl ammonium halide contain different halogens. Once the first solution is prepared, it may be applied 520 to a substrate. The applying step 520 may be by spin coating, dip coating, curtain coating, and/or any other suitable solution technique. For the case of spin coating, the applying step 520 may remove some or substantially all of the first solvent. Once applied, the solution may be thermally treated 530. The thermal treatment step 530 may include heating the solution to a final target temperature and then maintaining the solution at that target temperature for a defined period of time. In some cases the thermal treatment 530 may include a temperature ramp, such that the solution is heated over a specified range of temperature over a specified period of time. Alternatively, the solution may be allowed "dry" in ambient conditions, for example, at room temperature. The thermal treatment step 530 will cause the formation of an intermediate film that includes the metal halide and the alkyl ammonium halide. However, this intermediate film is only a transitory film. Eventually the thermal treating 530 removes substantially all of the alkyl ammonium halide and transforms 540 the intermediate film into a porous metal halide film. In some cases there may be significant residual alkyl ammonium halide (e.g., MAI, MAC1, or MABr) in the porous (or compact) metal halide film. Next, the metal halide film may be contacted 550 with a second solution. This second solution may include a second alkyl ammonium halide, different from the first, in a second solvent, which may be different from the first solvent. In some cases, the contacting step 550 will transform 560 the metal halide film into the final target perovskite halide film. In other cases, the contacting step 550 may also include thermally treating the second solution, by heating the solution above ambient and/or room temperature.

[0035] Referring again to Figure 5, the specific method 500 example shown, begins with preparing 510 a first solution of lead iodide and MACl in DMF solvent. The first solution is then applied 520 to a substrate by spin-coating the solution onto a substrate (e.g. titanium dioxide on a transparent conducting oxide film). After the first solution has been applied 520 to the substrate, the solution is then thermally treated 530 by heating the solution to about 130°C and maintaining that temperature for about 30 minutes. The thermal treatment step 540 results in the temporary formation of an intermediate film of PbI_2*MACl, which then degrades/decomposes/transforms 540 to a porous lead iodide film that is substantially free of solvent and MACl. The lead iodide film is then brought into contact 550 with a second solution prepared from a MAI in a second solvent, in this case isopropyl alcohol (IPA). In this case, the contacting step 550 is for 30 seconds at room temperature. However, in other embodiments, the contacting step 550 may be for longer or shorter periods of time at temperatures above room temperature (e.g. up to 250°C).

[0036] In general the second solvent should have a lower solubility for the final target perovskite film than the solubility of the first solvent for the final target perovskite film. IPA is one example, however, other common alcohol-containing solvents may also be used; e.g. butyl alcohol.

[0037] In some cases the thermal treatment step 530 may remove substantially all of the first solvent. However, in other cases small amounts of the first solvent may remain in the porous metal halide film. Similarly, in some cases the contacting step 550 may remove substantially all of the second solvent. However, in other cases small amounts of the second solvent may remain in the final target perovskite film.

[0038] The method illustrated in Figure 5 is referred to herein as a "three-step" method. In summary, the three-step method may be characterized by the formation of a transitory and thermally unstable stoichiometric precursor film of an PbI_2·alkyl ammonium halide film (e.g. deposited onto a mesoporous TiO_2 substrate), which then during thermal treatment 530 transforms to a porous PbI_2 film. In some cases (e.g., "drying" at room temperature) there may be significant residual alkyl ammonium halide in the PbI_2 film. Then, during a second contacting step 550, the PbI_2 film is converted into $CH_3NH_3PbI_3$ by contacting the PbI_2 film with a solvent solution (e.g. IPA) of CH_3NH_3I. Thus, embodiments of the three-step method shown in Figure 5, enable the formation of metal halide film, through the thermal decomposition of the metal halide·alkyl ammonium halide precursor film. This transition from a transitory intermediate film to a lead halide film enables the rapid conversion of metal halide film to the final target perovskite halide film, without any residual metal halide in the final target perovskite film, which results in improved device performance (e.g. solar cell).

EXAMPLES

[0039] The following examples are included to demonstrate certain embodiments of the present disclosure. It should be appreciated by those of skill in the art that the techniques disclosed in the examples which follow represent techniques discovered by the inventors to function well in the practice of the subject matter of the present disclosure, and thus can be considered to constitute modes for its practice. However, those of skill in the art should, in light of the present disclosure, appreciate that many changes can be made to the specific embodiments disclosed herein and still obtain a like or similar result without departing from the spirit and scope of the subject matter of the present disclosure.

EXAMPLE 1: ONE STEP METHOD

[0040] Disclosed herein is a one-step solution method for preparing perovskite $CH_3NH_3PbI_3$ films. The disclosed one-step solution method includes introducing a second alkyl ammonium halide, MAC1, to an equimolar mixture of a first alkyl ammonium halide, MAI, and a metal halide, lead iodide, in solution-to prepare perovskite $CH_3NH_3PbI_3$ on a substrate. Examples of substrates that may be used include mesoporous and planar TiO_2 substrates. Optical and structural characterizations show that the use of one or more alkyl ammonium halides adjusts the crystallization process for forming $CH_3NH_3PbI_3$. Depending on the amount of alkyl ammonium halides in the precursor solution, the crystallization process may take in a time period ranging from a few minutes to several tens of minutes. Using two or more alkyl ammonium halides not only improves absorption of $CH_3NH_3PbI_3$ but also enhances the $CH_3NH_3PbI_3$ coverage on planar substrates, leading to significant improvement of device performance. In this Example, methyl ammonium chloride (MAC1) was used as a second alkyl ammonium halide and was mixed into a solvent solution containing MAI and PbI_2)), to generate final target perovskite halide films of $CH_3NH_3PbI_3$. Charge transport and recombination properties were examined by intensity-modulated photocurrent/photovoltage spectroscopies (IMPS/IMVS) and impedance spectroscopy (IS).

Experimental Setup and Device Fabrication

[0041] Transparent conducting substrate and mesoporous TiO_2 films were fabricated. Initially, fluorine-doped transparent conducting SnO_2-coated glass substrate was pre-patterned by etching with Zn powder and -25 wt% HCl solution for about 2 minutes. The patterned FTO substrate was then cleaned by soaking in ~5 wt% NaOH in alcohol for ~16 hours and then rinsing it sequentially with deionized (DI) water and ethanol. The cleaned FTO substrate was subsequently coated with a compact TiO_2 layer by spray pyrolysis using 0.2 M Ti(IV) bis(ethyl acetoacetate)-diisopropoxide in 1-butanol solution at ~450°C, followed by annealing at ~450°C for about one hour. The 20-nm-sized TiO_2 nanoparticles were synthesized utilizing standard methods known in the field. The TiO_2 paste, together with~ 6 wt% of the 20-nm TiO_2 nanoparticles were mixed with terpineol and ethyl cellulose, and then screen-printed with 3-μm emulsion thickness on the patterned FTO substrates. The printed mesoporous TiO_2 film was annealed at ~500°C for about 0.5 hours. The average film thickness was determined by an Alpha-Step 500 surface profiler. The TiO_2 films were then soaked in ~0.04 M $TiCl_4$ solution at ~65°C for about 30 minutes, followed by rinsing with DI water and ethanol, and finally dried under N_2. The $TiCl_4$-treated TiO_2 films (for mesostructured cells) and compact TiO_2 films (for planar devices) on patterned FTO were annealed again at ~500°C for ~30 minutes before the $CH_3NH_3PbI_3$ perovskite films were deposited on these substrates.

[0042] In connection with device fabrication steps, CH_3NH_3I (MAI) was synthesized by reacting methylamine (33 wt% ethanol solution) and hydroiodic acid (57 wt% in water, Aldrich) with the molar ratio of 1.2:1 in an ice bath for 2 h with stirring followed by vacuum drying and cleaning with ethyl acetate. CH_3NH_3Cl (MACl) was synthesized by reacting methylamine (33 wt% ethanol solution) and 33 wt% hydrocholoride acid with the molar ratio of 1.2:1 in an ice bath for 2 h with stirring followed by vacuum drying and cleaning with acetonitrile. Four different $CH_3NH_3PbI_3$ precursor solutions were prepared by dissolving 0.693 g PbI_2 (1.5 mmol); 0.239 g MAI (1.5 mmol); and 0 g, 0.050 g (0.75 mmol), 0.100 g (1.5 mmol), or 0.200 g (3 mmol) MACl in 2.75 g dimethylformamide (DMF) at room temperature-noted as 0 molar (M) MACl, 0.5 M MACl, 1 M MACl, and 2 M MACl, respectively. Devices were fabricated in ambient condition (unless stated otherwise) as detailed below. The perovskite $CH_3NH_3PbI_3$ precursor solutions were spin-coated onto (1) 650-nm-thick TiO_2 mesoporous films on FTO at 3,000 rpm for ~30 seconds for mesostructured cells, and (2) compact TiO_2 films on FTO at 2,500 rpm for -10 seconds. The perovskite-coated films were then annealed on a hotplate at ~100°C for periods of time ranging from about 5 minutes to about 45 minutes. For both mesostructured and planar perovskite solar cells, a hole-transport material (HTM) solution was spin-coated on the perovskite-covered TiO_2 electrodes at 4,000 rpm for

~30 seconds. The HTM solution consisted of 0.1 M 2,2',7,7'-tetrakis-(*N,N*-di-*p*-methoxyphenyl-amine)-9,9'-spirobifluorene (spiro-MeOTAD), 0.035 M bis(trifluoromethane)sulfonimide lithium salt (Li-TFSi), and 0.12 M 4-*tert*-butylpyridine (tBP) in chlorobenzene/acetonitrile (10:1, v/v) solution. Finally, a 150-nm-thick Ag layer was deposited on the HTM layer by thermal evaporation. The active area of each device was about 0.15-0.28 cm^2.

[0043] In connection with characterizing the fabricated structures, the crystal structures of the perovskite films were measured by X-ray diffraction (XRD, Rigaku D/Max 2200 diffractometer with Cu K_α radiation). The absorption spectra of the mesoporous and planar perovskite films were characterized by a UV/Vis-NIR spectrophotometer (Cary-6000i). The photocurrent-voltage (*J-V*) characteristic of perovskite $CH_3NH_3PbI_3$ solar cells were measured with a Keithley 2400 source meter under the simulated AM 1.5G illumination (100 mW/cm^2; Oriel Sol3A Class AAA Solar Simulator), from open circuit to short circuit with a scan rate of 0.2 V/s. *J-V* hysteresis was observed when scanned from short circuit to open circuit, especially for planar devices. Charge transport and recombination properties of the mesostructured perovskite cells were measured by intensity-modulated photocurrent and photovoltage spectroscopies. Impedance spectroscopy (IS) was performed using a PARSTAT 2273 workstation with the frequency range of 0.1 Hz-100 kHz and the modulation amplitude of 10 mV. The IS spectra were analyzed using ZView 2.9c software (Scribner Associates).

Results and Discussion

[0044] Figure 6 shows perovskite films prepared from $CH_3NH_3PbI_3$ precursors with different amounts of CH_3NH_3Cl (or MACl; as indicated) and annealed at about 100°C with varying duration (as indicated). Figure 6 shows the effect of varying annealing time (from about 1 minute to about 45 minutes) at about 100°C on the appearance of perovskite $CH_3NH_3PbI_3$ films prepared by using the perovskite precursors with different amounts of added CH_3NH_3Cl (MAC1). The perovskite precursor solution contained PbI_2, CH_3NH_3I (or MAI), and MACl with a molar ratio of 1:1:*x*, where *x* varied from 0 to 2. The thickness of the mesoporous TiO_2 film was about 650 nm. When no MACl was used, the perovskite film turned brown within one minute of annealing at 100°C. The absorbance of this film stayed virtually unchanged at 5 minutes and then decreases when annealed for 10 minutes (Figure 7a). With an increasing amount of MACl added to the precursor solution, the process that turned the perovskite film brown/dark brown with annealing occurred at significantly slower rates. When 2 M MACl was used, it took more than 25 minutes for the perovskite film to turn brown. The annealing-time-dependent absorption spectra for these perovskite films prepared using different amounts of MACl are shown in Figures 7a-d. Adding MACl to the precursor solution not only slowed down the perovskite film darkening process but also darkened the color the final perovskite films (the color of the final perovskite film changed from brown with no MACl to dark brown with 1-2 MACl; Figure 6).

[0045] Figures 8a-c depict (a) XRD patterns of $CH_3NH_3PbI_3$ on mesoporous TiO_2 film as a function of the MACl amount in the precursors for different annealing time at about 100°C; magnified views of the XRD patterns (b) near 14 degrees for perovskite films using 0-2 M MACl with their respective optimum annealing time; and magnified views of the XRD patterns (c) for the 2 M MACl sample with different annealing times (from about 1 minute to about 45 minutes). Peaks associated with the perovskite $CH_3NH_3PbI_3$ structure are labeled. The other peaks are either from the TiO_2/FTO substrate or from a transient intermediate structure related to MACl.

[0046] Figure 8a compares the X-ray diffraction (XRD) patterns of $CH_3NH_3PbI_3$ on mesoporous TiO_2 film prepared from precursor solutions containing different amounts of MACl. When the absorption spectrum reached about maximum for each amount of added MACl (about 5 minutes for 0 M MAC1, 10 minutes for 0.5 M MAC1, 25 minutes for 1M MAC1, and 45 minutes for 2 M MAC1), the perovskite samples showed the same XRD patterns for $CH_3NH_3PbI_3$. The strongest $CH_3NH_3PbI_3$ (110) peak near 14 degrees increased slightly in intensity and became narrower as the amount of MACl added to the precursor solution increases (Figure 8b). This suggests an increase in crystallinity or a change in the preferred orientation of the final target perovskites with higher MACl concentration, which, without wishing to be bound by theory, is presumably caused by a slower crystallization process at higher MACl concentration. The perovskite film using 2 M MACl displayed the longest time to complete a color change, and its XRD pattern, as a function of the annealing time (from about 1 minute to about 45 minutes) at ~100°C, are shown in Figure 8a. The main characteristic $CH_3NH_3PbI_3$ (110) peak near 14 degrees only appeared after about 25 minutes of thermal treatment. At the early stage of thermal treatment (from about 1 minute to about 10 minutes), several intermediate peaks were present (Figure 8c), which all disappeared after 45 minutes of thermal treatment. Table 1 shows the energy dispersive X-ray (EDX) analysis of the perovskite halide films prepared with the 2 M MACl solution, suggesting that a significant amount of chlorine is initially incorporated into the film with an I:Cl ratio of about 2.7:1.6. The amount of chloride detected in the perovskite film decreased rapidly from 1.6 to 0.1 during thermal treatment times ranging from about 1 minute to about 25 minutes. Longer annealing time (~45 minutes) led to a complete loss of chloride (within the EDX detection limit of 1%). The intermediate XRD peaks for the 2 M MACl samples with short annealing times (from about 1 minute to about 10 minutes) are associated with the incorporation of MACl or its variation, which sublimes from the film with longer annealing times. The significant structural change for the 2 M MACl sample based on XRD measurement is consistent with the changes of its absorption spectra as a function of annealing time (Figure 7d). Similar to the 2 M MACl sample, no chloride was observed for other samples using zero molar or the other lower amounts of MACl with sufficient annealing times (Table 1). These results suggest that adding MACl to the $CH_3NH_3PbI_3$ precursor solution forms an intermediate crystal structure related to MACl, which slows down the crystallization of $CH_3NH_3PbI_3$. The intermediate structure subsequently appears to disappear with prolonged annealing to finally yield the targeted final perovskite halide film; e.g. $CH_3NH_3PbI_3$.

Table 1

Effect of MACl Amount (*x*) and Annealing Time on the Pb:I:Cl Ratio of Perovskite Films.

x MACl (time)	Pb	I	Cl
2 (1 min)	1	2.7 (0.3[a])	1.6 (0.2)
2 (10 min)	1	2.6 (0.3)	0.6 (0.1)
2 (25 min)	1	2.8 (0.3)	0.1 (0.1)
2 (45 min)	1	2.9 (0.3)	-
1 (25 min)	1	3.0 (0.3)	-
0.5 (10 min)	1	3.0 (0.4)	-
0 (5 min)	1	2.9 (0.4)	-

[a] The errors of the element ratios are obtained based on the EDX detection limit of 1%.

[0047] Figures 9a-h show the typical scanning electron microscopy (SEM) images of top views of the annealed perovskite films prepared from precursor solutions with different amounts of MACl. Figures 9a-d correspond to the perovskite films deposited on mesoporous TiO_2 films (650-nm thickness) using from 0 M to 2 M MACl, respectively. When no MACl was used, some islands of sub-micron-sized $CH_3NH_3PbI_3$ were observed on the top surface of the mesoporous TiO_2 film. These islands either disappeared or became less visible when MACl was used. Despite the slight difference of the perovskite appearance on the top surface of TiO_2 films, the overall appearances of these four films were similar and adopted the structure of the underlying mesoporous TiO_2 films. In contrast, adding MACl to the precursor solution lead to dramatic changes of the morphology of the perovskite $CH_3NH_3PbI_3$ films deposited directly on compact TiO_2 on the fluorine-doped tin oxide (FTO) glass substrate. Figure 9e-h correspond to the perovskite films deposited on compact TiO_2 using from 0 M to 2 M MACl, respectively. When no MACl was used, large elongated crystal plates formed, with a significant portion of the substrate being exposed without $CH_3NH_3PbI_3$ coverage. When 0.5 M MACl was used, the large crystal plates partially disappeared and some small crystals started to form, leading to enhanced surface coverage by the perovskite halide films. When using more MACl (1 M and 2 M), the elongated large crystal plates totally disappeared and the substrate was coated with interconnected, relatively small crystals with a high surface coverage. These differences in the surface coverage of perovskite films on the planar substrate are likely to affect final device characteristics.

[0048] Figures 10a-b depict the effect of MACl on the *J-V* curves of (a) mesostructured and (b) planar perovskite $CH_3NH_3PbI_3$ solar cells. All devices used spiro-MeOTAD as a hole conductor and silver as a top contact. Figure 10a shows the effect of MACl on the current density-voltage (*J-V*) characteristics of mesostructured perovskite solar cells based on 650-nm-thick TiO_2 mesoporous films. The cell with 0 M MACl demonstrated a short-circuit photocurrent density (J_{sc}) of ~16.91 mA/cm^2, open-circuit voltage (V_{oc}) of ~0.835 V, and fill factor (FF) of ~0.583 to yield an efficiency (η) of ~8.23%. The cell efficiency increased to about 9% to 10% when using MACl (0.5 M to 2 M) to adjust the crystallization process of the perovskite halide; $CH_3NH_3PbI_3$. The efficiency improvement resulted mainly from the higher J_{sc} associated with stronger light absorption (Figure 7) due to the use of the MACl. When $CH_3NH_3PbI_3$ was deposited directly on the planar compact TiO_2, the device performance (Figure 10b) showed a similar trend with MACl compared to the mesostructured perovskite solar cells. The degree of performance improvement by MACl for planar devices was greater than the performance improvement for the mesostructured devices. The J_{sc} increased from about 6 mA/cm^2 to about 18 mA/cm^2 when the amount of MACl was changed from 0 M to 0.5 M. When 1 M to 2 M MACl was used, the J_{sc} increased to > 20 mA/cm^2. The V_{oc} increased from about 0.8 V for 0 M MACl to > 1 V for 0.5 M to 2 M MACl. The FF increased from about 0.41 to a range of 0.57-0.61 for the same changes in MACl concentrations. As a result, the overall efficiency was improved from about 2% (0 M MACl) to ~11% (0.5 M MACl) to ~12% (1 M to 2 M MACl). The device parameters (J_{sc}, V_{oc}, FF, and η) for all these mesoporous and planar cells are summarized in Table 2.

Table 2

Effect of MACl Amount (x) on Short-Circuit Photocurrent Density J_{sc}, Open-Circuit Voltage V_{oc}, Fill Factor FF, and Conversion Efficiency η of Solid-State Mesostructured (Meso) and Planar Perovskite $CH_3NH_3PbI_3$ Solar Cells. The mean values and standard deviations of the PV parameters from 12-20 cells for each type of devices are given in parentheses.

Cell Type (x)	**J_{sc} (mA/cm^2)**	**V_{oc} (V)**	**FF**	**η (%)**
Meso (0)	16.91 (16.96±0.64)	0.835 (0.826±0.013)	0.583 (0.545±0.032)	8.23 (7.64±0.64)
Meso (0.5)	18.55 (17.91±0.67)	0.845 (0.836±0.016)	0.582 (0.552±0.039)	9.12 (8.25±0.54)
Meso (1)	19.31 (19.44±0.61)	0.833 (0.824±0.019)	0.595 (0.565±0.023)	9.57 (9.03±0.33)
Meso (2)	19.48 (19.38±0.50)	0.829 (0.823±0.016)	0.625 (0.597±0.020)	10.09 (9.52±0.37)
Planar (0)	5.55 (4.75±0.82)	0.813 (0.735±0.060)	0.413 (0.375±0.035)	1.86 (1.34±0.39)
Planar (0.5)	17.90 (17.38±0.66)	1.004 (0.974±0.022)	0.607 (0.561±0.038)	10.91 (9.50±0.85)
Planar (1)	20.85 (20.08±0.76)	1.016 (1.019±0.029)	0.566 (0.515±0.048)	11.99 (10.51±0.92)
Planar (2)	20.36 (19.84±0.63)	1.023 (1.013±0.042)	0.581 (0.540±0.029)	12.10 (10.85±0.79)

[0049] Figures 11a-b illustrate the effect of MACl on the recombination resistance (R_{rec}) as a function of voltage for (a) mesostructured and (b) planar perovskite $CH_3NH_3PbI_3$ solar cells. Impedance spectroscopy was used to study the effect of using MACl on the recombination resistance (R_{rec}) for mesostructured and planar perovskite $CH_3NH_3PbI_3$ solar cells. Figure 11a shows the R_{rec} values as a function of voltage for mesostructured perovskite solar cells. The R_{rec} for all mesostructured perovskite solar cells varied signifincantly with the bias voltage, following an approximately exponential decrease with voltage. All mesostructured perovskite cells exhibited essentially the same voltage dependence of R_{rec}, suggesting that using MACl as a second alkyl ammonium halide in the solution has minimal effect on the recombination kinetics in mesostructured cells. In contrast, a strong MACl effect was evident on the voltage dependence of R_{rec} for planar perovskite cells (Figure 11b.) The R_{rec} values for the planar device not using MACl were generally from about 1 to 2 orders of magnitude lower than those for the planar devices using MACl to assist the crystallization of $CH_3NH_3PbI_3$. Thus, the recombination rate for planar samples prepared without MACl was much faster than that for planar samples prepared with MACl. The observed difference in R_{rec} for these planar devices is consistent with their markedly different dark *J-V* characteristics (Figures 12a-b). The onset voltage of the dark current shifted from about 500 mV to over 700 mV when MACl was used as a second alkyl ammonium halide in the solution. Both R_{rec} and dark *J-V* results were consistent with the influence of MACl on the morphologies of planar perovskite $CH_3NH_3PbI_3$ films grown directly on the compact TiO_2 layer (Figures 9e-h). When no MACl was used, a significant portion of the substrate was exposed without $CH_3NH_3PbI_3$ coverage, which may lead to enhanced recombination and decreased solar cell performance.

[0050] To help understand the role of MACl on the perovskite film formation using the disclosed solution mixtures (i.e., a mixture of PbI_2, MAI, and a second alkyl ammonium halide with different molar ratios), perovskite films prepared from a solution containing only PbI_2 and MACl in the absence of MAI were evaluated. These films will be referred to herein as PbI_2-MACl. Figure 13 shows the effect of thermal treatement time (at about 100°C) on the XRD patterns of the PbI_2-MACl films prepared from the stoichiometric solution of PbI_2 and MACl with the same Pb concentration as used in the disclosed MACl-added solutions for making perovskite halides films; $CH_3NH_3PbI_3$. After about 1 minute of thermal treatment, the PbI_2-MACl film displayed the characteristic perovskite (110) peak near 14 degrees. There were two additional new XRD peaks at about 12.6 and 15.5 degrees, respectively. In contrast, the perovskite film using MACl-added $CH_3NH_3PbI_3$ precursor exhibited different XRD patterns during the early stage of annealing (Figures 8a-c). The peak near 12.6 degrees may be attributed to the formation of PbI_2, whereas the peak near 15.5 degrees may be attributed to the formation of $CH_3NH_3PbI_3$. With increased thermal treatment time, the intensities of both the 14- and 15.5-degree perovskite peaks decreased. In contrast, the 12.6-degree PbI_2 peak increased with thermal treatment time. With thermal treatment times longer than about 50 minutes, the two perovskite peaks near 14 and 15.5 degrees disappear completely. These XRD results show that the PbI_2-MACl film is not stable and decomposes to primarily PbI_2 with annealing. Consistent with the XRD results, the absorption spectrum of the PbI_2-MACl film also undergoes significant changes with thermal treatment time (Figure 15). The initial absorption spectrum of the PbI_2-MACl film was similar to that of $CH_3NH_3PbI_3$ with a brown color. The film turned yellowish after >20 minutes of thermal treatment, and its absorption spectrum become dominated by the absorption of PbI_2, which is consistent with the XRD results. Devices based on the PbI_2-MACl films with from 5 minutes to about 10 minutes of thermal treatment only show 2-3% efficiencies. These results suggest that direct reaction between PbI_2 and MACl (in the absence of MAI) may not lead to the formation of pure, high quality $CH_3NH_3PbI_3$ perovskite films. Furthermore, the maximum molar ratio of MACl:PbI_2 in the PbI_2-MACl precursor solutions was 1:1. Using a larger molar ratio for MACl:PbI_2 did not lead to a clear, fully-dissolved starting solution. In contrast, the solutions described heerein containing PbI_2, MAI, and from 0.5 M to 2 M MACl were clear and stable in ambient conditions. These results show that the exact precursor composition is critical to the formation of perovskite films. Thus, the success in preparing $CH_3NH_3PbI_3$ film in this study cannot be associated with PbI_2-MACl in the absence of MAI. Without wishing to be bound to by theory, it is believed that the $CH_3NH_3PbI_3$ films, with MACl-added to the MAI and PbI2 starting solution, are formed through a possible intermediate, MAI·PbI_2·xMACl, with an unknown crystalline structure. The additive MACl may act as a "sacrificial" agent to form this intermediate and then slowly decompose, volatilize, and/or sublime during the annealing process.

[0051] Charge transport and recombination properties in mesostructured perovskite $CH_3NH_3PbI_3$ solar cells were studied by IMPS and IMVS. Figure 14a shows the effect of using MACl on the diffusion coefficient (D) as a function of photoelectron density (n). All cells exhibited essentially the same power-law dependence ($D \propto n^{1/\alpha-1}$, with α being a disorder parameter) that is attributable to the electrons undergoing multiple trapping and detrapping through the mesoporous electrode film. There was no obvious difference of the D values for mesostructured perovskite cells using different amounts of MACl in the $CH_3NH_3PbI_3$ precursor solution, suggesting that using MACl does not affect the trap distribution on the TiO_2 surface. Similarly, no significant difference is observed for the recombination lifetime as a function of voltage for mesostructured cells prepared using different amounts of MACl (Figure 14b).

[0052] Figures 16a-c provide (a) an SEM image, (b) XRD patterns, and (c) EDX analysis of the mixed halide $CH_3NH_3PbI_{3-x}Cl_x$ prepared from the starting solution containing MAI and $PbCl_2$ (at about a 3:1 molar ratio). Figure 16a shows the SEM image of the $CH_3NH_3PbI_{3-x}Cl_x$ film thermally treated at about 100°C for ~45 minutes. The overall film morphology was similar to the $CH_3NH_3PbI_3$ films prepared using the $CH_3NH_3PbI_3$ precursors with the addition of from about 1 M to about 2 M MACl (Figures 9g and 9h). The crystal structure evolution of the $CH_3NH_3PbI_{3-x}Cl_x$ film was examined by the thermal treatment time dependence of the XRD patterns. With ~1 minute of thermal treatment at 100°C, the film exhibited three XRD peaks near 12.6, 14, and 15.5 degrees, which were similar to the XRD patterns of the PbI_2-MACl films (Figure 13) during the early stage of annealing. Again, the perovskite film using MACl-added added to the MAI and PbI_2 starting solution exhibited different XRD patterns during the initial thermal treatment stage, implying the existence of different crystal structures formed during the early stage of thermal treatment. With increasing thermal treatment time, to about 45 minutes, only the perovskite peak near 14 degrees is left for the $CH_3NH_3PbI_{3-x}Cl_x$ film, similar to the XRD patterns for $CH_3NH_3PbI_3$ shown in Figure 8. Consistent with this observation, the EDX analysis (Figure 16c) of the $CH_3NH_3PbI_{3-x}Cl_x$ film shows that with increasing thermal treatment time, the Cl:I ratio decreased from about 1.6:2.7 at 1 about minute to 0.5:2.8 at about 20 minutes. The $CH_3NH_3PbI_{3-x}Cl_x$ film thermally treated for ~45 minutes did not show any detectable trace of chloride.

[0053] Figure 17 illustrates recombination resistance R_{rec} as a function of voltage for a planar perovskite solar cell based on the mixed halide $CH_3NH_3PbI_{3-x}Cl_x$ prepared from the starting solution containing MAI and $PbCl_2$ (3:1 molar ratio). The R_{rec} values for the planar $CH_3NH_3PbI_3$ cells prepared from the $CH_3NH_3PbI_3$ precursor with 2-MACl additive are also plotted for comparison. The *J-V* curve for a planar $CH_3NH_3PbI_{3-x}Cl_x$ perovskite cell is shown in Figure 18. The cell efficiency was ~11.86% with a J_{sc} of ~20.57 mA/cm^2, V_{oc} of ~0.995 V, and FF of ~0.579. The performance of the planar $CH_3NH_3PbI_{3-x}Cl_x$ perovskite cell was similar to that of the planar $CH_3NH_3PbI_3$ cells prepared from the starting solutions containing from 1 M to 2 M amounts of MACl additives, as previously described. Referring again to Figure 17, the R_{rec} values for the planar $CH_3NH_3PbI_3$ cells prepared with 2-MACl additive are also plotted for comparison. It is apparent that these two samples follow almost identical voltage dependence of the recombination resistances. Taken together the results of SEM, XRD, *J-V,* and impedance spectroscopy, it is reasonable to believe that the $CH_3NH_3PbI_{3-x}Cl_x$ perovskite film prepared from the 3MAI-$PbCl_2$ precursor is similar to the $CH_3NH_3PbI_3$ perovskite film prepared from the MACl-added to the solution containing MAI and PbI_2. Despite these similarities, significant differences between these two approaches exist. (1) First, the crystal structures of the perovskite films prepared with these two approaches during the early stage of thermal treatment are different (Figures 8a-c and 16a-c), indicating that the exact precursor composition is critical to the process of perovskite formation. (2) It was also found that the ratio of MAI:$PbCl_2$ in the starting solution for preparing $CH_3NH_3PbI_{3-x}Cl_x$ should not be less than 3; otherwise, $PbCl_2$ cannot be fully dissolved. This may explain why the $CH_3NH_3PbI_{3-x}Cl_x$ precursor has a molar ratio of 3:1 for MAI:$PbCl_2$. In contrast, a starting solution utilizing wide ranging amounts of MACl added to MAI and PbI_2, enhanced the ability to control the kinetics of the perovskite crystallization process. (3) Moreover, this example shows that the 3MAI-$PbCl_2$ precursor solution turned from green-yellow to brown-yellow after one week of storage in air. In contrast, the PbI_2-MAI-2MACl starting solution (with the same Pb concentration as in the 3MAI-$PbCl_2$ precursor solution) stays clear with a green-yellow color for more than three months when stored in air.

[0054] In summary, the present disclosure provides a one-step solution approach to prepare perovskite halide films ($CH_3NH_3PbI_3$) on a mesoporous TiO_2 film or on a planar, compact TiO_2 layer on FTO. In this Example, CH_3NH_3Cl (or MACl) was added to a standard equimolar solution of CH_3NH_3I and PbI_2 to favorably adjust the crystallization process for the final target perovskite halide film; $CH_3NH_3PbI_3$. Depending on the amount of MACl used in the precursor solution, the optimum crystallization time for forming pure $CH_3NH_3PbI_3$ with the strongest absorption varied from a few minutes to several tens of minutes. The use of MACl not only led to enhanced absorption of $CH_3NH_3PbI_3$, but also to significantly improved coverage of $CH_3NH_3PbI_3$ on a planar substrate. Compared to a typical, standard one-step solution approach for producing $CH_3NH_3PbI_3$ films, the additional use of an alkyl ammonium halide such as MACl improves the performance of perovskite solar cells. For the mesostructured device architecture, the efficiency was enhanced from about 8% to 10%, whereas for the planar cell structure, the efficiency was improved from about 2% to 12%. The recombination resistance for planar cells was reduced by 1-2 orders of magnitude by using MACl. The significant performance improvement for planar perovskite cells is attributed primarily to the improved morphology of the perovskite films resulting from the additional use of MACl to control the crystallization process for forming the final target perovskite halide film, $CH_3NH_3PbI_3$.

EXAMPLE 2: ONE-STEP METHOD

[0055] Figures 19a-c depict typical SEM images of CH_3NH PbI_2Br films deposited on c-TiO_2/FTO substrates from various precursor solutions: (a) PbI_2+MABr; (b) PbI_2+MABr+MACl; and (c) PbI_2+MABr+2MACl. Figures 20a-c illustrate the effect of annealing time (as indicated) at 125°C on the XRD patterns of $CH_3NH_3PbI_2Br$ films deposited on c-TiO_2/FTO substrate from various precursor solutions: (a) PbI_2+MABr; (b) PbI_2+MABr+MACl; and (c) PbI_2+MABr+2MACl. Figure 21 illustrates photocurrent density-photovoltage (J-V) curves of perovskite solar cells prepared from different precursor compositions (i.e., PbI_2+MABr or 0 MACl; PbI_2+MABr+MACl or 1 MACl; and PbI_2+MABr+2MACl or 2MAC1).

[0056] This one-step solution approach provided by the present disclosure comprises introducing CH_3NH_3Cl (or MACl) to the standard $CH_3NH_3PbI_2Br$ precursor solution to prepare perovskite $CH_3NH_3PbI_2Br$ films. It has been found that the use of CH_3NH_3Cl alters the crystallization process for forming $CH_3NH_3PbI_2Br$. The amount of CH_3NH_3Cl in the perovskite precursor solution strongly affects the film morphology (Fig. 19), crystal structure formation (Fig. 20), and device characteristics (Fig. 21).

EXAMPLE 3: THREE-STEP METHOD

[0057] This example illustrates a three-step sequential deposition method for preparing PbI_2-free $CH_3NH_3PbI_3$ films. Using typical, known two-step approaches, it is often difficult to completely convert PbI_2 into final target perovskite halide film, e.g.$CH_3NH_3PbI_3$, without causing significant degradation of the perovskite film. In contrast, the disclosed three-step sequential solution deposition approach provides a thermally unstable stoichiometric $PbI_2 \cdot CH_3NH_3Cl$ (PbI2·MACl) transitory, intermediate film that is first deposited on the mesoporous TiO_2 substrate, followed by thermal decomposition to form a PbI_2 film. Using this disclosed method, the PbI_2 film can be rapidly converted into $CH_3NH_3PbI_3$ without any PbI_2 residue by using a MAI IPA solution at room temperature, which ultimately leads to improved device performance.

Experimental Setup and Device Fabrication

[0058] Preparation of material for fabricating the disclosed structures, and for fabricating conventional devices used for purposes of comparison, used to quantify the improved performance of the disclosed structures proceeded as follows. MAI and MACl were synthesized by reacting methylamine (MA) with HI and HCl, respectively, followed by purification. A patterned fluorine-doped tin oxide (FTO) was first deposited with a blocking layer by spray pyrolysis at ~450°C using ~0.2 M Ti(IV) bis(ethyl acetoacetate)-diisopropoxide 1-butanol solution, followed by ~450°C annealing in air for one hour. A 500-nm-thick mesoporous TiO_2 film was then screen coated onto FTO followed by ~500°C annealing in air for 30 minutes. The TiO_2 film was then treated in 40 mM $TiCl_4$ aqueous solution at ~65°C for about 30 minutes. These $TiCl_4$-treated TiO_2 films were then sequentially rinsed by deionized (DI) water, blown dry in air, and finally annealed at about 500°C for about 30 minutes.

[0059] "Standard" two-step deposition of perovskites proceeded as follows. From 0.4 M to about 1.0 M PbI_2 (99.99%) DMF solution was spin coated onto a mesoporous TiO_2 film at 3000 rpm for about 20 seconds. The deposited PbI_2 film was then thermally treated at about 70°C for about 5 minutes. The PbI_2 film was cooled to room temperature and then immersed into a 10 mg MAI/mL isopropyl alcohol (IPA) solution for different times (from 2 minutes to about 60 minutes), followed by rinsing with IPA, blown dry with N_2, and then thermally treated at 70°C for about 5 minutes.

[0060] Three-step methods for the formation perovskites halides, performed pursuant to methods provided by the present disclosure, as follows. A first solution in DMF of 1.0 M equal molar ratio PbI_2 and MACl was first spin coated onto the mesoporous TiO_2 film at 3000 rpm for about 20 seconds. The applied solution was then thermally treated at about 130°C for about 30 minutes, resulting in the formation of a yellow PbI_2 film, which was then cooled to room temperature. The yellow PbI_2 film was then immersed into a 10 mg MAI/mL IPA solution for about 30 seconds, followed by rinsing with IPA, blown dry by N_2, and then thermally treated at ~70°C for about 5 minutes.

[0061] In connection with device preparation, the perovskite-deposited electrodes were first coated with a layer of hole transport material (HTM) by spin coating at 4,000 rpm for 20 seconds using 0.1 M spiro-MeOTAD, 0.035 M bis(trifluoromethane)sulfonimide lithium salt (Li-TFSi), and 0.12 M 4-tert-butylpyridine (tBP) in chlorobenzene/acetonitrile (10:1, v/v) solution. A 150-nm-thick Ag contact layer was then deposited by thermal evaporation.

[0062] The crystalline structures of the perovskite films were measured by X-ray diffraction (XRD, Bruker D8 ADVANCE with Cu Kα radiation). The absorption spectra of the planar perovskite films were characterized by an ultraviolet-visible (UV-vis) spectrophotometer (Cary-60). The photocurrent density-voltage (J-V) characteristic of perovskite solar cells was measured with a Keithley 2400 source meter under simulated AM 1.5G illumination (100 mW/cm2; Oriel Sol3A Class AAA Solar Simulator).

Results and Discussion

[0063] In a standard two-step method, a 1.0 M PbI_2 precursor solution is normally used to obtain sufficient deposition of $CH_3NH_3PbI_3$ to absorb light. In this Example, the time evolution of the conversion of PbI_2 into the final target perovskite halide film, $CH_3NH_3PbI_3$, was examined by using UV-vis and XRD measurements. Figures 22a-b show the effect of MAI contacting times on changes of the XRD patterns. When the PbI_2 film was contacted with MAI for about 2 minutes, there was an incomplete conversion as evidenced by the existence of both the PbI_2 (near 12.6°) and $CH_3NH_3PbI_3$ (near 14°) diffraction peaks with similar peak intensities. The intensity of the $CH_3NH_3PbI_3$ peak increased, whereas the PbI_2 peak intensity decreased with longer MAI contact times (from 10 minutes to 60 minutes). Even with a 60 minutes of contact time, there was still a noticeable amount of PbI_2 in the film as indicated by the characteristic PbI_2 diffraction peak. However, the intensity of the PbI_2 peak was much smaller and almost negligible compared to the $CH_3NH_3PbI_3$ peak when the contact time was more than 30 minutes.

[0064] During the conversion process to the final perovskite film, the initial yellow PbI_2 film slowly changed color to brown or dark brown, depending on the contact time in the second MAI-containing solution. Figures 22b shows the UV-vis absorption spectra of the resulting films as a function of the contact time. Although the XRD measurement indicates a significant fraction of PbI_2 existed after 2 minutes of contact time, the UV-vis spectrum of this sample showed a typical $CH_3NH_3PbI_3$ absorbance as shown in Figure 22b. The direct absorbance by the residue PbI_2 is likely hidden by the absorption spectrum from the partially converted $CH_3NH_3PbI_3$ within the film. Because the regular IPA solution can dissolve $CH_3NH_3PbI_3$, longer contact times eventually led to a significant drop of absorption across the entire wavelength range, despite more conversion of PbI_2 to the final target perovskite film, $CH_3NH_3PbI_3$, as suggested by the XRD results. Therefore, the sample contacted for about 60 minutes with the second solution only displayed about half the absorbance compared to the sample contacted with the second solution for about 2 minutes.

[0065] The impact of the MAI-containing contact time on the photovoltaic parameters of the perovskite solar cells are presented in Table 3. When the contact time was increased from 2 minutes to 60 minutes, the short-circuit photocurrent density first increased and then decreased, with a peak value (14.84 mA/cm2) reached at 30 minutes contact time, which reflects the balance between perovskite conversion and dissolution during the second contacting step, as shown in Figures 22a-b. Fill factor of these devices increased significantly with the increased contact times, from 0.346 at 2 minutes to 0.455 at 60 minutes. The overall conversion efficiency essentially followed the trend of photocurrent, increasing from ~2.55% at 2 minutes to ~5.75% at 30 minutes, and then decreases to ~4.59% at 60 minutes. These results indicate that it is important to have more complete conversion of PbI_2 to the final target perovskite halide film, $CH_3NH_3PbI_3$, without significant dissolution of $CH_3NH_3PbI_3$ in order to reach reasonable device performance.

Table 3

Effect of the MAI dipping time on the perovskite solar cell photovoltaic parameters short-circuit photocurrent density, J_{sc}; open-circuit voltage, V_{oc}; fill factor, FF; and conversion efficiency, η.

Dipping Time [min]	J_{sc} [mA/cm^2]	V_{oc} [V]	FF	η [%]
2	8.58	0.859	0.346	2.55
10	11.41	0.837	0.403	3.85
30	14.84	0.899	0.431	5.75
60	11.07	0.911	0.455	4.59

[0066] Figures 23a-b illustrate the effect of PbI_2 concentration (from 0.4 M to 1.0 M) on the (a) XRD patterns and (b) UV-vis absorption spectra of the perovskite films deposited on mesoporous TiO_2 films after contacting the PbI_2 films with a 10 mg MAI/mL IPA solution for about 10 minutes. The impact of varying PbI_2 concentration on the PbI_2-to-$CH_3NH_3PbI_3$ conversion using a typical two-step method was also analyzed. The concentration of the PbI_2 precursor solution was changed from 0.4 M to 1.0 M. To avoid the dissolution of $CH_3NH_3PbI_3$ in the IPA solution, the dipping time of PbI_2 film in the MAI IPA solution was fixed at about 10 minutes for all samples. Figure 23a shows the XRD measurements of the perovskite films using different PbI_2 concentration with a -10 minute contact time during the second contacting step with the second solution. The intensity of the characteristic PbI_2 diffraction peak decreased significantly when the PbI_2 concentration was reduced from 1.0 M to 0.8 M. The PbI_2 peak disappeared from the diffraction pattern when the PbI_2 concentration was further reduced to 0.6 M and 0.4 M, suggesting a complete conversion of PbI_2 to $CH_3NH_3PbI_3$ using a low-concentration PbI_2 first solution, with -10 minute contact time in the second MAI IPA solution. Without wishing to be bound to theory, it is believed that a lower concentration PbI_2 first solutions (e.g., from 0.4 M to 0.6 M) can lead to less infiltration of PbI_2 into the mesoporous TiO_2 films than the higher concentration first solutions (e.g., from 0.8 M to about 1.0 M PbI_2). A lower degree of pore filing of PbI_2 may promote the conversion of PbI_2 into $CH_3NH_3PbI_3$ by facilitating the intercalation of MAI into PbI_2; but it may also result in lower absorbance due to less $CH_3NH_3PbI_3$ deposition. Figure 23b compares the effect of PbI_2 concentration on the UV-vis absorption spectra of the perovskite films. A higher PbI_2 concentration in the first solution for the first contacting step, generally led to stronger absorbance. The perovskite film based on a 0.4 M PbI_2 first solution displayed only about half the absorbance of the perovskite film based on a 1.0 M PbI_2 first solution.

[0067] Table 4 summarizes the photovoltaic parameters (J_{sc}, V_{oc}, FF and η) of the solar cells based on the $CH_3NH_3PbI_3$ films prepared using different concentrations of PbI_2 in the first solution of the two-step method, with 10 minute contact times in the second MAI solution during the second contacting step. The 0.8-M sample exhibited a low photocurrent density similar to the 1.0-M sample, which may be attributed to the residue PbI_2 observed by XRD. In contrast, the 0.6 M sample without any PbI_2 residue exhibited a reasonable photocurrent density despite its lower absorption than the 1.0 M sample (Figure 22b). However, the lowest J_{sc} value was observed for the 0.4 M sample, for which the poor light absorption clearly limits the device performance. As a balance for optimizing both the light absorption and conversion of PbI_2 to $CH_3NH_3PbI_3$, the best device performance efficiency was obtained for the 0.6 M sample with a cell efficiency of about 7.23%. Thus, it appears that isopropanol may not be suitable for a standard two-step method because of the dissolution of $CH_3NH_3PbI_3$ dissolution and the difficulty of obtaining a PbI_2-free $CH_3NH_3PbI_3$ film with sufficient absorption.

Table 4

Effect of PbI_2 concentration (0.4-1.0 M) on the perovskite solar cell photovoltaic parameters. The second-step MAI dipping time is 10 min for all samples.

Concentration [M]	J_{sc} [mA/cm^2]	Voc [V]	FF	η [%]
0.4	10.27	0.842	0.609	5.27
0.6	14.79	0.836	0.585	7.23
0.8	11.73	0.830	0.55	5.35
1.0	11.40	0.837	0.403	3.85

[0068] In order to overcome the deficiencies of the two-step deposition, the three-step sequential deposition method, per embodiments of the present invention, was investigated. In the three-step method, a first solution of PbI_2 and MACl (in equimolar concentration) was first applied onto a mesoporous TiO_2 film. Upon thermal treatment at ~130°C for about 1 minute, the resulting film exhibited a light brown color with an unknown XRD pattern. Its XRD pattern and UV-vis absorption spectra are shown in Figure 24a and 24b (Step 1), respectively. The absorption spectra were similar to those of $CH_3NH_3PbI_3$; however, their XRD patterns were very different. This unknown compound (denoted as PbI_2+MACl) was likely a mixture of $CH_3NH_3PbCl_3$, $CH_3NH_3PbI_3$, and some unknown structure. When thermally treated at 130°C in air, the brown film slowly turned to a yellow color. After thermally treating at 130°C for 30 min, the PbI_2+MACl film was thermally decomposed to PbI_2, as suggested by its UV-vis spectra and XRD pattern (Figures 24a -b, Step 2). No traceable chlorine content could be found in this film by the energy dispersive X-ray (EDX) analysis.

[0069] The PbI_2 film formed from thermal treatment turned dark brown almost immediately after contacting with the second MAI-containing solution (with regular IPA). It took only about 30 seconds for the yellow PbI_2 film to convert into a dark-brown $CH_3NH_3PbI_3$ film (Figure 24a, step 3) without any traceable PbI_2 evident from its XRD pattern (Figure 24b, step 3). The perovskite halide target film, $CH_3NH_3PbI_3$, prepared from the initial 1.0 M $PbI_2 \cdot MACl$ precursor by the three-step method exhibited strong absorption (especially in the long-wavelength region) similar to the film prepared from the regular two-step approach using a 1.0 M PbI_2 first solution.

[0070] Figure 25 is a graphical illustration of a *J-V* characteristic of a perovskite solar cell based on the $CH_3NH_3PbI_3$ film prepared from the disclosed three-step method. The cell efficiency was about 10.11%, with a J_{sc} of ~18.64 mA/cm^2, V_{oc} of ~0.868 V, and FF of ~0.625. Both forward and backward J-V scans are shown in Figure 25. The hysteresis was about 1%, and thus, can be considered negligible.

[0071] The above results demonstrate that the three-step method provides a promising way to address the challenges associated with the PbI_2 conversion for a standard two-step method. Without wishing to be limited by theory, it is believed that the quick PbI_2-to-$CH_3NH_3PbI_3$ conversion kinetics observed results from the higher exposed surface of the PbI_2 film prepared through the thermal treatment step of the three-step deposition method. The formation of pores resulting from the release of MACl in the thermal treatment step is expected to form a PbI_2 film with a larger exposed surface area than the PbI_2 film deposited directly from the PbI_2 precursor. The higher exposed surface of the PbI_2 film may facilitate the intercalation reaction between MAI with PbI_2 during the contacting step with the second solution, leading to a complete conversion of PbI_2 within about 30 seconds. With such a short contact time, the issue of $CH_3NH_3PbI_3$ dissolution in the IPA solution may be effectively mitigated.

[0072] For a typical two-step method, with a high-concentration (1.0 M) PbI_2 first solution, the conversion of the PbI_2 film to the final target perovskite halide, $CH_3NH_3PbI_3$, required a long conversion time in the MAI IPA second solution. The long exposure to the second IPA solution caused the dissolution of the converted $CH_3NH_3PbI_3$ perovskite film, leading to reduced photocurrent generation, and consequently, poor device performance. On the other hand, a short exposure of the PbI_2 film to the second MAI IPA solution resulted in only a partial conversion of the film with significant PbI_2 residue, which also limited the device performance. Using a less concentrated first PbI_2 solution (e.g., 0.4 M) showed complete conversion of the PbI_2 film with a fixed contact time of about 10 minutes. However, the poorer light absorption for the final perovskite film prepared with a low concentration of PbI_2 in the first solution also limited the final device performance. To address this dilemma, the present disclosure provides a three-step solution method to prepare $CH_3NH_3PbI_3$ perovskite halide films by using a second MAI-containing solution with regular (non-anhydrous) IPA. In comparison to the typical two-step approach using similar processing conditions, the disclosed three-step method enables the formation of a PbI_2 film through the thermal decomposition of an intermediate and transitory PbI_2+MACl film. This intermediate film facilitates a rapid conversion of the subsequently formed PbI_2 film to the final target perovskite halide film, $CH_3NH_3PbI_3$, without any detectable residual PbI_2 in the perovskite film, leading to improved device performance. Thus, the disclosed three-step solution method using regular IPA represents a promising alternative deposition method for preparing low-cost, high-efficiency perovskite solar cells.

EXAMPLE 4: MODIFIED THREE STEP METHOD

[0073] In this Example, the three-step method provides a facile morphology-controllable sequential deposition of a planar $CH_3NH_3PbI_3$ film by stepping through a transitory intermediate $PbI_2{\cdot}x$MAI (x: 0.1-0.3) precursor film. Adding a small amount of MAI to the PbI_2 first solution, may lead to about a 10-fold faster complete formation of the final target perovskite halide film, $CH_3NH_3PbI_3$, without any PbI_2 residue after the contacting step with the MAI-containing second solution, resulting in a much improved device performance with higher reproducibility, especially when using about 0.1 M to about 0.2M MAI in the second solution. The best cell efficiency recorded was ~16.76% using this modified $PbI_2{\cdot}0.15$MAI first solution with the maximum power output stabilized at about 16.5% under one-sun illumination. This demonstrates that the morphologies of $PbI_2{\cdot}x$MAI intermediate films and the corresponding final target perovskite halide films, $CH_3NH_3PbI_3$, can be adjusted by tuning the relative amount of MAI.

[0074] Figure 26a shows the ultraviolet-visible (UV-vis) absorption spectra evolution of a pure PbI_2 film after dipping in a second solution of 10 mg/mL MAI isopropanol (IPA) for contact times up to about 30 minutes. The absorption shoulder near 750 nm for perovskite $CH_3NH_3PbI_3$ increased slowly with the MAI dipping time up to 20 min. The absorption spectrum increased very little after 20 minutes of contacting, which indicates that most PbI_2 had been converted to $CH_3NH_3PbI_3$. The baseline of the absorption spectra also increased simultaneously with longer dipping time, reflecting the stronger light scattering effect associated with a rougher perovskite morphology. Although the absorption measurements suggest that the $CH_3NH_3PbI_3$ perovskite film grown with 6 minutes dipping exhibited strong $CH_3NH_3PbI_3$ absorbance spectrum, the X-ray diffraction (XRD) pattern of the same sample (Figure 26b) still exhibited the characteristic peaks for PbI_2 along with the $CH_3NH_3PbI_3$ diffraction peaks, which is an indication of incomplete conversion of PbI_2 to $CH_3NH_3PbI_3$. The intensity of PbI_2 diffraction peak was substantially reduced with longer contacting times up to 20 minutes. The PbI_2 peak disappeared completely when the contact time was further increased to 30 minutes. The typical scanning electron microscopy (SEM) images of planar PbI_2 and $CH_3NH_3PbI_3$ (20-min dipping/conversion) films are compared in Figure 26c and 26d, respectively. The planar PbI_2 film appeared porous with a coarse top surface, which may be caused by the shrinkage of the precursor film during the drying process. The resulting $CH_3NH_3PbI_3$ film was also full of tiny pinholes and its surface is covered with rough perovskite nanocrystals; this appearance is similar to that of the perovskite capping layer grown on a mesoporous substrate using two-step sequential deposition. The increased roughness of the $CH_3NH_3PbI_3$ film compared to the initial PbI_2 film may be attributed to space expansion during the second step of MAI intercalation reaction with PbI_2.

[0075] Taken together, the results of XRD and absorption measurements in Figures 26a and 26b illustrate the deficiencies associated with planar $CH_3NH_3PbI_3$ thin films prepared from PbI_2 using the standard two-step sequential solution deposition method. The effect of varying MAI dipping time on the device characteristics is shown in Figure 27 and the corresponding photovoltaic parameters are listed Table 5. The cell efficiency increased significantly with longer contact time from 3.145% at 0.5 min to 6.105% at 2 min to 9.301% at 6 min, which was consistent with the more complete conversion of PbI_2 to $CH_3NH_3PbI_3$. However, when the contact time was increased to 20 min, the device performance dropped in all parameters to an overall efficiency of only 1.290%, despite the fact that the $CH_3NH_3PbI_3$ film with 20 min contact time showed a reduced amount of residue PbI_2 and also had stronger light absorption than the $CH_3NH_3PbI_3$ film with 6 minute contact times. Thus, simply lengthening the conversion time to complete the PbI_2-to-$CH_3NH_3PbI_3$ conversion presents a challenge for the typical two-step sequential solution processing. The long contacting/reaction duration caused damage to the $CH_3NH_3PbI_3$ layer resulting from the back extraction of MAI from $CH_3NH_3PbI_3$, thus deteriorating the device performance.

Table 5

Device parameters of planar $CH_3NH_3PbI_3$ solar cells prepared from PbI_2 precursor films.

PbI_2 in MAI time	J_{sc} (mA/cm^2)	V_{oc} (V)	FF	η (%)
0.5 min	6.539	0.979	0.491	3.145
2 min	8.847	0.969	0.712	6.105
6 min	15.515	0.961	0.624	9.301
20 min	4.512	0.489	0.584	1.290

[0076] To address the challenges associated with the incomplete conversion of PbI_2 and rough perovskite surface discussed above and associated with the known two-step approach, the modified three-step deposition process provided by the present disclosure has been developed. The disclosed modified three-step method utilizes an alkyl ammonium halide in combination with the typical perovskite precursor, a mixture of PbI_2 and x alkyl ammonium halide with x varying from 0.1-0.3, during a first contacting step to deposit a resulting precursor film denoted as $PbI_2 \cdot x$ alkyl ammonium halide. Even in the presence of the alkyl ammonium halide, the deposited $PbI_2 \cdot x$ alkyl ammonium halide films still looked yellowish without any indication of the formation of perovskite $CH_3NH_3PbI_3$.

[0077] In this Example, the alkyl ammonium halide was methyl ammonium iodide (MAI). Figure 28a shows the UV-vis absorption spectra of the $PbI_2 \cdot x$MAI precursor films. All of these films exhibited an absorption onset near 510 nm, which is characteristic for PbI_2. The sharp absorption edge associated with PbI_2 became less clear with increasing MAI. At x=0.3, the baseline of the absorption of precursor film increased substantially, indicating an enhanced light scattering effect. Figure 28b compares the XRD patterns of $PbI_2 \cdot x$MAI (x: 0-0.3) precursor films. In the absence of MAI (x: 0), the PbI_2 film displayed a strong characteristic XRD peak at about 12.5°. The intensity of PbI_2 peaks decreased significantly with the increase of the MAI amount used in the first-step precursor solution. The addition of xMAI into PbI_2 during the first deposition step did not result in any detectable $CH_3NH_3PbI_3$ diffraction peaks, such as the main (110) peak near 14°. This is consistent with the yellow appearance and the corresponding absorption spectra. The intensity of the main PbI_2 diffraction peak (~12.5°) decreased substantially with increased amounts of MAI in the precursor. This observation suggests that a partial incorporation of MAI in the PbI_2 film decreased the PbI_2 crystallinity in the $PbI_2 \cdot x$MAI films (compared to the pure PbI_2 film) without forming the perovskite $CH_3NH_3APbI_3$ phase.

[0078] In contrast to the slow conversion of planar PbI_2 film into $CH_3NH_3PbI_3$ via the standard two-step sequential deposition, using the disclosed $PbI_2 \cdot x$MAI precursor films was found to convert to red-brown planar $CH_3NH_3PbI_3$ film relatively quickly when using the same sequential deposition processes. It took from about 1 minute to about 3 minutes for all $PbI_2 \cdot x$MAI (x: 0.1-0.3) films to convert completely into $CH_3NH_3PbI_3$ without any PbI_2 residue as evidenced by the XRD measurements (Figure 29). This contrasts significantly to the about 20 minutes to about 30 minutes required for the pure PbI_2 film to reach full conversion to $CH_3NH_3PbI_3$ (Figure 26b) for the standard two-step sequential deposition process. Figure 28c shows the UV-vis absorption spectra of the planar $CH_3NH_3PbI_3$ films using various $PbI_2 \cdot x$MAI (x: 0.1-0.3) precursor films. The absorption spectrum for PbI_2 is also shown for comparison. Consistent with their XRD results, all of these films exhibited the same absorption shoulder near 750 nm, which is typical for $CH_3NH_3PbI_3$. The variation of the absorption intensity is presumably due to differences in $CH_3NH_3PbI_3$ film thicknesses due to different precursors. A noticeable increase of the baseline was observed for the $PbI_2 \cdot 0.3$MAI sample, corresponding to a larger light scattering effect as discussed in connection with Figure 28a. Using the $PbI_2 \cdot 0.15$MAI precursor film as an example, Figure 26d demonstrates the effect of MAI on the evolution of the absorption spectra of the precursor films. The rapid increase of absorbance near 750 nm indicated a quick conversion process from the $PbI_2 \cdot 0.15$MAI precursor film to the final perovskite $CH_3NH_3PbI_3$ film. Furthermore, there was no obvious increase of the baseline of the absorption spectra during the entire conversion process, suggesting that the $CH_3NH_3PbI_3$ film sequentially deposited from $PbI_2 \cdot 0.15$MAI may have a similar surface roughness as the initial $PbI_2 \cdot 0.15$MAI film.

[0079] Figures 30a-d show the typical SEM images of top views of the $PbI_2 \cdot x$MAI (x=0.1, 0.15, 0.2, and 0.3) precursor films. These films had very different morphologies than the pure PbI_2 film and their morphologies varied with the amount of MAI used in the precursor. When $x \leq 0.2$, the introduction of MAI into PbI_2 led to the formation of a smoother $PbI_2 \cdot x$MAI film with less pinholes than the pure PbI_2 film. However, the morphologies of the $PbI_2{\cdot}0.3MAI$ films became even coarser than pure PbI_2 films, which is consisted with the higher absorption baseline of the $PbI_2{\cdot}0.3MAI$ film as shown in Figure 28a. Figures 30e-h show the typical SEM images of the $CH_3NH_3PbI_3$ films prepared from $PbI_2{\cdot}x$MAI films after the second contacting/conversion step. Note that the $CH_3NH_3PbI_3$ films fabricated from $PbI_2{\cdot}x$MAI (x=0.1-0.2) were nearly pinhole free and showed a relatively uniform, smooth surface, especially for the 0.15MAI sample, which was significantly different from the relatively rough $CH_3NH_3PbI_3$ films prepared from the pure PbI_2 film (See Figure 26). The grain sizes of the $CH_3NH_3PbI_3$ films also showed a dependence on the amount of MAI used in the precursor. When x=0.1, the $CH_3NH_3PbI_3$ film consisted mainly of relatively small $CH_3NH_3PbI_3$ nanocrystals with sizes less than 200 nm. When using 0.15-0.2 MAI, the $CH_3NH_3PbI_3$ films were composed of many relatively large (~500 nm) crystals filled with ~200 nm small crystals; such film morphology is comparable to that of the vapor-phase-grown perovskite films. This result is also consistent with the absence of absorption baseline increase during the sequential deposition as shown in Figure 28d. When starting with the relatively coarse $PbI_2{\cdot}0.3MAI$ film, the $CH_3NH_3PbI_3$ film looked similar to that prepared from the pure PbI_2 film. These results clearly demonstrate that the new $PbI_2{\cdot}x$MAI-based modified three-step deposition method described herein allows for the control of the morphology of the final $CH_3NH_3PbI_3$ film.

[0080] In the standard two-step sequential solution deposition of $CH_3NH_3PbI_3$, the layer structured PbI_2 crystal was intercalated by MAI to form the $CH_3NH_3PbI_3$ as shown in Figure 31a. This significant phase transformation normally leads to approximately a factor of two volume expansion per formula during the second conversion step. To help understand the effect of adding MAI (during the first step deposition) on the $CH_3NH_3PbI_3$ film formation, the thickness (or volume) expansion ratios of converting $PbI_2{\cdot}_x$MAI to $CH_3NH_3PbI_3$ films were examined by using a surface profiler. Figure 31b shows the result of the expansion ratios for the films prepared with different amounts (x) of MAI from 0 to 0.3. The ratio continuously decreased with increasing amount of MAI. Without wishing to be bound by any theory, it is believed that, for the $PbI_2{\cdot}x$MAI films, the added MAI was likely incorporated into the PbI_2 matrix and partially pre-expanded the volume of PbI_2 matrix. The degree of this pre-expansion may depend on the amount of MAI used during the first step deposition. This pre-expansion may decrease the final film expansion ratio with increasing amounts of MAI. Assuming the pre-expansion ratio per formula of reactant MAI is the same as the expansion ratio in the standard conversion process with pure PbI_2, the expansion ratio of the final $CH_3NH_3PbI_3$ film thickness (d_f) to the thickness of the initial $PbI_2{\cdot}x$MAI film (d_i) can be calculated with the expression $d_f/d_i = m/[1 + (m - 1)x]$, where m is the expansion ratio. A best fit of the data yields $m = 2.02 \pm 0.07$; the corresponding best-fit line is shown in Figure 31b. The expansion is approximately two, suggesting that the pre-expansion to form $PbI_2{\cdot}x$MAI and the standard expansion to form $CH_3NH_3PbI_3$ have essentially the same volume expansion ratio. Considering the absence of the crystalline $CH_3NH_3PbI_3$ phase in the $PbI_2{\cdot}x$MAI films (Figure 28b), the additive MAI likely forms an amorphous structure with the nearby PbI_2. The formation of this amorphous structure may strongly affect the crystallinity of the remaining PbI_2 phase. The XRD intensity of the PbI_2 peak is much reduced even when the PbI_2 phase still constitutes the majority of the $PbI_2{\cdot}x$MAI film (e.g., x=0.15; Figure 28b). Thus, the addition of small amounts of MAI may result in several features that favor the rapid conversion reaction during the second step. These features may include the formation of amorphous $PbI_2{\cdot}MAI$, the pre-expansion of the PbI_2 matrix, and reduced crystallinity of PbI_2. Moreover, using different amounts of MAI may allow the control of the pre-expansion of the $PbI_2{\cdot}x$MAI precursor film, which may give rise to the advantageous morphology shown in Figure 30 and may also affect the final photovoltaic performance of the perovskite solar cells based on the planar $CH_3NH_3PbI_3$ films.

[0081] Figure 32 summarizes photocurrent density-voltage (J-V) curves of planar $CH_3NH_3PbI_3$ solar cells prepared using different $PbI_2{\cdot}x$MAI (x: 0-0.3) under simulated one-sun illumination. These $PbI_2{\cdot}x$MAI films were dipped in the MAI solution for 2 min to form the $CH_3NH_3PbI_3$ layers, which were adjusted to about 250 nm thick. In the absence of MAI (i.e., using the standard PbI_2 precursor), the device shows a short-circuit photocurrent density (J_{sc}) of 8.847 mA/cm^2, open-circuit voltage (V_{oc}) of 0.969 V, fill factor (FF) of 0.712, and overall conversion efficiency (η) of 6.105%. The cell efficiency increases significantly when 0.1-0.2 MAI along with PbI_2 is used during the first-step deposition, especially when 0.15 MAI is used. A typical efficiency for the 0.15 MAI based device is increased to 15.622% with the J_{sc} of 19.888 mA/cm^2, V_{oc} of 1.065 and FF of 0.738. The performance improvement is largely determined by the increased J_{sc} value associated with enhanced PbI_2 conversion process and less perovskite damage resulting from minimized interaction with IPA solvent. The V_{oc} and FF values for the devices based on 0.1-0.2 MAI are also significantly larger than those of the cells based on the standard, pure PbI_2. However when 0.3 MAI is used, all device parameters are reduced with a typical J_{sc} of 13.867 mA/cm^2, V_{oc} of 0.967 V and FF of 0.668, yielding an efficiency of 8.977%. This is presumably due to the coarser morphology of $CH_3NH_3PbI_3$ when 0.3 MAI is used, since there is no PbI_2 residue found in the perovskite film. The significant drop in cell performance of the 0.3 MAI based device is consistent with its much reduced recombination resistance (or faster recombination) compared to the 0.1-0.2 MAI-based cells (Figure 33). The details of photovoltaic parameters of all these devices including the statistical analysis (mean values and standard deviations) for each type of devices are given in Table 6. Using 0.15 MAI, the best cell efficiency recorded is 16.76% (Figure 34a). The maximum power output of this device stabilizes at the efficiency of about 16.5% (Figure 34b), which is in good agreement with the value obtained from the J-V measurement.

Table 6

Effect of $PbI_2 \cdot x$MAI precursor composition (x: 0-0.3) on the device parameters of typical planar perovskite $CH_3NH_3PbI_3$ solar cells using two-step sequential deposition. The mean values and standard deviations of the device parameters from about 8 to 16 cells for each type of devices are given in parentheses.

Precursor Type	J_{sc} (mA/cm^2)	V_{oc} (V)	FF	η (%)
PbI_2 (standard)	8.847 (9.067±0.790)	0.969 (0.995±0.036)	0.712 (0.657±0.069)	6.105 (5.914±0.479)
PbI_2+0.1MAI	17.069 (18.009±1.603)	1.089 (1.097±0.013)	0.726 (0.714±0.039)	13.494 (14.087±1.208)
PbI_2+0.15MAI	19.888 (20.388±0.815)	1.065 (1.085±0.009)	0.738 (0.714±0.027)	15.622 (15.798±0.618)
PbI_2+0.2MAI	18.372 (18.526±0.792)	1.041 (1.056±0.020)	0.729 (0.721±0.063)	13.928 (14.263±1.253)
PbI_2+0.3MAI	13.867 (14.013±1.300)	0.967 (0.949±0.024)	0.668 (0.642±0.034)	8.977 (8.519±0.712)

[0082] In summary, the present disclosure provides the use of a precursor composition comprising a mixture of PbI_2 and MAI (molar ratio 1:x, where x varies from 0.1 to 0.3) to replace the pure PbI_2 used in the standard two-step sequential solution deposition of $CH_3NH_3PbI_3$. In comparison to the standard two-step approach, the use of additive MAI during the first step deposition leads to about 10-fold faster $CH_3NH_3PbI_3$ formation without any PbI_2 residue during the second MAI intercalation step and ultimately results in a much improved device performance when 0.1-0.2 MAI is used. The morphology of the $CH_3NH_3PbI_3$ film depends on the relative amount of MAI used in the $PbI_2 \cdot x$MAI precursor films during the first-step deposition, and generally demonstrates a smoother surface morphology when 0.1-0.2 MAI is used. Adding a small amount of MAI is found to lead to the formation of amorphous $PbI_2 \cdot$MAI, the pre-expansion of the PbI_2 matrix, and reduced crystallinity of PbI_2, all of which favor the complete conversion within a short period of time and thus minimizes the negative impact of the IPA solvent on the integrity of the $CH_3NH_3PbI_3$ film during the second dipping/conversion step of the standard two-step process. This new first-step precursor ($PbI_2 \cdot x$MAI) is promising for facile preparation of high-quality planar $CH_3NH_3PbI_3$ films with controllable morphologies via the new two-step sequential solution deposition methods described herein, to fabricate high-performance perovskite solar cells.

Experimental Setup and Device Preparation

[0083] CH_3NH_3I (MAI) was synthesized by reacting methylamine (33 wt% ethanol solution) and hydroiodic acid (57 wt% in water, Aldrich) and purified as previously reported. Unless otherwise stated, the mixtures of 0.784 g PbI_2 (1.7 mmol) and 0, 0.027g (0.17 mmol), 0.041g (0.26 mmol), 0.054 g (0.34 mmol), or 0.081g MAI (0.51 mmol) were dissolved in 2 mL dimethylformamide (DMF) at room temperature to form five different precursor solutions with mixed PbI_2 and MAI with a molar ratio of 1:x-noted as $PbI_2 \cdot x$MAI (x=0, 0.1, 0.15, 0.2, 0.3, respectively).

[0084] A patterned fluorine-doped tin oxide (FTO) was first deposited with a blocking layer by spray pyrolysis at 450°C using 0.2 M Ti(IV) bis(ethyl acetoacetate)-diisopropoxide 1-butanol solution, followed by 450 °C annealing in air for one hour. The different $PbI_2 \cdot x$MAI films were prepared by spin coating different $PbI_2 \cdot x$MAI precursor solutions (pre-warmed at 65°C) onto the substrate at 65°C at 6,000 rpm for 15 s. The spin coated $PbI_2 \cdot x$MAI films were dried in air for about 30-60 min before dipping in the 10 mg/mL MAI solution at 55°C for different duration. After quickly rinsed by anhydrous IPA twice, the $CH_3NH_3PbI_3$ perovskite films were annealed on a hotplate at 150°C for about 1 min, and then washed again by spin coating IPA at 4,000 rpm for 15 s, followed by an additional annealing at 150°C for 1 min. A hole-transport material (HTM) solution was spin-coated on the perovskite-covered TiO_2 electrodes at 4,000 rpm for 30 s. The HTM solution consists of 0.065 M spiro-MeOTAD, 0.053 M bis(trifluoromethane)sulfonimide lithium salt (Li-TFSi) and 0.20 M 4-*tert*-butylpyridine (tBP) in chlorobenzene/acetonitrile (30:1, v/v) solution. Finally, a 150-nm-thick Ag layer was deposited on the HTM layer by thermal evaporation. A typical cell area was about 0.12 cm^2 as defined by a shadow mask.

[0085] The crystal structures of the perovskite films were characterized by X-ray diffraction (XRD, Shimadzu XRD-6100 diffractometer with Cu K_α radiation). The morphologies of the perovskite films were examined on a FEI Sirion 200 scanning electron microscope (SEM). The optical absorption spectra of $CH_3NH_3PbI_3$ perovskite films were measured by a UV/Vis spectrophotometer (Cary-60). The photocurrent-voltage (J-V) characteristic and continuous power output of perovskite $CH_3NH_3PbI_3$ solar cells were measured respectively with a Keithley 2400 source meter and a potentiostat (Princeton Applied Research, VersaSTAT MC) under the simulated AM 1.5G illumination (100 mW/cm^2; Oriel Sol3A Class AAA Solar Simulator). Film thickness was measured by a surface profilometer (Dektak 8). Impedance spectroscopy

(IS) was done using a PARSTAT 2273 workstation with the frequency range of 0.1 Hz-100 kHz and the modulation amplitude of 10 mV. The IS spectra were analyzed using ZView 2.9c software (Scribner Associates).

EXAMPLE 5: AMMONIA SENSING

[0086] It has been found that $(CH_3NH_3)PbI_3$ is not stable (with color bleaching) under polar solvents or in solutions containing high iodine/iodide concentrations. Although the exact mechanism underlying this stability issue is unclear, the reported color bleaching for $(CH_3NH_3)PbI_3$ is irreversible. The $(CH_3NH_3)PbI_3$ film changes its color from brown to yellow when exposed to water, and cannot turn back from yellow to brown after the removal of water. This disclosure shows that the NH_3 gas induces a phase transformation of the perovskite $(CH_3NH_3)PbI_3$ film, leading to a rapid (<1 s) change of its color from brown to transparent across the entire visible spectral range. This color change is reversed within seconds upon removing the NH_3 gas. These findings suggest the potential use of perovskite halides (e.g., $(CH_3NH_3)PbI_3$) for NH_3 sensor applications. It is believed that this special material property of $(CH_3NH_3)PbI_3$ or similar halide perovskites could inspire a broader range of applications and fundamental investigations.

[0087] The $(CH_3NH_3)PbI_3$ films were deposited onto mesoporous TiO_2 nanocrystalline films on fluorine-doped tin oxide (FTO) by spin coating using a γ-butyrolactone solution comprising 35 wt% of stoichiometric PbI_2 and CH_3NH_3I, as described in previous reports. The effects of ammonia on the structural and optical properties of perovskite $(CH_3NH_3)PbI_3$ films were studied by X-ray diffraction (XRD, Rigaku D/Max 2200 diffractometer with Cu K_α radiation) and ultraviolet-visible (UV-vis, Cary-6000i) absorption techniques. The transient photoresponse of $(CH_3NH_3)PbI_3$ associated with the introduction and removal of the NH_3 source was probed with a 660-nm illumination using a silicon detector connected to a potentiostat (PARSTAT 2273).

[0088] Figures 35a-c show the sequence (left to right) of the color change of a $(CH_3NH_3)PbI_3$ film passing through the top opening of a bottle containing a 3% NH_3 solution. The perovskite film is deposited on a mesoporous TiO_2 film on FTO. The sample is held at each position for about 1-2 seconds. Interestingly, we find that the brown $(CH_3NH_3)PbI_3$ film (Fig. 35a) immediately becomes nearly colorless when it is in contact with the NH_3 gas (Fig. 35b), and rapidly turns back to the brown color once the NH_3 source is removed (Fig. 35c).

[0089] Figures 36a-b includes (a) UV-vis absorption spectra of a $(CH_3NH_3)PbI_3$ film in the absence and in the presence of NH_3 gas. (b) Photoresponse (transmitted light intensity) of a $(CH_3NH_3)PbI_3$ film at 660 nm as measured by a silicon detector in response to the introduction (on) and removal (off) of NH_3 gas. Figure 36a compares the UV-vis absorption spectra of the perovskite $(CH_3NH_3)PbI_3$ film in the absence and in the presence of NH_3. In the absence of NH_3, the $(CH_3NH_3)PbI_3$ film starts to absorb around 750-800 nm and absorbs strongly below 600 nm, which agrees with our previous study. In contrast, the absorption spectrum of the $(CH_3NH_3)PbI_3$ film across the entire visible region is essentially reduced to zero(i.e., the film becomes transparent in the visible region) when the perovskite film is exposed to the NH_3 gas.

[0090] The significant contrast of the optical absorption of the perovskite $(CH_3NH_3)PbI_3$ film in the presence and in the absence of NH_3 suggests that the $(CH_3NH_3)PbI_3$ film could potentially be used for optical NH_3 sensing applications. Because the perovskite $(CH_3NH_3)PbI_3$ film has a very wide response over the entire visible spectral range (i.e., the disappearance/substantial decrease of the entire absorption spectrum from 400 to 800 nm), the change of the absorption spectrum of the $(CH_3NH_3)PbI_3$ film at any single wavelength or wavelength range from 400 to 800 nm can be used. Figure 36b shows the photoresponse (transmitted light intensity) at 660 nm as measured by a silicon detector. The transmitted light intensity increases immediately (<1 s) after the introduction of NH_3 and also decreases quickly (1-2 s) after NH_3 is removed. It is noteworthy that other perovskite halides (e.g., $(CH_3NH_3)PbI_{3-x}Cl_x$ and $(CH_3NH_3)PbBr_3$) exhibit similar optical changes in the presence of NH_3.

[0091] To understand the effect of NH_3 on the optical change of the perovskite film, we carried out XRD measurements on the perovskite samples in the presence and in the absence of the NH_3 environment (Fig. 37). For comparison, the XRD patterns of the TiO_2/FTO substrate and PbI_2 deposited on the TiO_2/FTO substrate are also shown in Fig. 37. The perovskite $(CH_3NH_3)PbI_3$ film shows the standard XRD pattern, as we described previously. Several characteristic peaks associated with the perovskite structure are denoted with asterisks. The XRD pattern of the perovskite film changes substantially after the film is exposed to the NH_3 gas. The characteristic XRD peaks (e.g., at 14.02°) for $(CH_3NH_3)PbI_3$ either disappear or become indistinguishable from the background signal. Interestingly, an unknown peak at about 11.6° arises after the NH_3 treatment. This characteristic peak cannot be assigned to either $(CH_3NH_3)PbI_3$ or PbI_2. It is also noteworthy that the XRD pattern of the $(CH_3NH_3)PbI_3$ film in the presence of NH_3 cannot be matched to other possible compounds such as NH_4PbI_3, $Pb(NH_3)_4I_3$ and $NH_4PbI_3.xH_2O$. Thus, further studies are required to identify the crystal structure of the perovskite film subjected to the NH3 treatment. Based on the results above, it is evident that the dramatic change of the optical property of the perovskite film results from its interaction with NH_3 at room temperature.

[0092] To our knowledge, previous studies provide virtually no information on the phase transition of organometallic halide perovskites induced by NH_3 at room temperature. It is well known that metal oxide perovskites (e.g., Sr_2RuO_4) are layered materials (due to their strong in-plane chemical bonding and weak out-of-plane bonding) and thus can be easily exfoliated by a solution process. The metal oxide perovskites are usually exfoliated through a liquid-phase transformative process via ion-exchange and intercalation reactions. PbI_2 also has a layered structure. It was shown previously that the yellow PbI_2 can turn colorless by reacting with nitrogen-containing molecules (e.g., ammonia or pyridine) to form either an intercalation compound or a coordination complex; these colorless products can largely reverse back to the yellow PbI_2 once the nitrogen source is removed. Inasmuch as $(CH_3NH_3)PbI_3$ shows essentially the same optical change as PbI_2 when NH_3 is introduced to or removed from the perovskite film, we hypothesize that NH_3 either intercalates into or forms a new coordination complex with the perovskite network and that the crystal structure of $(CH_3NH_3)PbI_3$ can also be largely restored once the NH_3 source is removed. It is noteworthy that the $(CH_3NH_3)PbI_3$ film exposed to NH_3 for a long period of time (e.g., tens of minutes) does not turn back to the brown color when the NH_3 source is removed. The exact mechanism of NH_3-induced phase transformation of $(CH_3NH_3)PbI_3$ is still uncertain. Further studies are required to understand how the crystal structure of $(CH_3NH_3)PbI_3$ evolves in the presence of NH_3 and then how the crystal structure of NH_3-treated $(CH_3NH_3)PbI_3$ changes with the removal of the NH_3 environment.

[0093] In summary, we investigated the impact of a NH_3 gas environment on the structural and optical properties of perovskite $(CH_3NH_3)PbI_3$. A mild treatment of NH_3 to $(CH_3NH_3)PbI_3$ at room temperature strongly affects its crystal structure and physical appearance. The color of the $(CH_3NH_3)PbI_3$ film changes immediately (<1 s) from brown to colorless (i.e., transparent from 400 to 800 nm) in the presence of NH_3. The color of the NH_3-treated $(CH_3NH_3)PbI_3$ film turns back to brown within 1-2 s after the NH_3 environment is removed. XRD measurements show that the crystal structure of perovskite $(CH_3NH_3)PbI_3$ changes significantly when the perovskite film is exposed to NH_3. This structure change could result from the formation of either an intercalation compound or a coordination complex from $(CH_3NH_3)PbI_3$ and NH_3. The results of this study imply that organometallic halide perovskites (e.g., $(CH_3NH_3)PbI_3$) could potentially be used as ammonia sensors with both a fast response time and a wide range of spectral response. Thus, understanding how halide perovskites interact with their surrounding environment will help researchers fully use the unique properties of this new absorber system for solar cell applications, but may also lead to potential applications of these materials in different fields.

EXAMPLE 6: MOLYBDENUM OXIDE TOP CONTACT

[0094] At present, perovskite solar cells are often made with two types of common device architectures, i.e., either mesostructured or planar thin-film solar cells. The first type is similar to the conventional solid-state dye-sensitized solar cells (DSSCs). A key component of this device configuration is a mesoporous metal-oxide (e.g., TiO_2) layer that is first coated with nanostructured perovskite absorbers and then infiltrated with a hole transport material (HTM; e.g., spiro-MeOTAD). In addition to being the light absorber, perovskite can also be used as a hole conductor. In this situation, the standard HTM layer can be avoided. For the planar perovskite solar cells, a thin layer (a few hundred nanometers) of perovskite absorber is sandwiched between the electron- and hole-contact layers (e.g., TiO_2 and spiro-MeOTAD, respectively). For both the mesostructured and planar perovskite solar cells, a layer (about 80-150 nm thick) of Au or Ag is often used as the top metal contact for carrier extraction. Replacing Au or Ag with a low-cost material/structure that can also effectively extract photogenerated holes would help reduce the overall cost for producing perovskite solar cells.

[0095] This disclosure demonstrates that a thin layer (10 nm) of molybdenum oxide (MoO_x) coupled with Al can be used as an effective top-contact structure for extracting photogenerated holes from perovskite $CH_3NH_3PbI_3$ solar cells. In recent years, transition metal oxides (TMO; e.g., MoO_x) have been used as either an interlayer or buffer layer for a variety of optoelectronic devices to improve either hole injection (e.g., in organic light-emitting diodes) or hole extraction (e.g., in organic photovoltaics, CdTe, Si, and quantum-dot solar cells). We find that the device performance of perovskite solar cells using a MoO_x/Al top contact is comparable to that of cells using the standard Ag top contact. Analysis of impedance spectroscopy measurements shows that using 10-nm-thick MoO_x and Al does not affect charge-recombination properties. However, a thicker (20-nm) MoO_x layer leads to decreased cell performance resulting primarily from a reduced fill factor.

[0096] The precursor of CH_3NH_3I was synthesized and purified as previously reported. The pre-patterned fluorine-doped SnO_2-coated glass substrate (FTO; TEC15, Hartford, USA) was coated with a compact TiO_2 layer by spray pyrolysis using 0.2 M Ti(IV) bis(ethyl acetoacetate)-diisopropoxide in 1-butanol at 450°C. A mixture of $PbCl_2$ and CH_3NH_3I (1:3 molar ratio) was dissolved in dimethylformamide (DMF) to form the precursor solution, which was spin-coated onto the TiO_2/FTO substrate at 2500 rpm for 10 s, followed by annealing at 100°C for 45 min in air. A spiro-MeOTAD-based HTM solution with a previously reported recipe was spin-coated on the perovskite-covered TiO_2 electrodes at 4000 rpm for 30 s. A thin layer (0-20 nm) of MoO_x was deposited by thermal evaporation. Finally, a 150-nm-thick metal (Ag or Al) layer was deposited by thermal evaporation. The active area of each device was about 0.2-0.3 cm^2. The X-ray diffraction (XRD) patterns of the perovskite films were conducted using Rigaku D/Max 2200 diffractometer with Cu K_α radiation. The ultraviolet/visible (UV/vis) spectra were characterized by an ultraviolet/visible-near infrared (UV/vis-NIR) spectrophotometer (Cary-6000i). The morphology of perovskite film was examined by a field-emission scanning electron microscopy (FE-SEM, JEOL JSM-7000F). The photocurrent density-voltage (J-V) characteristic of perovskite solar cells were studied using a class AAA solar simulator (Oriel Sol3A). Impedance spectroscopy (IS) was done with a PARSTAT

2273 workstation with the frequency range of 0.1 Hz-100 kHz and modulation amplitude of 10 mV.

[0097] Figure 38 displays the XRD patterns of a perovskite $CH_3NH_3PbI_3$ film deposited on a compact TiO_2 layer on the FTO-coated glass substrate. We observe characteristic perovskite diffraction peaks (denoted by stars) at about 14.1, 28.44, 31.88, and 43.24°, respectively, corresponding to the diffractions from (110), (220), (310), and (314) crystal planes of the $CH_3NH_3PbI_3$ perovskite structure. The positions of these diffraction peaks are consistent with previous reports. The other XRD peaks are attributable to the TiO_2/FTO substrate. No secondary phases (e.g., PbI_2) are found. The typical UV-vis absorption spectrum for the same perovskite $CH_3NH_3PbI_3$ film is shown in the inset of Fig. 38. Consistent with our previous reports, the $CH_3NH_3PbI_3$ film strongly absorbs the illumination below 600 nm. The absorbance of $CH_3NH_3PbI_3$ decreases slightly with increasing wavelength from about 600 to 750 nm and then drops rapidly when the wavelength approaches the bandgap near 800 nm.

[0098] Figure 39a shows the typical cross-sectional SEM image of the planar perovskite $CH_3NH_3PbI_3$ solar cell with the following layered structure: FTO/compact TiO_2/perovskite absorber/spiro-MeOTAD/MoO_x/metal. In this study, the metal layer is either Ag or Al. Although it is not evident in the SEM image, a 10-nm MoO_x interlayer is deposited by thermal evaporation between the spiro-MeOTAD and metal layers. The average thickness of the $CH_3NH_3PbI_3$ layer is about 300 nm, and the average thickness of the HTM layer (spiro-MeOTAD) is about 280 nm. In Figure 39b, we test the effect of MoO_x interlayer thickness on the *J-V* characteristics of perovskite $CH_3NH_3PbI_3$ solar cells using the Ag top contact. In the absence of MoO_x, the device displays a short-circuit photocurrent density (J_{sc}) of 19.94 mA/cm^2, open-circuit voltage (V_{oc}) of 1.011 V, and fill factor (FF) of 0.613 to yield an efficiency (η) of 12.36%. When 5-nm and 10-nm MoO_x layers are used, the respective efficiencies are 11.49% and 12.04%. The mean values and standard deviations of the PV parameters from 8-20 cells for these device architectures are given in Table 7. It is evident that the 5-nm and 10-nm MoO_x cells have essentially the same performance level as the cell without the MoO_x layer, within experimental error. However, when a 20-nm-thick MoO_x layer is used, the cell efficiency is significantly reduced from about 12% to 9.33%. The decrease of cell efficiency is primarily caused by the much reduced FF, which is in agreement with a recent study on the effect of MoO_x layer thickness on the device characteristics of Si solar cells. The details of the photovoltaic parameters (J_{sc}, V_{oc}, FF, and η) for all these cells are given in Table 7.

Table 7

Effect of the top layer (hole-contact) structure on the short-circuit photocurrent density J_{sc}, open-circuit voltage V_{oc}, fill factor FF, and conversion efficiency η of champion planar perovskite $CH_3NH_3PbI_3$ solar cells. The mean values and standard deviations of the PV parameters from 8-20 cells for each type of devices are given in parentheses.

Cell Type	J_{sc} (mA/cm^2)	V_{oc} (V)	FF	η (%)
HTM/Ag	19.94 (19.45±0.90)	1.011 (0.967±0.040)	0.613 (0.538±0.043)	12.36 (10.13±0.99)
HTM/5-nm MoO_x/Ag	19.60 (19.43±0.60)	0.985 (0.952±0.026)	0.595 (0.544±0.027)	11.49 (10.08±0.81)
HTM/10-nm MoO_x/Ag	20.14 (20.37±0.95)	0.993 (0.962±0.021)	0.602 (0.543±0.036)	12.04 (10.63±0.70)
HTM/20-nm MoO_x/Ag	19.56 (19.22±0.82)	1.008 (0.964±0.024)	0.473 (0.439±0.025)	9.33 (8.15±0.64)
HTM/10-nm MoO_x/Al	19.55 (19.31±0.85)	0.990 (0.972±0.023)	0.590 (0.542±0.030)	11.42 (9.85±0.91)
HTM/Al	0.92 (0.67±0.26)	0.182 (0.119±0.104)	0.165 (0.203±0.060)	0.027 (0.015±0.011)
10-nm MoO_x/Ag	0.84 (0.66±0.13)	0.045 (0.034±0.016)	0.261 (0.254±0.025)	0.01 (0.006±0.003)

[0099] Having established that MoO_x works as an effective interlayer for hole extraction in our regular device architecture, we compare in Fig. 40a the *J-V* characteristics of perovskite $CH_3NH_3PbI_3$ solar cells using different top-contact structures, including: (1) HTM/Ag, (2) HTM/MoO_x/Ag, (3) HTM/MoO_x/Al, (4) HTM/Al, and (5) MoO_x/Ag (no HTM). For top-contact structures (2), (3), and (5), we used a fixed 10-nm-thick MoO_x layer. The composition of the spiro-MeOTAD-based HTM layer is given in detail in the experimental section. Using the HTM/MoO_x/Al contact structure, the cell efficiency is 11.42% with a J_{sc} of 19.55 mA/cm^2, V_{oc} of 0.990 V, and FF of 0.590. All of these parameters are comparable to those of the cells using HTM/Ag and HTM/MoO_x/Ag contact structures (Table 7). Consistent with the *J-V* results, the incident photon-to-current efficiency (IPCE) spectra for cells based on contact structures (1)-(3) are essentially identical (Fig. 40b). These results suggest that the junction between MoO_x and the metal contact is not critical to hole extraction in perovskite solar cells. This observation agrees with other studies where MoO_x is used as an interlayer in organic solar cells and quantum-dot solar cells[28] to facilitate extraction of photogenerated holes. It is worth noting that these studies demonstrated improved cell performance using the MoO_x interlayer than the control sample without the MoO_x layer. In contrast, our study shows that cells using HTM/MoO_x/Ag or HTM/MoO_x/Al have comparable performance to the control cells using HTM/Ag. This is presumably caused by the use of HTM in this study, whereas in other studies the MoO_x layer is deposited directly on the absorber layer. Interestingly, we find that when Al is deposited directly on top of the HTM layer (i.e., no MoO_x is used), the perovskite solar cell only shows a conversion efficiency of 0.027% with a J_{sc} of 0.92 mA/cm^2, V_{oc} of 0.182 V, and FF of 0.165. This could be attributed to the formation of a back diode at the HTM/A1 interface, which creates an energy barrier limiting hole extraction. It was shown previously for PbS quantum dot solar cells that the back-diode effect can be significantly reduced when using higher work-function metals (e.g., Au or Ag) or can be completely removed by using a MoO_x interlayer. It is worth noting that using MoO_x/Ag directly on the perovskite absorber layer (i.e., no HTM layer) leads to a 0.01% device (Table 7). This is presumably caused by shorting associated with pinholes on the absorber layer. The use of the HTM layer appears to be effective in suppressing shorting in perovskite cells.

[0100] Impedance spectroscopy is used to study the impact of top-contact structure on the recombination resistance (R_{rec}) for the perovskite solar cells. Fig. 41a shows the typical Nyquist plots of the complex impedance Z (i.e., the imaginary component Im [Z] versus the real component Re [Z] of the impedance) for a perovskite cell with three different bias voltages. The impedance spectra are dominated by a large semicircle at low frequencies. This feature has been attributed to charge recombination either at the interface between perovskite and contact layers or within the bulk perovskite layer. A larger semicircle corresponds to a larger recombination resistance R_{rec}, which is inversely proportional to the recombination rate. The model used for impedance analysis has been previously discussed in detail by others. From these Nyquist plots, the recombination resistance of the perovskite cells can be determined. Fig. 41(b) shows the R_{rec} values as a function of voltage for perovskite solar cells using the top-contact structures (1)-(3). The R_{rec} for all these cell structures depends strongly on the bias voltage, following an approximately exponential decrease with voltage. Similar voltage dependence of recombination resistance for perovskite solar cells has been reported previously. Interestingly, there is not much difference in recombination resistance among the three samples despite the significant difference in their top-contact structures, which suggests that the MoO_x/metal interface does not affect charge transfer at the back contact. This is in agreement with the *J-V* measurements in Fig. 40a. Thus, the *J-V* and impedance results suggest that MoO_x/Al can be used as an effective hole-extraction contact to replace more expensive metal contacts (e.g., Ag or Au) for perovskite solar cells.

[0101] In summary, we demonstrate the effectiveness of using a combination of a thin layer of molybdenum oxide and aluminum as the top-contact structure for extracting photogenerated holes from perovskite solar cells. MoO_x is deposited by thermal evaporation. The device performance of perovskite solar cells using a MoO_x/Al top contact is comparable to that of cells using the standard Ag top contact. Impedance measurements suggest that the extraction of photogenerated holes is not affected by the MoO_x/metal interface when proper MoO_x thickness (e.g., 10 nm) is used. Using a thicker (20-nm) MoO_x layer leads to decreased cell performance resulting primarily from a reduced fill factor.

[0102] Figure 42 shows the pictures of the perovskite solar cells after 15 hour continuous light soaking under simulated one sun illumination. The devices using MoOx showed essentially no color change of the illuminated areas. In contrast, the device without MoOx layer showed significant color change from brown to yellow, suggesting the degradation of the perovskite layer under illumination.

[0103] Figure 43 shows the dependence of solar cell efficiencies as a function of continuous light soaking under simulated one sun illumination for 15 hours. The efficiencies are normalized for easy comparison. The devices using MoO_x/Al layer showed the best devices stability among the cells tested.

[0104] While a number of exemplary aspects and embodiments have been discussed above, those of skill in the art will recognize certain modifications, permutations, additions and sub combinations thereof. It is therefore intended that the following appended claims and claims hereafter introduced are interpreted to include all such modifications, permutations, additions and sub-combinations as are within their true spirit and scope.

[0105] Finally, it should be noted that there are alternative ways of implementing the embodiments disclosed herein. Accordingly, the present embodiments are to be considered as illustrative and not restrictive, and the claims are not to be limited to the details given herein, but may be modified within the scope and equivalents thereof.

[0106] From the foregoing description, various modifications and changes in the compositions and methods of the present disclosure will occur to those skilled in the art. All such modifications coming within the scope of the appended claims are intended to be included therein.

Claims

1. A method of forming a perovskite film, the method comprising:

applying a first solution onto a substrate, the first solution comprising in a first solvent, a first alkyl ammonium

halide with a first halogen, and a metal halide with a second halogen different from the first halogen;
completing a first thermal treatment of the first solution to form a first film of the metal halide on the substrate; and
contacting a second solution with the first film, the second solution comprising in a second solvent, a second alkyl ammonium halide with the second halogen, wherein the second alkyl ammonium halide reacts with the first film to form a final crystalline alkyl ammonium metal halide perovskite film that is substantially free of the first film and the first halogen.

2. The method of claim 1, further comprising, during at least a portion of the contacting, completing a second thermal treatment of the second solution and the first film.

3. The method of either claims 1 or 2, wherein the first thermal treatment forms an unstable intermediate film comprising the metal halide and an alkyl ammonium metal halide with the first halogen, wherein the intermediate film subsequently changes to form the first metal halide film.

4. The method of any one of claims 1-3, wherein the first halogen and the second halogen comprise fluorine, chlorine, bromine, iodine, or astatine.

5. The method of any one of claims 1-4, wherein the first halogen has a lower molecular weight than the second halogen.

6. The method of any one of claims 1-5, wherein the first halogen is chlorine and the second halogen is iodine.

7. The method of any one of claims 1-6, wherein an alkyl group for at least one of the first alkyl ammonium halide or the second alkyl ammonium halide comprises at least one of a methyl group, an ethyl group, a propyl group, or a butyl group.

8. The method of any one of claims 1-7, wherein a metal of the metal halide comprises at least one of lead, tin, germanium, or any other metal in the 2+ valence state.

9. The method of any one of claims 1-8, wherein the first solvent comprises at least one polar solvent.

10. The method of any one of claims 1-9, wherein the second solvent comprises isopropyl alcohol.

11. The method of any one of claims 1-10, wherein the metal halide and the first alkyl ammonium halide are present in the first solution at a molar ratio ranging from about 1:0.1 to about 1:3.

12. The method of any one of claims 1-11, wherein at least one of the metal halide and the first alkyl ammonium halide are present in the first solution at a concentration ranging from about 0.1 M to about 3.0 M.

13. The method of any one of claims 1-12, wherein the second alkyl ammonium halide is present in the second solution at a concentration ranging from 0.1 mg/ml solvent to about 100 mg/ml solvent.

14. The method of any one of claims 1-13, wherein at least one of the thermal treatments comprises heating at least one of the solutions at a temperature ranging from about 40°C to about 250°C.

15. The method of any one of claims 1-14, wherein at least one of the thermal treatments comprises heating at least one of the solutions for a period of time ranging from about 30 seconds to about 6 hours.

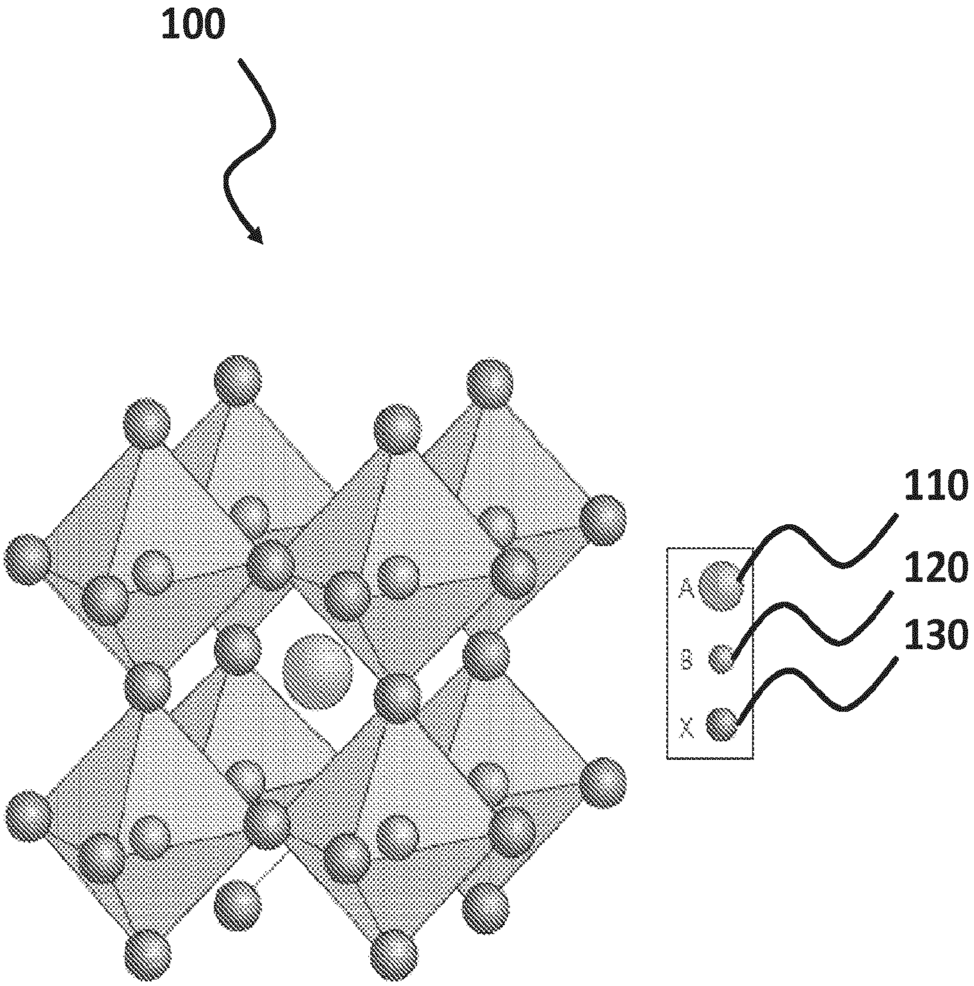

Fig. 1

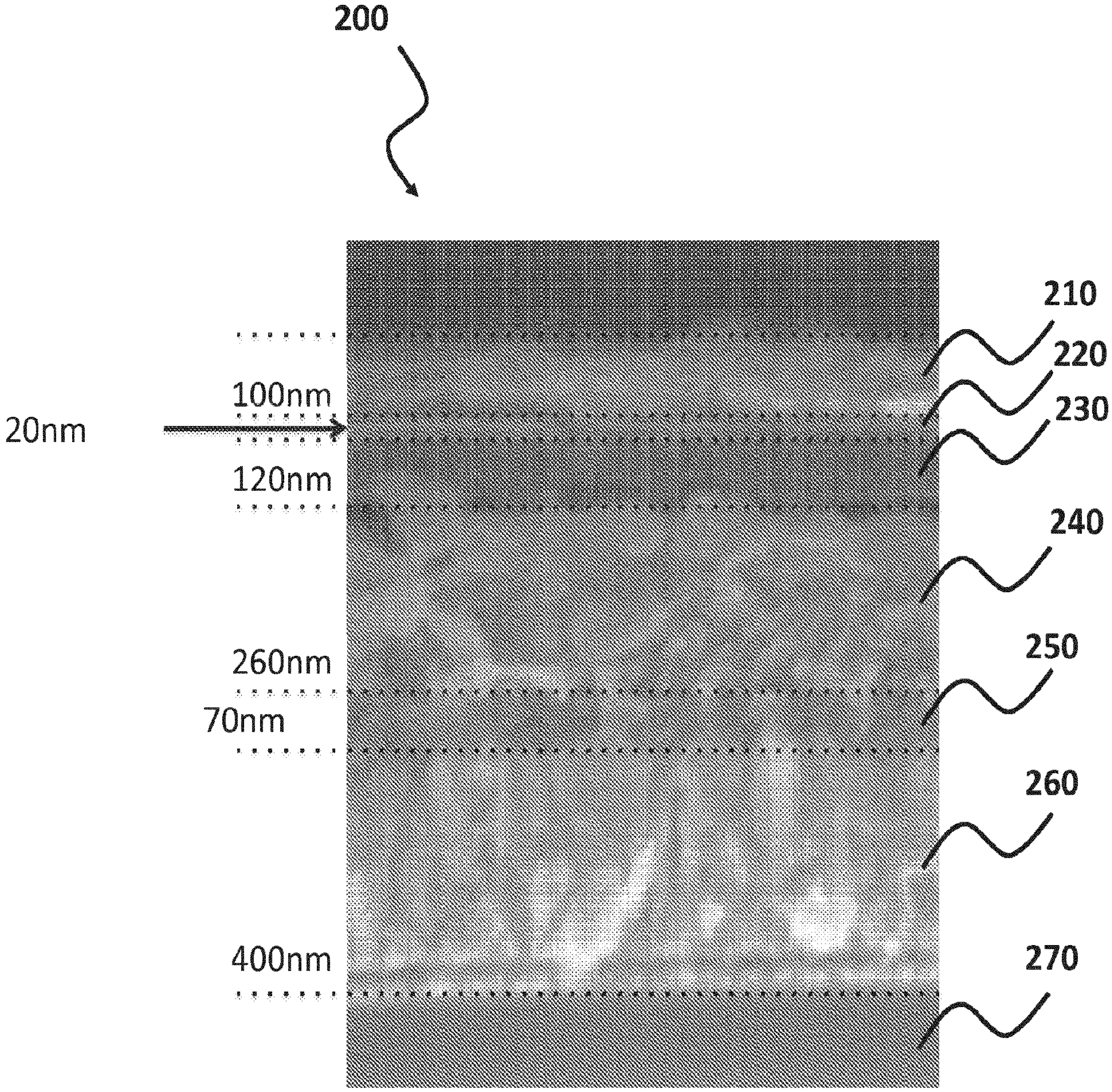
200
210
220
230
240
250
260
270
20nm
100nm
120nm
260nm
70nm
400nm

Fig. 2

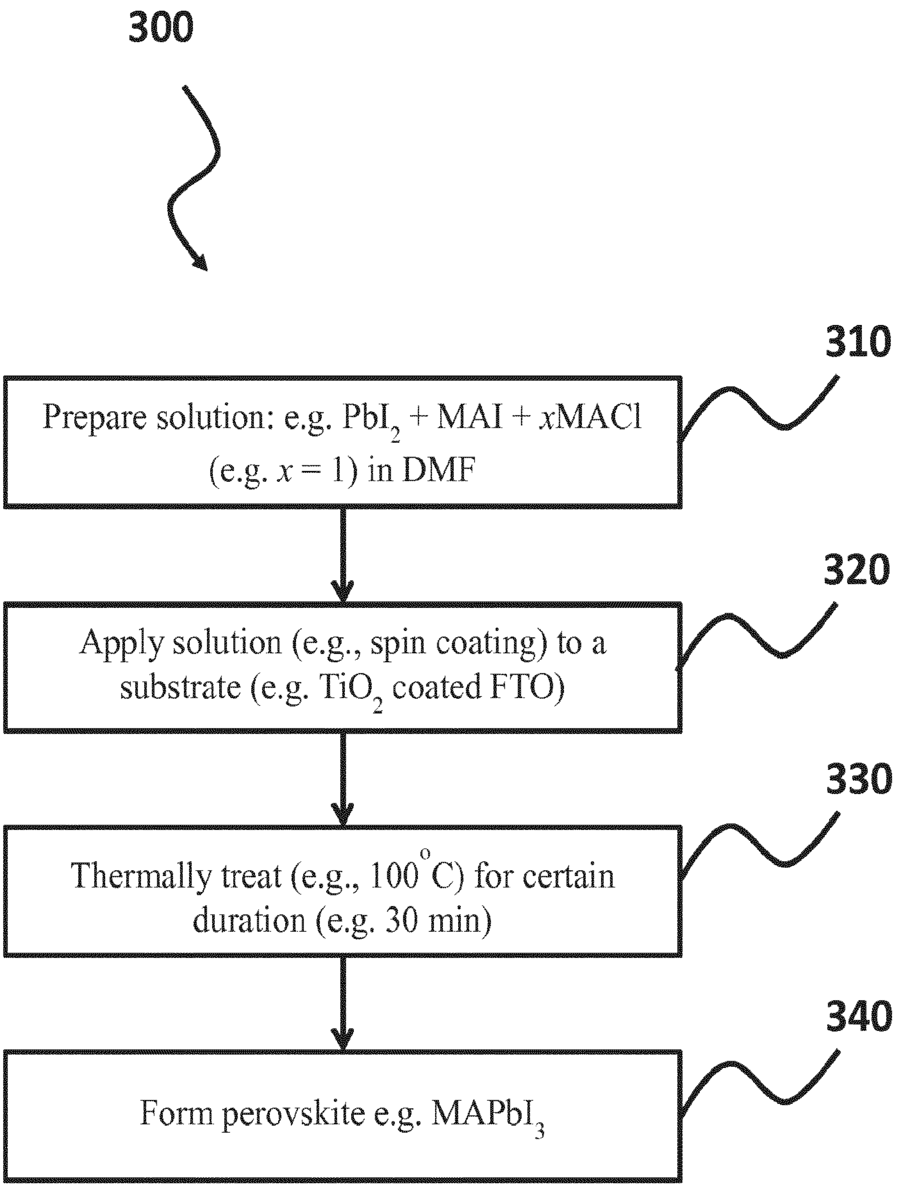
300
310
Prepare solution: e.g. PbI2 + MAI + xMACl (e.g. x = 1) in DMF
320
Apply solution (e.g., spin coating) to a substrate (e.g. TiO2 coated FTO)
330
Thermally treat (e.g., 100°C) for certain duration (e.g. 30 min)
340
Form perovskite e.g. MAPbI3

Fig. 3

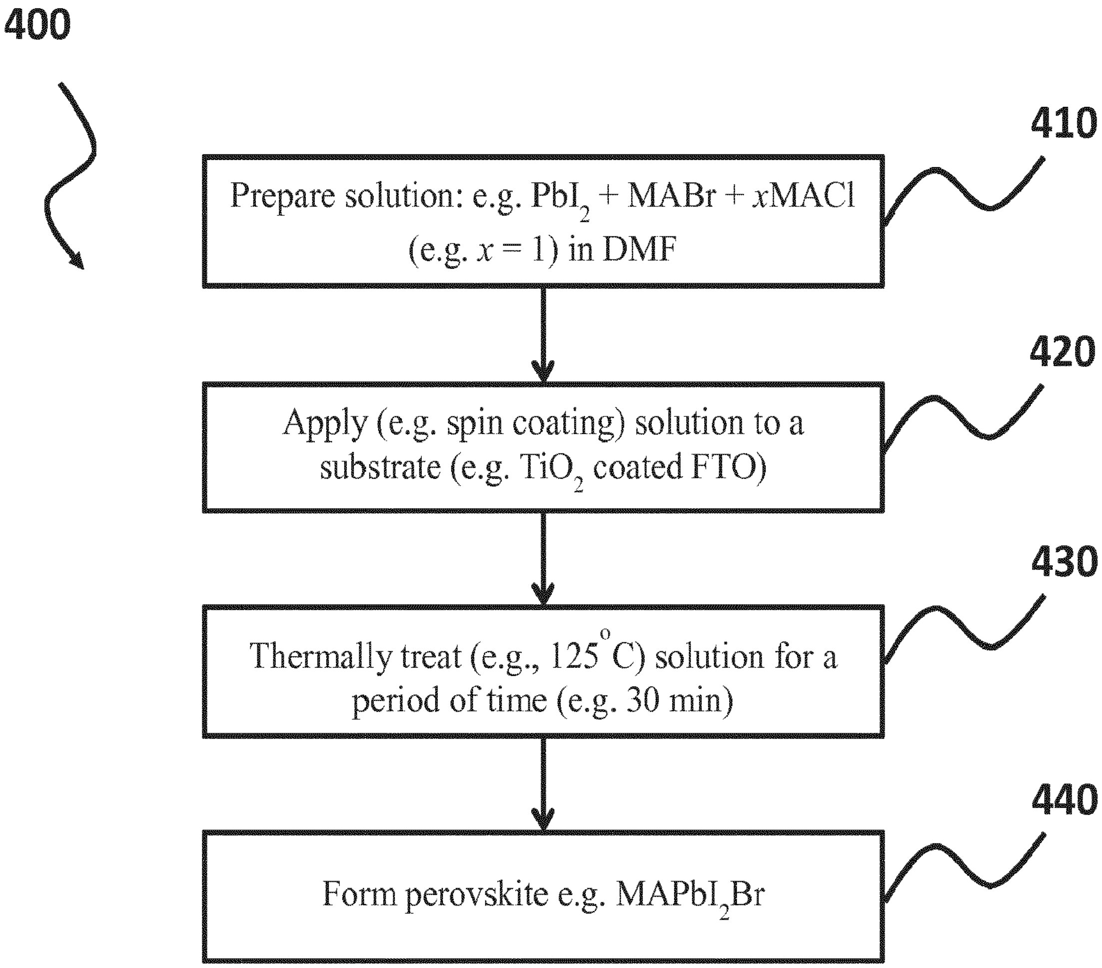
400
410
Prepare solution: e.g. PbI2 + MABr + xMACl (e.g. x = 1) in DMF
420
Apply (e.g. spin coating) solution to a substrate (e.g. TiO2 coated FTO)
430
Thermally treat (e.g., 125°C) solution for a period of time (e.g. 30 min)
440
Form perovskite e.g. MAPbI2Br

Fig. 4

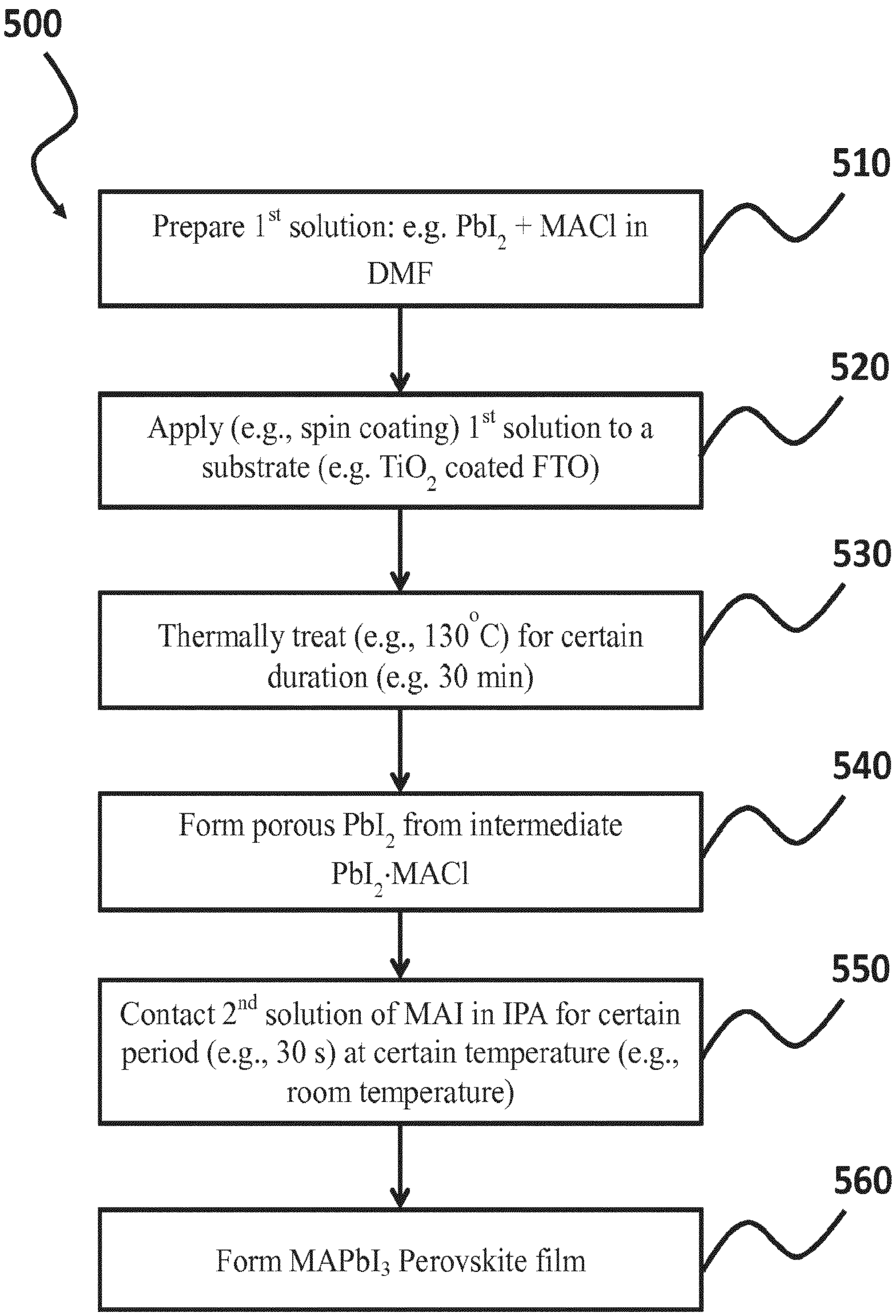
500
510
Prepare 1st solution: e.g. PbI_2 + MACl in DMF
520
Apply (e.g., spin coating) 1st solution to a substrate (e.g. TiO_2 coated FTO)
530
Thermally treat (e.g., 130°C) for certain duration (e.g. 30 min)
540
Form porous PbI_2 from intermediate PbI_2·MACl
550
Contact 2nd solution of MAI in IPA for certain period (e.g., 30 s) at certain temperature (e.g., room temperature)
560
Form $MAPbI_3$ Perovskite film

Fig. 5

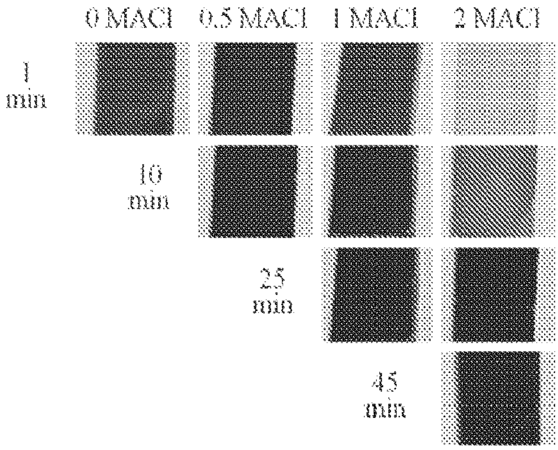

Fig. 6

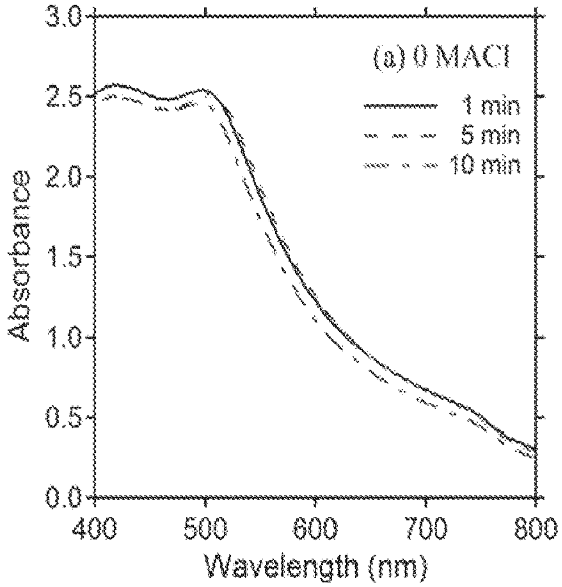

Fig. 7a

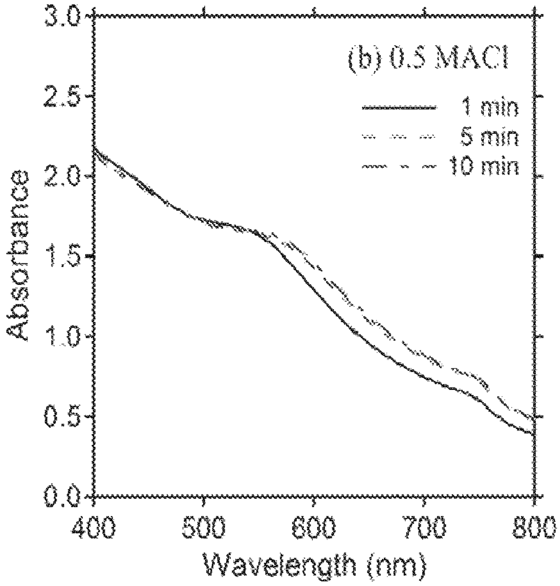

Fig. 7b

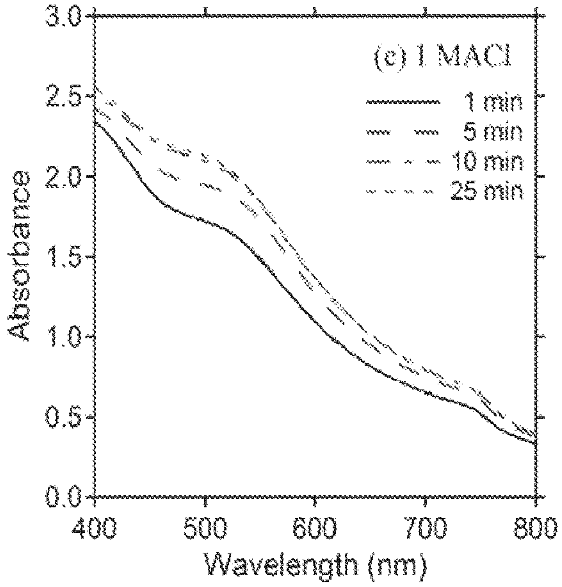

Fig. 7c

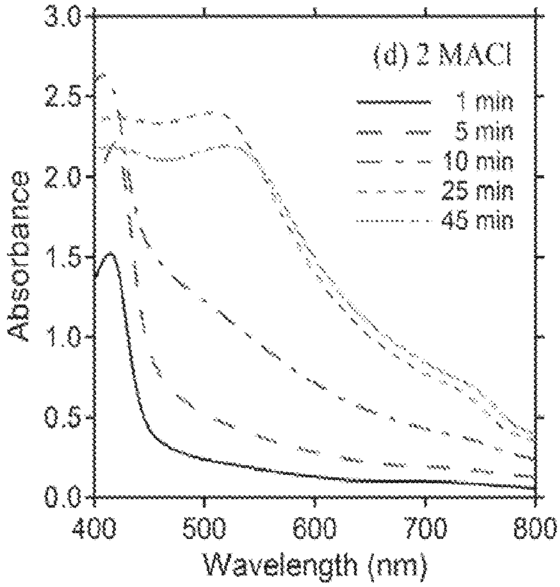

Fig. 7d

Fig. 8a

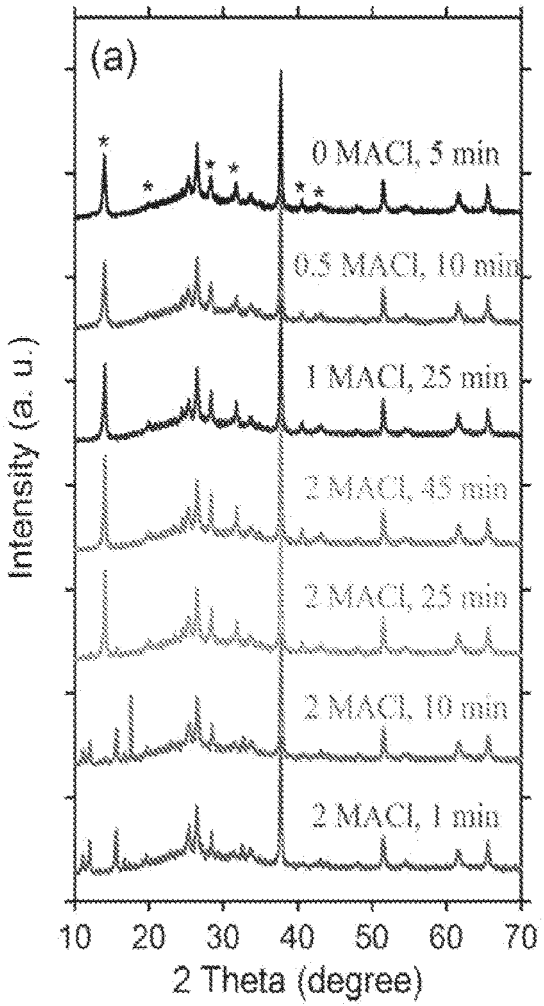

Fig. 8b

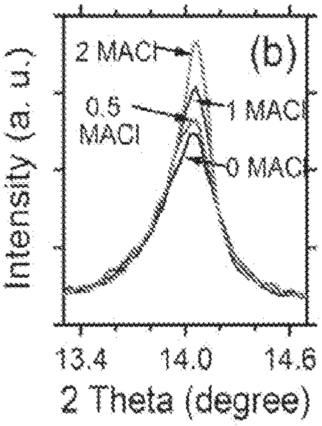

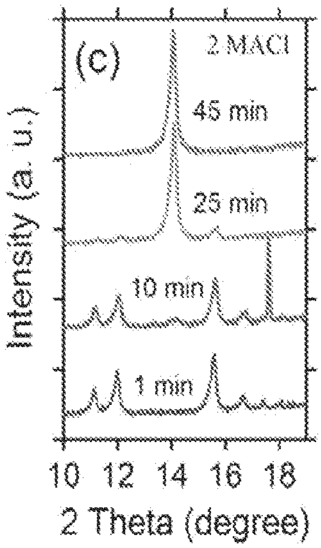

Fig. 8c

Fig. 9a

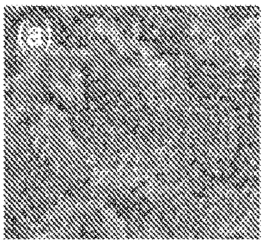

Fig. 9b

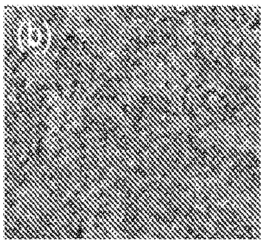

Fig. 9c

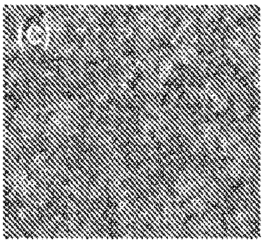

Fig. 9d

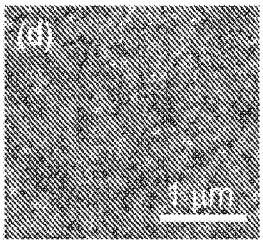

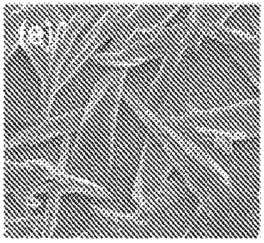

Fig. 9e

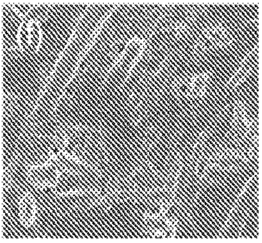

Fig. 9f

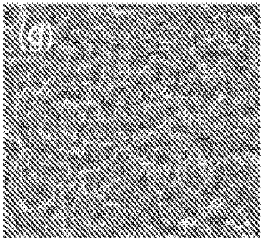

Fig. 9g

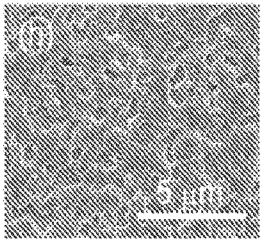

Fig. 9h

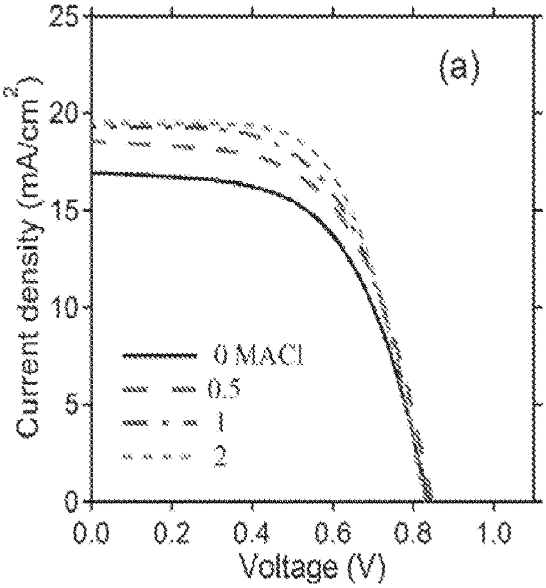

Fig. 10a

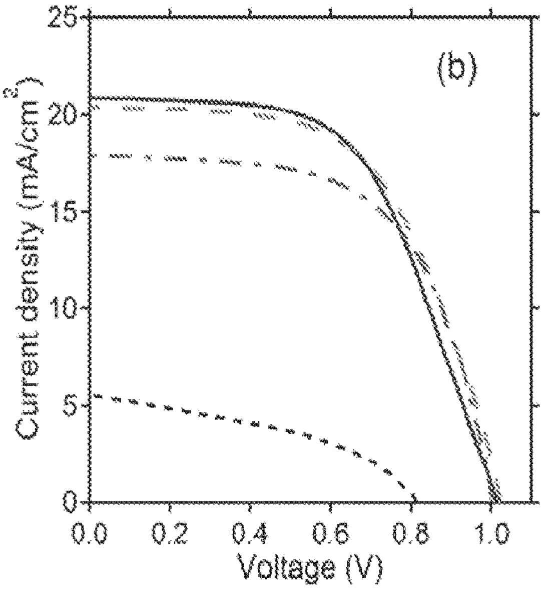

Fig. 10b

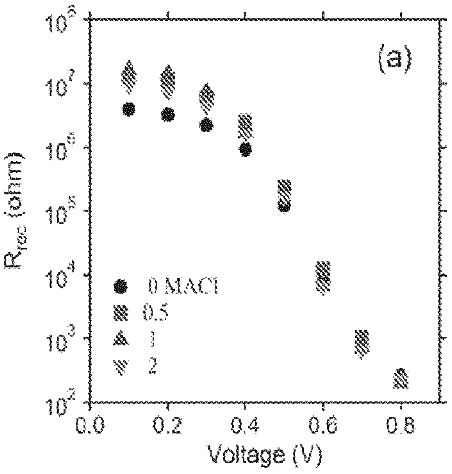

Fig. 11a

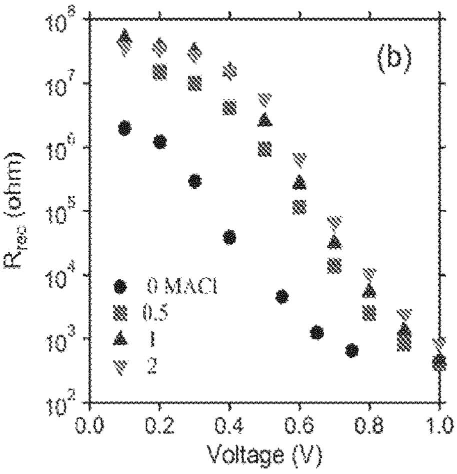

Fig. 11b

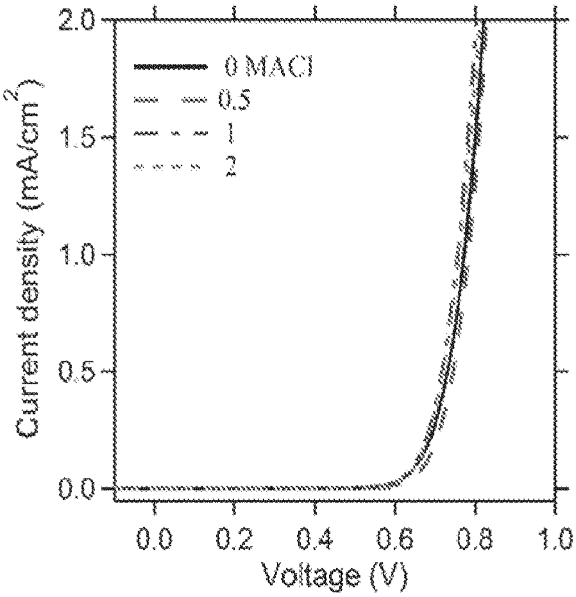

Fig. 12a

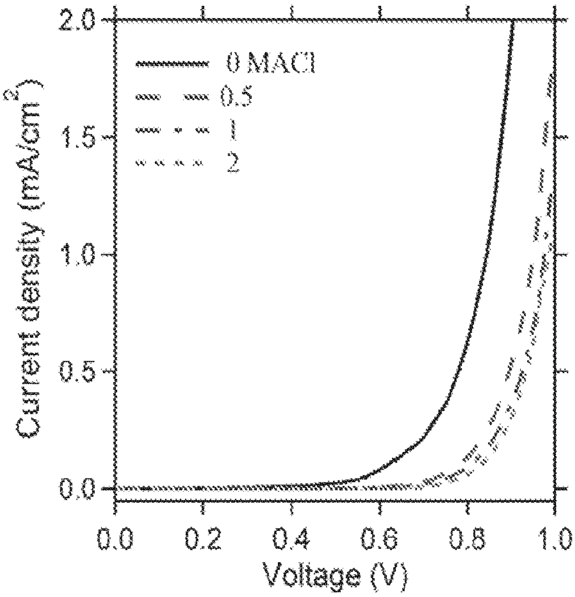

Fig. 12b

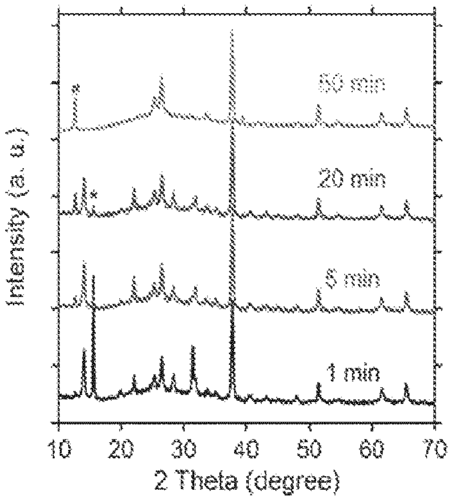
Intensity (a. u.)
2 Theta (degree)
10
20
30
40
50
60
70
*
60 min
*
20 min
5 min
1 min

Fig. 13

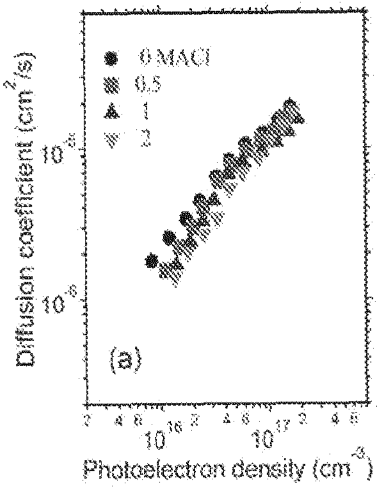

Fig. 14a

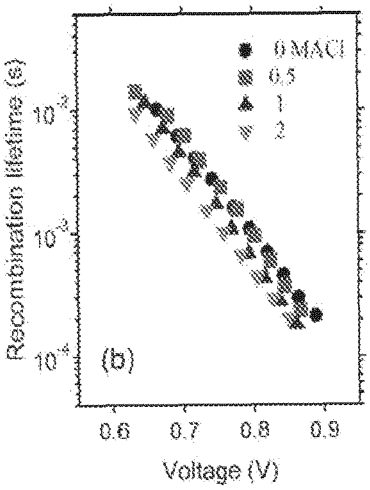

Fig. 14b

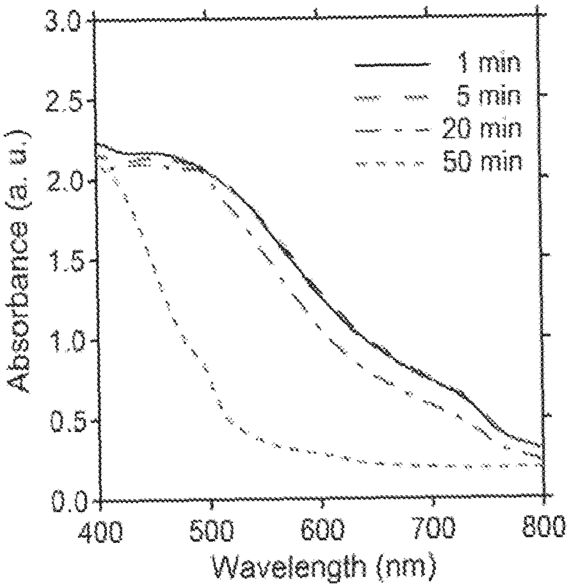
3.0
2.5
2.0
1.5
1.0
0.5
0.0
Absorbance (a. u.)
400
500
600
700
800
Wavelength (nm)
1 min
5 min
20 min
50 min

Fig. 15

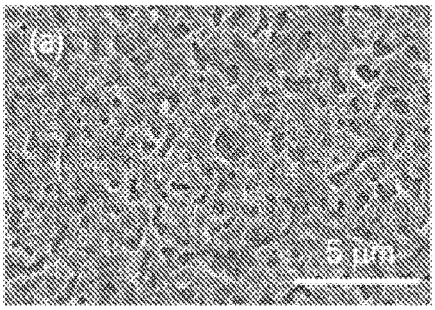

Fig. 16a

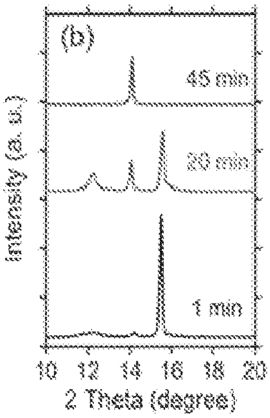

Fig. 16b

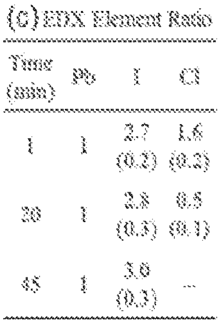

(c) EDX Element Ratio

Time (min)	Pb	I	Cl
1	1	2.7 (0.2)	1.6 (0.2)
20	1	2.8 (0.3)	0.5 (0.1)
45	1	3.0 (0.3)	–

Fig. 16c

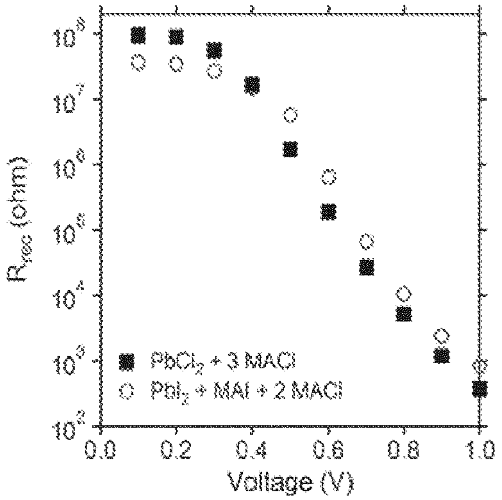
10^8
10^7
10^6
10^5
10^4
10^3
10^2
R_{rec} (ohm)
0.0
0.2
0.4
0.6
0.8
1.0
Voltage (V)
■ $PbCl_2$ + 3 MACl
○ PbI_2 + MAI + 2 MACl

Fig. 17

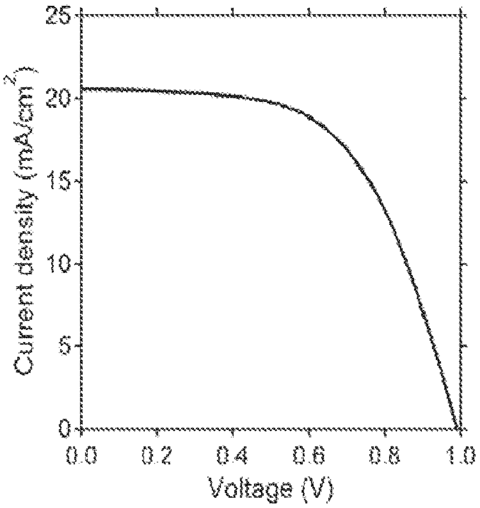

Fig. 18

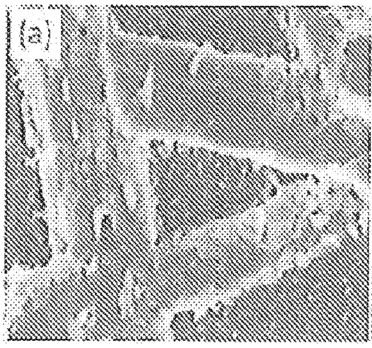

Fig. 19a

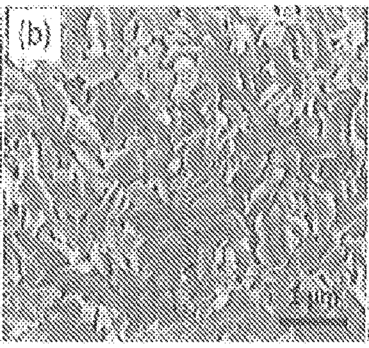

Fig. 19b

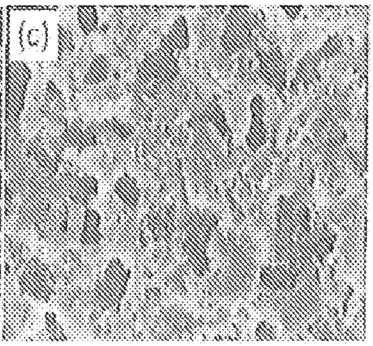

Fig. 19c

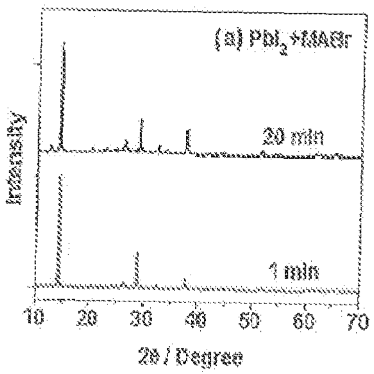

Fig. 20a

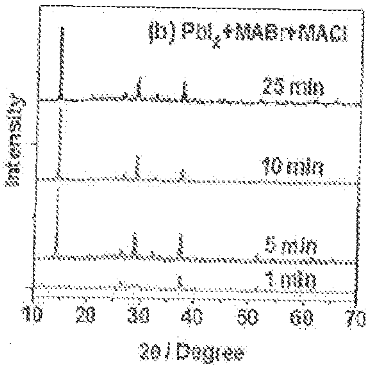

Fig. 20b

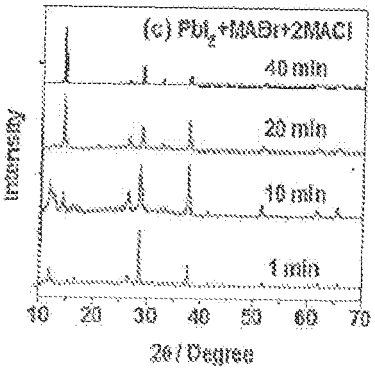

Fig. 20c

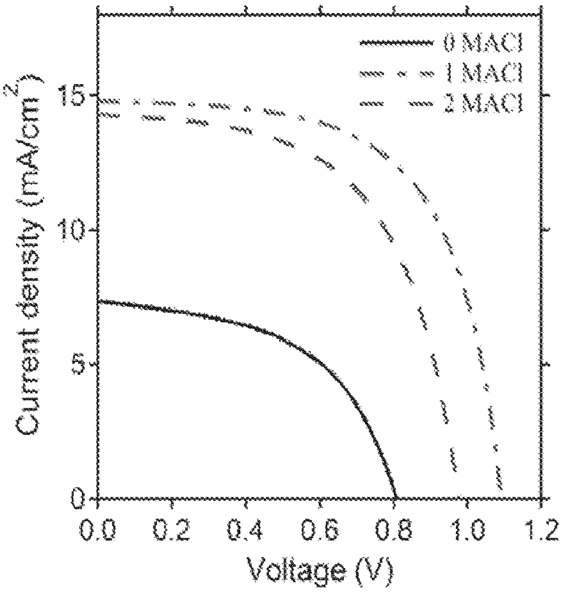
0 MACl
1 MACl
2 MACl
Current density (mA/cm^2)
15
10
5
0
0.0
0.2
0.4
0.6
0.8
1.0
1.2
Voltage (V)

Fig. 21

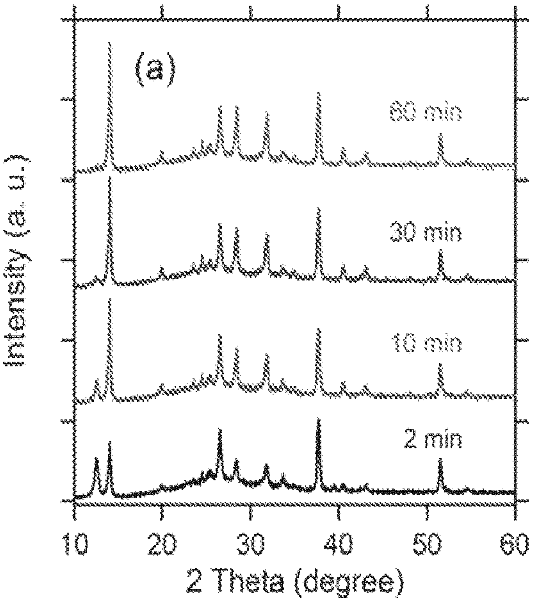

Fig. 22a

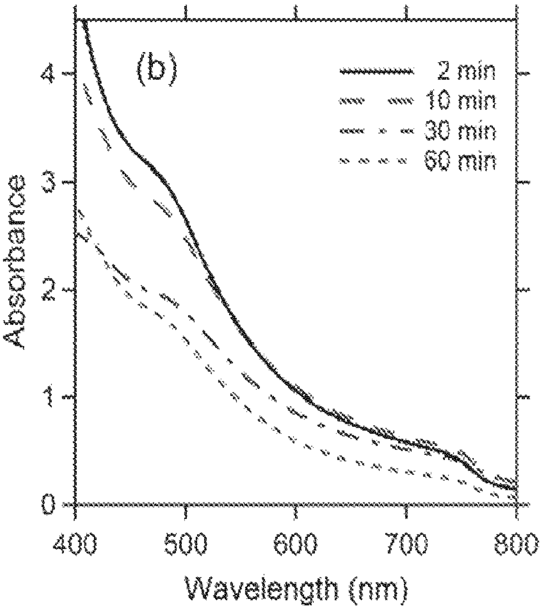

Fig. 22b

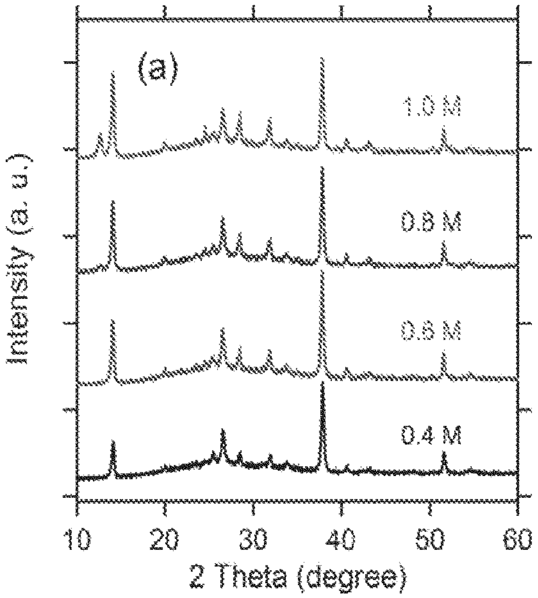

Fig. 23a

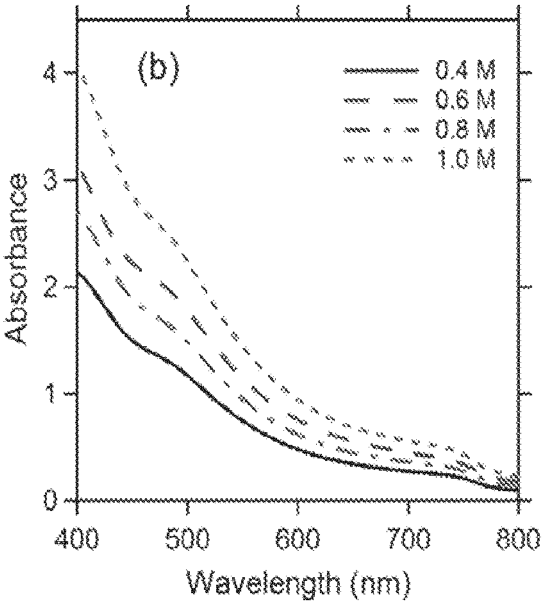

Fig. 23b

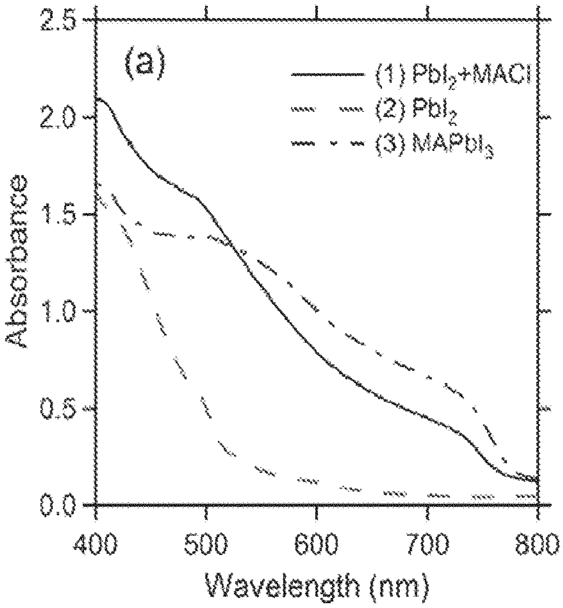

Fig. 24a

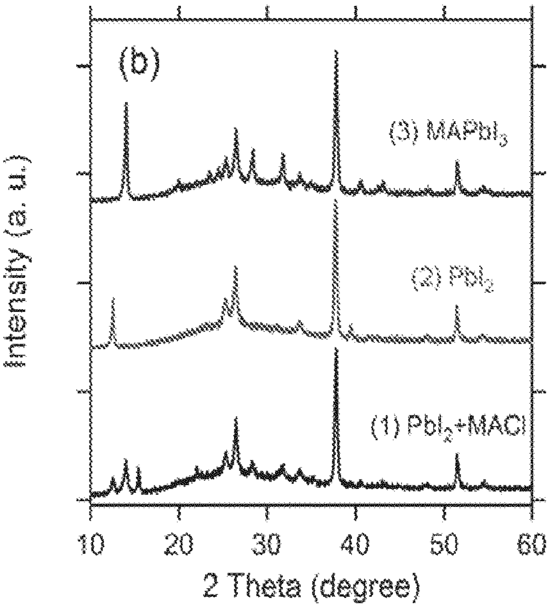

Fig. 24b

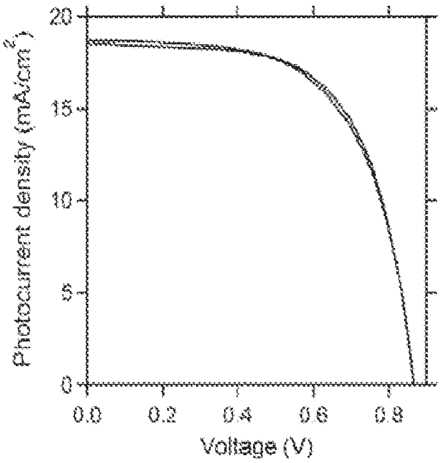

Photocurrent density (mA/cm^2)
20
15
10
5
0
0.0
0.2
0.4
0.6
0.8
Voltage (V)

Fig. 25

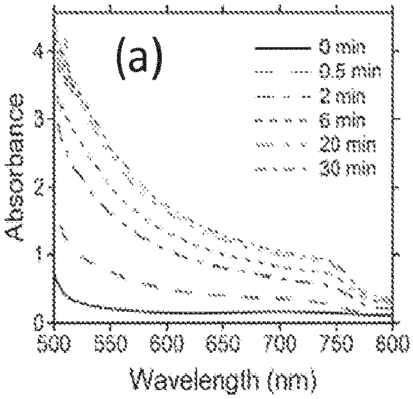

Fig. 26a

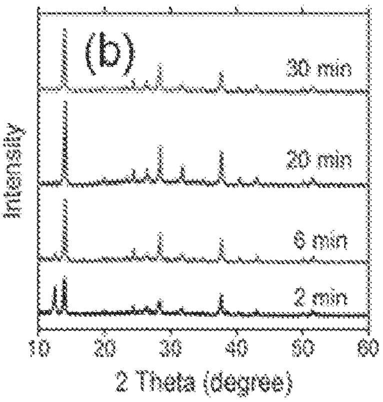

Fig. 26b

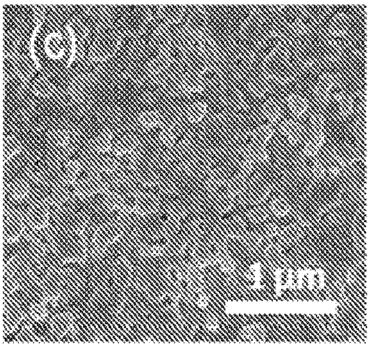

Fig. 26c

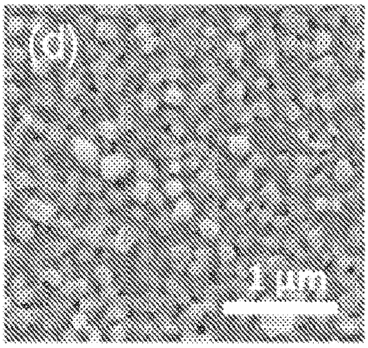

Fig. 26d

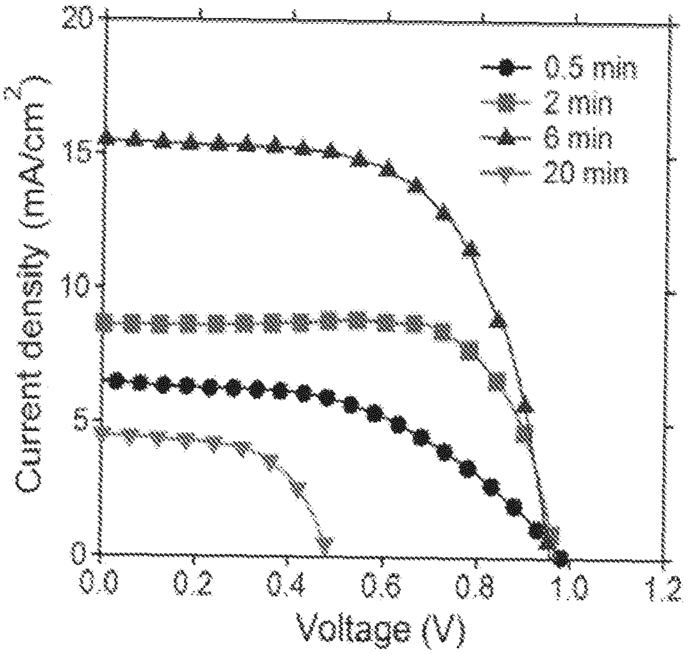
Current density (mA/cm^2)
20
15
10
5
0
0.0
0.2
0.4
0.6
0.8
1.0
1.2
Voltage (V)
0.5 min
2 min
6 min
20 min

Fig. 27

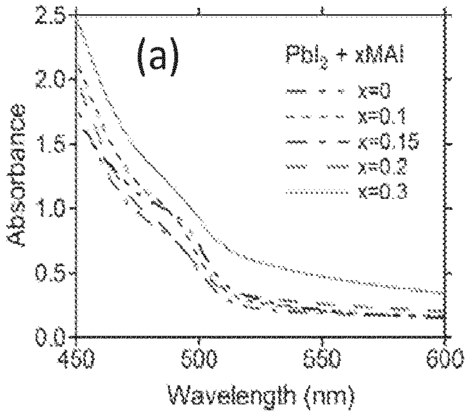

Fig. 28a

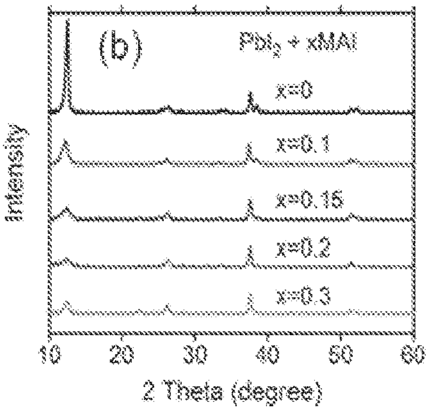

Fig. 28b

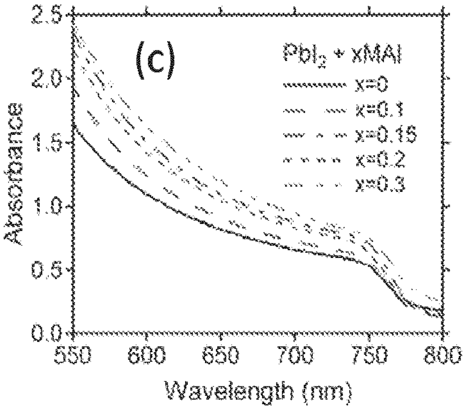

Fig. 28c

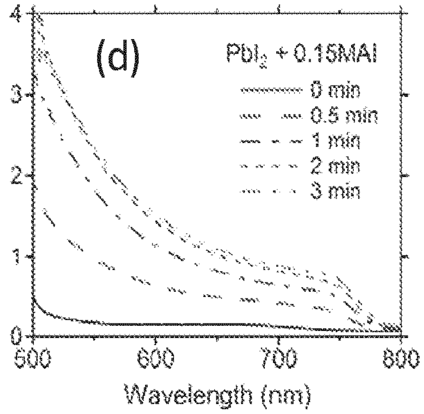

Fig. 28d

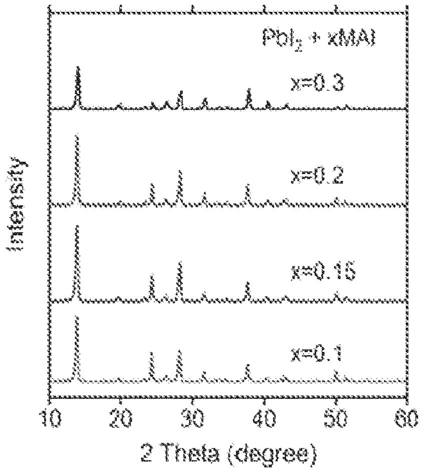
PbI_2 + xMAI
x=0.3
x=0.2
x=0.15
x=0.1
Intensity
10
20
30
40
50
60
2 Theta (degree)

Fig. 29

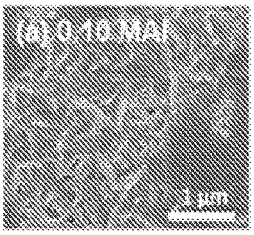

Fig. 30a

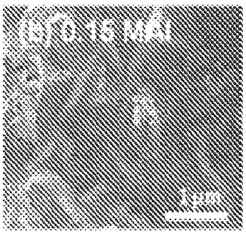

Fig. 30b

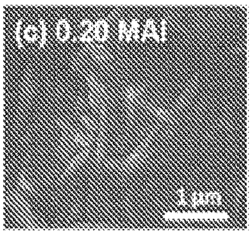

Fig. 30c

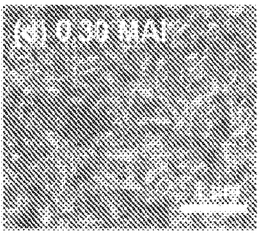

Fig. 30d

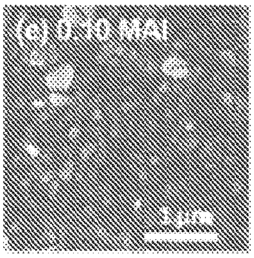

Fig. 30e

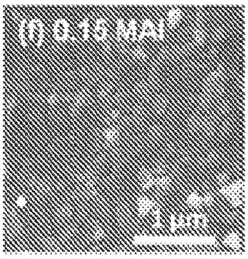

Fig. 30f

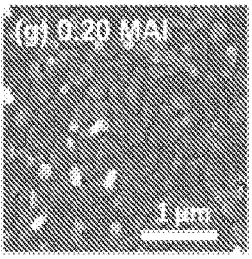

Fig. 30g

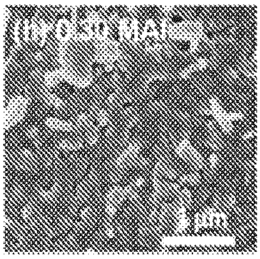

Fig. 30h

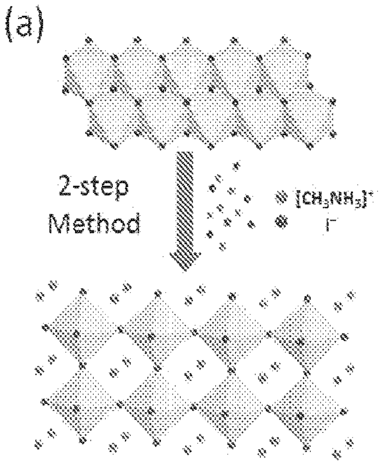

Fig. 31a

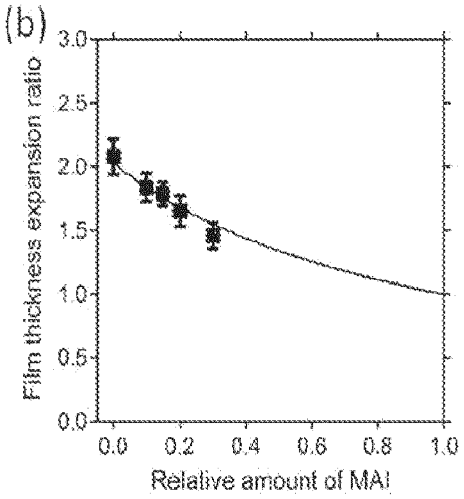

Fig. 31b

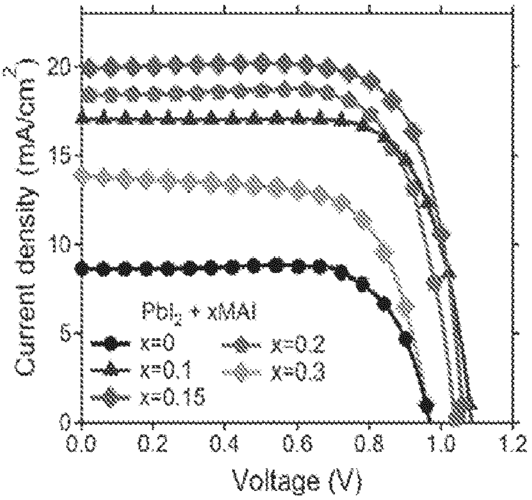
Current density (mA/cm^2)
Voltage (V)
0
5
10
15
20
0.0
0.2
0.4
0.6
0.8
1.0
1.2
PbI$_2$ + xMAI
x=0
x=0.1
x=0.15
x=0.2
x=0.3

Fig. 32

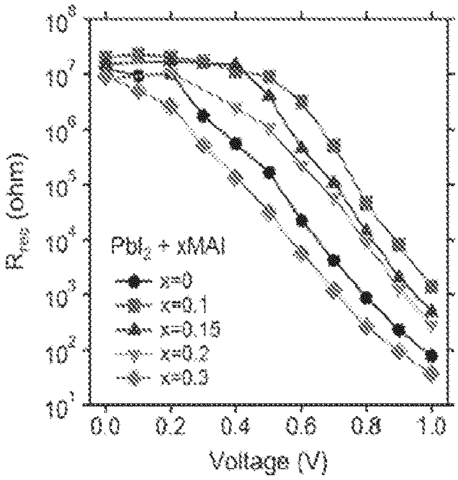
R_{res} (ohm)
10^8
10^7
10^6
10^5
10^4
10^3
10^2
10^1
0.0
0.2
0.4
0.6
0.8
1.0
Voltage (V)
PbI_2 + xMAI
x=0
x=0.1
x=0.15
x=0.2
x=0.3

Fig. 33

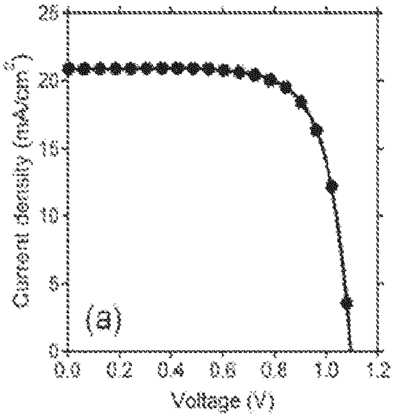

Fig. 34a

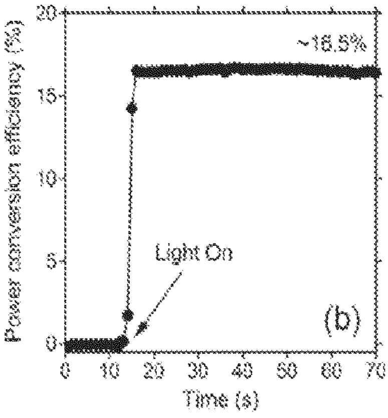

Fig. 34b

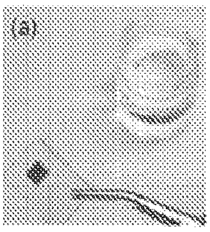

Fig. 35a

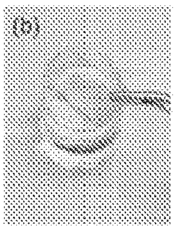

Fig. 35b

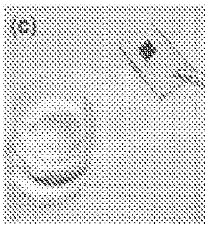

Fig. 35c

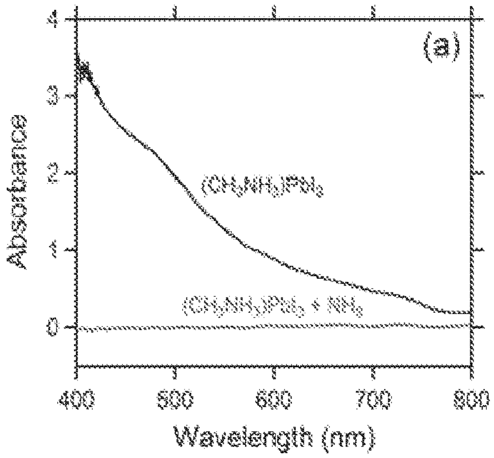

Fig. 36a

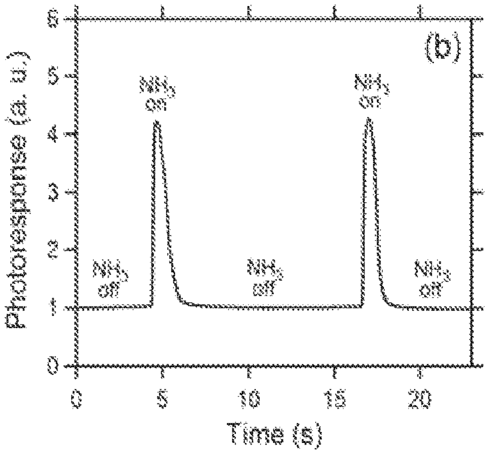

Fig. 36b

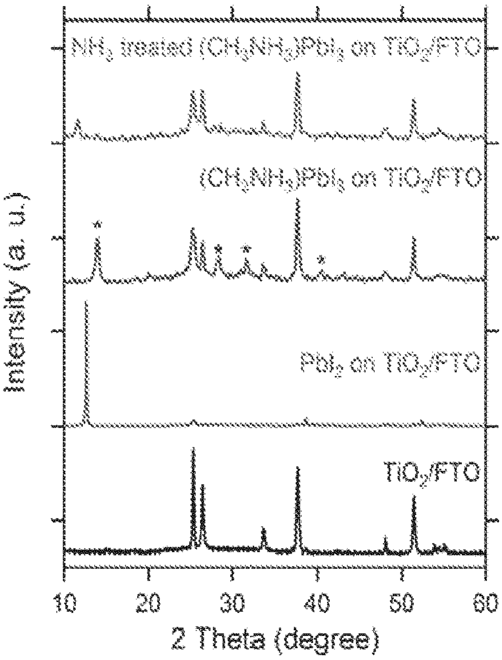
NH$_3$ treated (CH$_3$NH$_3$)PbI$_3$ on TiO$_2$/FTO
(CH$_3$NH$_3$)PbI$_3$ on TiO$_2$/FTO
PbI$_2$ on TiO$_2$/FTO
TiO$_2$/FTO
Intensity (a. u.)
10
20
30
40
50
60
2 Theta (degree)

Fig. 37

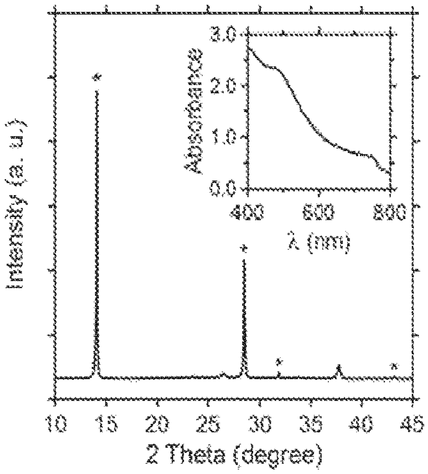
Intensity (a. u.)
2 Theta (degree)
10
15
20
25
30
35
40
45
*
*
*
*
Absorbance
3.0
2.0
1.0
0.0
400
600
800
λ (nm)

Fig. 38

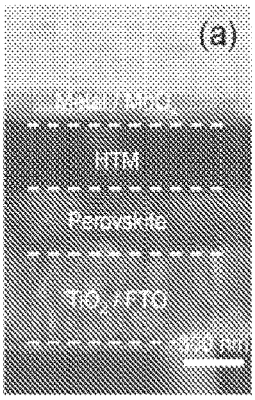

Fig. 39a

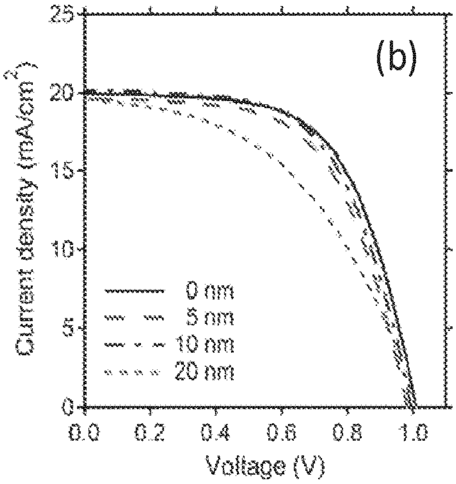

Fig. 39b

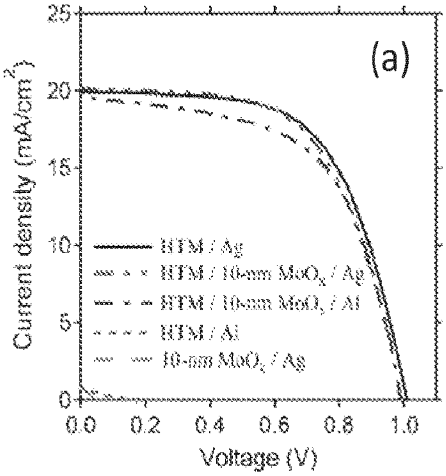

Fig. 40a

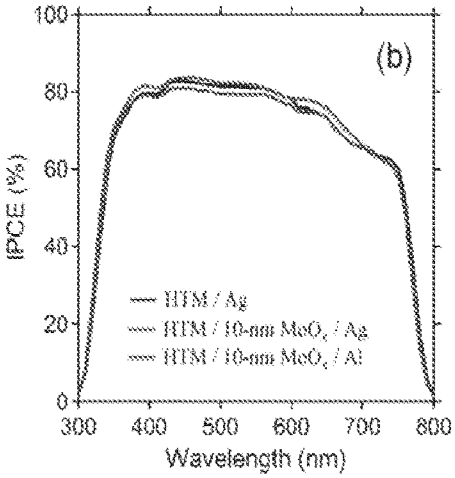

Fig. 40b

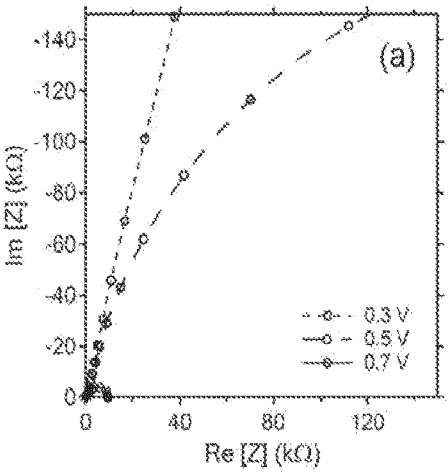

Fig. 41a

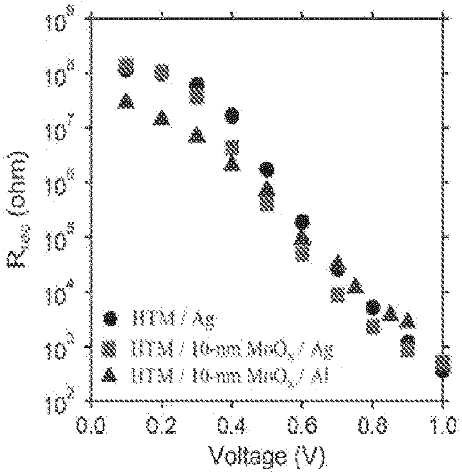

Fig. 41b

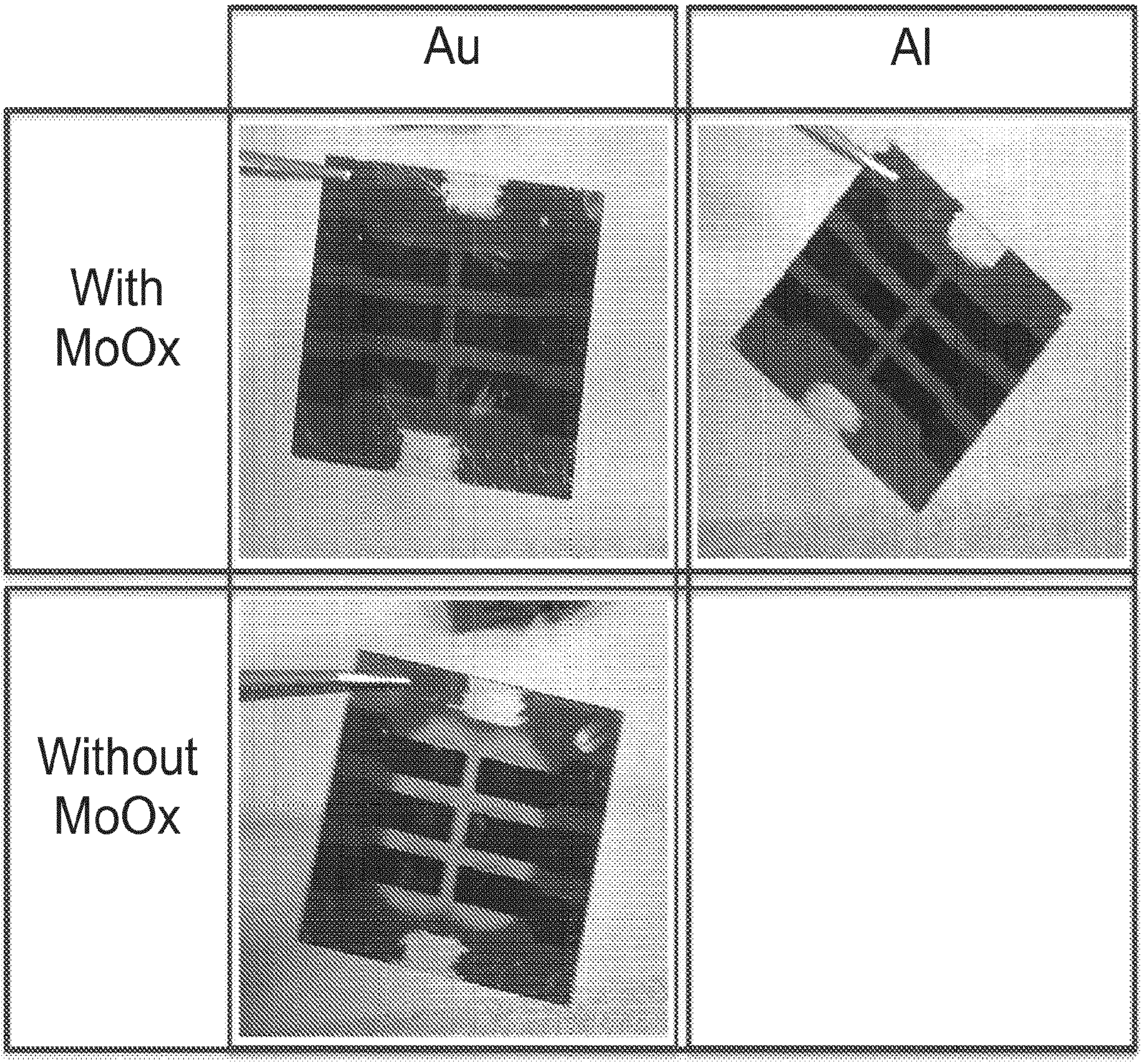

Fig. 42

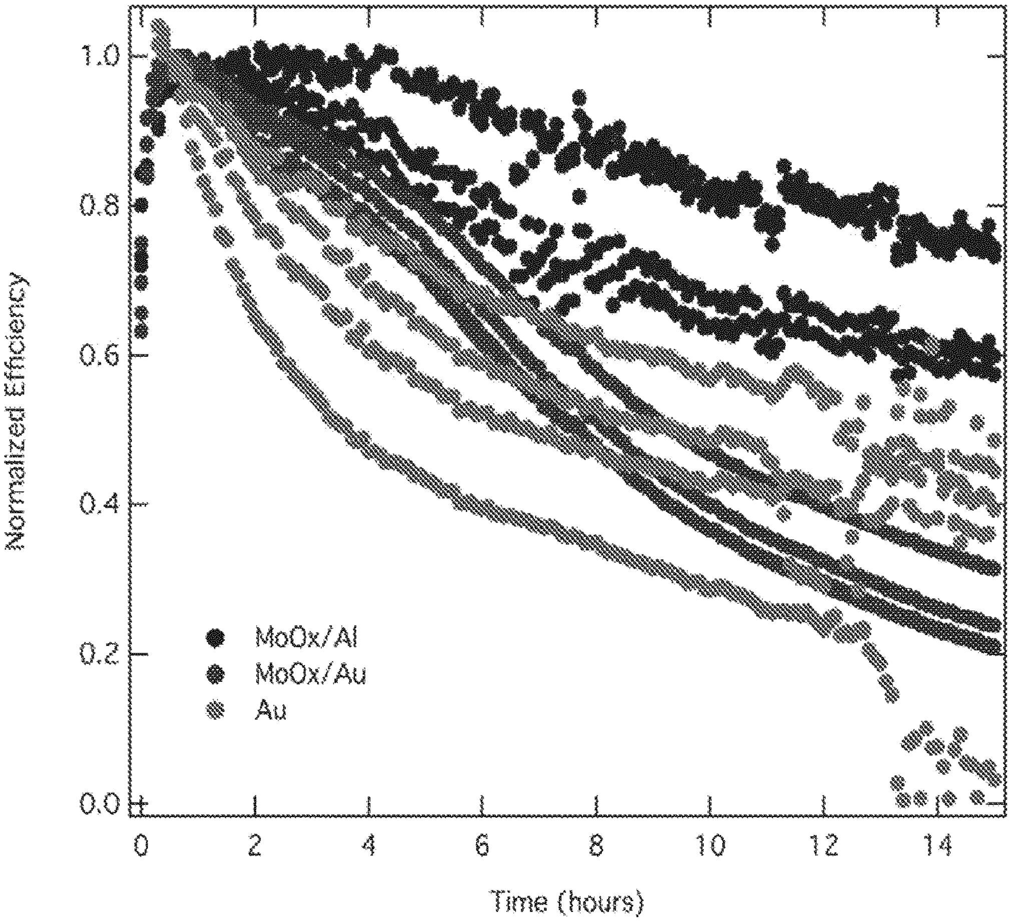
Normalized Efficiency
1.0
0.8
0.6
0.4
0.2
0.0
0
2
4
6
8
10
12
14
Time (hours)
MoOx/Al
MoOx/Au
Au

Fig. 43

Europäisches Patentamt
European Patent Office
Office européen des brevets

EUROPEAN SEARCH REPORT

Application Number
EP 18 16 8162

DOCUMENTS CONSIDERED TO BE RELEVANT

Category	Citation of document with indication, where appropriate, of relevant passages	Relevant to claim	CLASSIFICATION OF THE APPLICATION (IPC)
A	JULIAN BURSCHKA ET AL: "Sequential deposition as a route to high-performance perovskite-sensitized solar cells", NATURE, vol. 499, no. 7458, 10 July 2013 (2013-07-10), pages 316-319, XP055131813, ISSN: 0028-0836, DOI: 10.1038/nature12340 * page 1, lines 3-21, paragraph right * -----	1-15	INV. H01L51/42 H01L21/20
A	Yingzhunag Ma ET AL: "A highly efficient mesoscopic solar cell based on CH 3 NH 3 PbI 3Àx Cl x fabricated via sequential solution deposition", Chem. Commun, vol. 50 19 May 2014 (2014-05-19), pages 12458-12461, XP055418161, Retrieved from the Internet: URL:http://pubs.rsc.org/en/content/articlepdf/2014/cc/c4cc01962h [retrieved on 2017-10-23] Scheme 1; * abstract; figure 1 * -----	1-15	TECHNICAL FIELDS SEARCHED (IPC) H01L

The present search report has been drawn up for all claims

1

Place of search	Date of completion of the search	Examiner
The Hague	14 September 2018	Welter, Steve

CATEGORY OF CITED DOCUMENTS

X : particularly relevant if taken alone
Y : particularly relevant if combined with another document of the same category
A : technological background
O : non-written disclosure
P : intermediate document

T : theory or principle underlying the invention
E : earlier patent document, but published on, or after the filing date
D : document cited in the application
L : document cited for other reasons

& : member of the same patent family, corresponding document